REDUCTIVE DEHALOGENATION OF POLYHALOGENATED SOLVENTS AND FLAME RETARDENTS USING ZERO VALENT IRON BASED BIMETALLIC PARTICLES

by

WEN LIU

A Dissertation submitted to the

Graduate School-New Brunswick

Rutgers, The State University of New Jersey

in partial fulfillment of the requirements

for the degree of

Doctor of Philosophy

Graduate Program in Environmental Sciences

written under the direction of

Dr. WEILIN HUANG

and approved by

_____

_____

_____

_____

New Brunswick, New Jersey

[OCTOBER, 2012]

ABSTRACT OF THE DISSERTATION

REDUCTIVE DEHALOGENATION OF POLYHALOGENATED SOLVENTS AND FLAME RETARDENTS USING ZERO VALENT IRON BASED BIMETALLIC PARTICLES

By WEN LIU

Dissertation Director:
DR. WEILIN HUANG

Abiotic reductive dehalogenation is considered to be a fast and effective way for the detoxification of various polyhalogenated compounds. This dissertation consists of four studies intended to identify materials for fast and effective dehalogenation of halogenated benzenes and flame retardants.

In *Study I*, bimetallic particles were synthesized by chemically depositing a second metal onto micro-scale zero valent iron particles, and then characterized by Brunauer-Emmet-Teller surface area analyzer, scanning electron microscopy and X-ray photoelectron spectrometry.

In *Study II*, it was found that 1,2,4-trichlorobenzene and 1,2,4-tribromobenzene were rapidly dehalogenated by Pd/Fe with a half-life of 165 minutes and 71 minutes, respectively. Benzene was the major final product. Under the same reaction conditions, 1,2,4-trifluorobenzene, however, showed no dehalogenation activity.

Pd/Fe bimetallic particles were found to be effective in dehalogenation of dichlorobenzenes, chlorobenzene, dibromobenzenes and bromobenzene. The order of dechlorination rates among

dichlorobenzenes was 14-DCB ≥ 13-DCB ≥ 12-DCB. The order of debromination rates among DBBs was 14-DBB ≥ 13-DBB ≥ 12-DBB.

The following reactivity trend for 1,2,4-trichlorobenzene and 1,2,4-tribromobenzene was identified: Pd/Fe >> Ni/Fe > Cu/Fe > Ag/Fe ≈ Fe. A near linear correlation was found between the heat of hydrogen solution and $1/k_{obs}$ for 1,2,4-TCB dechlorination/1,2,4-TBB debromination by different bimetallic particles.

In *Study III*, it was demonstrated that the dehalogenation of tetrabromobisphenol A (TBBPA)/ tetrachlorobisphenol A (TCBPA) by Pd/Fe was rapid at ambient temperature. The dehalogenation rate constant k_{obs} of TBBPA/TCBPA was proportional to the Pd/Fe particle dosage and surface loading of Pd. Lower solution pH also favored the debromination of TBBPA. Higher initial TCBPA concentrations had a negative impact on the k_{obs}. The k_{obs} values measured at constant solution pH correlated linearly with the Pd mass introduced to the reactors, regardless of Pd/Fe particle dosage or Pd surface coverage. The greater amount of Pd also resulted in more complete of transformation of TBBPA/TCBPA to bisphenol-A (BPA) within a short period of time.

In *Study IV*, an optimized quantitative structure–activity relationship (QSAR) model was developed using 5 descriptors to establish the correlation between the reaction rates of structurally similar halogenated benzenes with ZVI based bimetallic particles and their molecular properties. A significant correlation (R^2=0.924, $p<0.05$) between Q_X^+ and the observed $\log k_{obs}$ was established. A pathway prediction model for TBBPA/TCBPA was constructed based on the QSAR modeling results for the halogenated benzenes.

ACKNOWLEDGEMENTS

First and foremost, I would like to thank my adviser Dr. Weilin Huang for providing me numerous research opportunities, extensive guidance and much needed direction over the years. Dr. Weilin Huang was always an exceptionally supportive, encouraging and helpful advisor. His interest in my research, patient guidance throughout my experiments, and continuous encouragement make me the researcher I am today. Much of what I have learned under him will help me throughout my professional career.

I would also like to thank my dissertation committee members Dr. Lisa Rodenburg, Dr. Peter Strom and Dr. Zev Gerstl for their suggestions and advice regarding my PhD work. I graciously offer thanks for their input and advice on various aspects of this work. I would like to thank Dr. Bichun Huang and Dr. Guining Lu from South China University of Technology (SCUT), Qiang Huang from Guangzhou Institute of Geochemistry for their help on the various aspects of this work.

I acknowledge the grants that supported me during my PhD: Excellence Fellowship and Teaching Assistantship from the Department of Environmental Sciences, New Jersey Department of Environmental Protection (NJEDP) Grant (SR08-039) and Philadelphia Water Department (PWD) Grant (Impacts of tidal sediment pollution on stream water quality). Without their support, this work would literally not have been possible. I also acknowledge a scholarship from the NJ Water Environment Association (NJWEA) that I received in 2012.

I also express my warm thanks and gratitude to my colleagues and friends here at Rutgers. I would always be indebted to Huang lab members Baohua, Yingjun, Il and Kelly for the wonderful time I have had working and being friends with them, for our insightful discussions

about experiments, career and life in general. I thank my friends, Songyan, Jia, Yun, Youyou, and many others for their support and company throughout the years.

Finally, I thank my parents for their support and encouragement to pursue my academic goals. I must acknowledge my husband, Yilun Yao, for his calm manner, natural optimism and bountiful assistance during the preparation of this dissertation. He is an amazing person from whom I have sought counsel many times. I cannot thank him enough.

Contents

Abstract……ii

Acknowledgements……..iv

1 Chapter 1 Introduction..... 1

1.1 Polyhalogenated compounds pollution..... 1

1.2 Remediation technologies for PHCs polluted groundwater..... 1

1.3 Nano-sized ZVI and bimetallic reductants/ particles..... 3

1.4 Research objectives..... 6

2 Chapter 2 Literature Review..... 7

2.1 Historical development of ZVI for environmental remediation..... 7

2.1.1 History of ZVI-mediated reduction..... 7

2.1.2 History of ZVI based bimetallic particles mediated reduction..... 8

2.2 Zero valent iron mediated degradation..... 9

2.2.1 Reductive transformation of inorganic contaminants..... 9

2.2.2 Reductive degradation of organic compounds..... 11

2.3 ZVI applications..... 17

2.3.1 Permeable Reactive Barrier..... 17

2.3.2 *Insitu* injection methods..... 19

2.4 Synthesis of ZVI based bimetallic particles..... 21

2.5 Summary..... 22

3 Chapter 3 Methodology 24
3.1 Chemicals and reagents 24
3.2 Solution phase synthesis of ZVI based bimetallic particles 25
3.3 ZVI based bimetallic particles characterization 26
3.3.1 Brunauer, Emmett, and Teller (BET) surface area analysis 26
3.3.2 Scanning electron microscopy analysis 27
3.3.3 X-ray photoelectron spectroscopy analysis 27
3.4 Batch degradation study 27
3.4.1 1, 2, 4-Trichlorobenzene, dichlorobenzenes and chlorobenzene 27
3.4.2 1, 2, 4-Tribromobenzene, dibromobenzenes and bromobenzene 30
3.4.3 1, 2, 4-Trifluorobenzene 31
3.4.4 Tetrabromobisphenol A 31
3.4.5 Tetrachlorobisphenol A 34
3.5 Method of analysis 35
3.5.1 GC-MS 35
3.5.2 HPLC 36
4 Chapter 4 Results and Discussion 38
4.1 Characterization of bimetallic particles 38
4.1.1 Surface area analysis 38
4.1.2 Scanning electron microscopy analysis 39
4.1.3 X-ray photoelectron spectroscopy analysis 41

4.2 Dechlorination of 1, 2, 4-trichlorobenzene, dichlorobenzenes and chlorobenzene by Pd/Fe 47

4.3 Dechlorination of 1, 2, 4-trichlorobenzene by Ni/Fe, Cu/Fe and Ag/Fe 51

4.4 Debromination of 1, 2, 4-tribromobenzene, dibromobenzenes and bromobenzene by Pd/Fe 59

4.5 Debromination of 1, 2, 4-tribromobenzene by Ni/Fe, Cu/Fe and Ag/Fe 63

4.6 Reaction of 1, 2, 4-trifluorobenzene with Pd/Fe 68

4.7 Debromination of tetrabromobisphenol A by Pd/Fe 68

4.7.1 Rates of debromination 68

4.7.2 Effect of Pd coverage 71

4.7.3 Effect of bimetallic particle dosage 74

4.7.4 Effect of solution pH 76

4.7.5 Mechanisms 79

4.8 Degradation of tetrachlorobisphenol A by Pd/Fe 81

4.8.1 Rates of dechlorination 81

4.8.2 Effect of bimetallic particle dosage 84

4.8.3 Effect of initial concentration of TCBPA 85

4.8.4 Effect of Pd coverage 87

4.8.5 Mechanism 89

4.9 Summary 90

5 Chapter 5 Quantitative Structure–Activity Relationship Modeling 93

5.1 Introduction 93

5.2 Background 94
5.3 Computational method 96
5.4 QSAR modeling for halogenated benzenes 97
5.4.1 Response variables 97
5.4.2 Descriptors 97
5.4.3 Quantitative modeling 98
5.4.4 Modeling results 101
5.4.5 Analysis and discussion 104
5.5 Dehalogenation pathway prediction for TBBPA/ TCBPA 106
5.5.1 Pathway prediction for TBBPA debromination 107
5.5.2 Pathway prediction for TCBPA dechlorination 109
6 Chapter 6 Conclusions 110
6.1 Summary of results 110
6.2 Further research needs 114
7 References 116

List of Tables

Table 1 Comparison of four in-situ methods: nZVI, conventional PRB, thermal treatment and chemical oxidation, adapted from Müller (2010). 5

Table 2 Groundwater contaminants treated by ZVI[b] 8

Table 3 Bimetallic particles mediated reductive dehalogenation of PHCs 13

Table 4 Received chemicals 24

Table 5 Basic property data for 1,2,4-TCB, DCBs, MCB and Benzene at 25°C * 28

Table 6 Basic property data for 1,2,4-TBB, DBBs and MBB at 25°C *..... 30

Table 7 Basic property data for 1,2,4-TFB, DFBs and MFB at 25°C *..... 31

Table 8 Basic property data for TBBPA and BPA at 25°C*..... 32

Table 9 TBBPA experimental sets..... 33

Table 10 Basic property data for TCBPA at 25°C*..... 34

Table 11 TCBPA experimental sets..... 35

Table 12 Surface areas of bimetallic particles and commercial iron particles 38

Table 13 Rate constants and half-lives for MCB, DCBs and 124-TCB dechlorination with 5 g/L of 0.011% Pd/Fe 49

Table 14 Rate constants and half-lives for 124-TCB dechlorination by Pd/Fe, Ni/Fe, Cu/Fe and Ag/Fe 54

Table 15 Standard reduction Potentials at 25°C 55

Table 16 Rate constants and half-lives for MBB, DBBs and 124-TBB debromination with 5 g/L 0.011% Pd/Fe 60

Table 17 Rate constants and half-lives for 124-TBB debromination by Pd/Fe, Ni/Fe, Cu/Fe and Ag/Fe 66

Table 18 Apparent rate constants of TBBPA debromination..... 70

Table 19 Apparent Rate Constants of TCBPA Dechlorination 83

Table 20 Response variables* 95

Table 21 Descriptor variables* 95

Table 22 Pseudo-first-order reaction rate constants (k_{obs}) for chemicals of interests 97

Table 23 Descriptors for 124-TCB, DCBs, MCB, 124-TBB, DBBs and MBB 98

Table 24 Symbols in PLS model 100

Table 25 Fitting results for PLS models I, II and III 102

Table 26 The variable coefficients of the Model II 102

Table 27 The variable coefficients of the optimized model 104

Table 28 Experimental and predicted logk_{obs} values for 10 compounds 106

Table 29 Charge on each chlorine atom of the 1,2,4-TCB molecule (Unit: atomic charge unit) 107

Table 30 Secondary maximum contaminant levels for public water systems 115

List of Illustrations

Figure 1 Permeable Reactive Barriers (Interstate Technology & Regulatory Council, 1999a) 3

Figure 2 A conceptual model for metal removal with nZVI (Li and Zhang, 2007)..... 11

Figure 3 Schematic of possible pathways for the reductive degradation of halocarbon (Matheson and Tratnyek, 1994)..... 12

Figure 4 Permeable reactive barrier for groundwater plume remediation (USEPA, 2001) 18

Figure 5 PRBs and zero-valent metals..... 18

Figure 6 Schematic of two methods of groundwater remediation using *insitu* injection (Tratnyek and Johnson, 2006)..... 20

Figure 7 Solution phase synthesis of ZVI based bimetallic particles 26

Figure 8 Major steps of batch degradation study for halogenated benzenes..... 29

Figure 9 Major steps of batch degradation study for TBBPA/TCBPA..... 33

Figure 10 Pd/Fe SEM images, from left to right: 20 µm, 5 µm and 2 µm..... 39

Figure 11 Ni/Fe SEM images, from left to right: 20 µm, 5 µm and 2 µm..... 39

Figure 12 Cu/Fe SEM images, from left to right: 20 µm, 5 µm and 2 µm..... 39

Figure 13 Ag/Fe SEM images, from left to right: 20 µm, 5 µm and 2 µm 40

Figure 14 Size distribution curve for 4 bimetallic particles 40

Figure 15 XPS spectra of commercial iron particles 41

Figure 16 XPS spectra of Pd/Fe 0.011 wt %..... 42

Figure 17 XPS spectra of Pd/Fe 0.022 wt %..... 42

Figure 18 XPS spectra of Pd/Fe 0.044 wt %..... 43

Figure 19 XPS spectra of Ni/Fe 1 wt%..... 43

Figure 20 XPS spectra of Cu/Fe 1 wt% 44

Figure 21 XPS spectra of Ag/Fe 1 wt%..... 44

Figure 22 Pd on the surface of Pd/Fe, 0.011 wt % 45

Figure 23 Ni on the surface of Ni/Fe 45

Figure 24 Cu on the surface of Cu/Fe 46

Figure 25 Ag on the surface of Ag/Fe 46

Figure 26 Reaction of 5 g/L of 0.011% Pd/Fe with 1,2,4-trichlorobenzene 47

Figure 27 Reaction of 5 g/L of 0.011% Pd/Fe with chlorobenzene 48

Figure 28 Reaction of 5 g/L of 0.011% Pd/Fe with 1,2-dichlorobenzene 49

Figure 29 Reaction of 5 g/L of 0.011% Pd/Fe with 1,3-dichlorobenzene 50

Figure 30 Reaction of 5 g/L of 0.011% Pd/Fe with 1,4-dichlorobenzene 50

Figure 31 Reaction of 5 g/L of 1% Ni/Fe with 1,2,4-trichlorobenzene 52

Figure 32 Reaction of 5 g/L of 1% Cu/Fe with 1,2,4-trichlorobenzene 52

Figure 33 Reaction of 5 g/L of 1% Ag/Fe with 1,2,4-trichlorobenzene 53

Figure 34 Reaction of 5 g/L of Fe^0 with 1,2,4-trichlorobenzene 53

Figure 35 Reaction standard potential (ΔE°) vs $\ln k_{obs}$ for 1,2,4-TCB 56

Figure 36 Schematic of the potential energy of a hydrogen atom at the surface of Pd (*left side*) and the immediate vacuum (*right side*), (Pundt and Kirchheim, 2006) 56

Figure 37 Hydrogen uptake rate R of a 130 nm thick yttrium film at 420 K and 2 bar hydrogen (Borgschulte et al., 2006). 57

Figure 38 The heat of hydrogen solution ΔH_{sol} vs. $1/k_{obs}$ (the observed rate constants) (a) and the heat of hydrogen chemisorption ΔH_{chem} vs. $\ln k_{obs}$ (b) for 1,2,4-TCB 58

Figure 39 Reaction of 5 g/L 0.011% Pd/Fe with 1,2,4-tribromobenzene 59

Figure 40 Reaction of 5 g/L 0.011% Pd/Fe with bromobenzene 60

Figure 41 Reaction of 5 g/L 0.011% Pd/Fe with 1,2-dibromobenzene 61

Figure 42 Reaction of 5 g/L 0.011% Pd/Fe with 1,3-dibromobenzene 61

Figure 43 Reaction of 5 g/L 0.011% Pd/Fe with 1,4-dibromobenzene 62

Figure 44 Coefficient of determination from the overall regression analysis 62

Figure 45 Reaction of 5 g/L 1% Ni/Fe with 1,2,4-tribromobenzene 64

Figure 46 Reaction of 5 g/L 1% Cu/Fe with 1,2,4-tribromobenzene..... 64

Figure 47 Reaction of 5 g/L 1% Ag/Fe with 1,2,4-tribromobenzene 65

Figure 48 Reaction of 5 g/L Fe^0 with with 1,2,4-tribromobenzene 65

Figure 49 Reaction standard potential ($\Delta E°$) vs lnk_{obs} for 1,2,4-TBB..... 66

Figure 50 The heat of hydrogen solution ΔH_{sol} vs. 1/k_{obs} (the observed rate constants) (a) and the heat of hydrogen chemisorption ΔH_{chem} vs. lnk_{obs} (b) for 1,2,4-TBB 67

Figure 51 Debromination of TBBPA with 4 g L^{-1} of 0.022% Pd/Fe and solution pH 6.2 69

Figure 52 Effect of Pd coverage on TBBPA transformation rates 72

Figure 53 TBBPA: correlations between the rate constants (k_{obs}) and the Pd loading (a), k_{obs} and the Pd/Fe dosage (b), and log k_{obs} and the solution pH (c) 73

Figure 54 The effect of bimetallic particle dosage on the rate of TBBPA debromination (0.022% Pd/Fe and solution pH 7.2)..... 75

Figure 55 The effect of solution pH on the rate of TBBPA debromination (4 g L^{-1} of 0.022% Pd/Fe)..... 77

Figure 56 Correlation between the rate constant (k_{obs}) for TBBPA debromination and the Pd dosage. 80

Figure 57 Dechlorination of TCBPA (20 μM) with 4 g L^{-1} of 0.044% Pd/Fe and solution pH 4.0 81

Figure 58 The effect of Pd/Fe dosage on TCBPA transformation rates..... 85

Figure 59 The effect of initial concentration on the rate of TCBPA dechlorination 86

Figure 60 TCBPA: correlations between the rate constants (k_{obs}) and the Pd/Fe dosage (a), k_{obs} and initial TCBPA concentration (b), and k_{obs} and Pd loading (c) 87

Figure 61 The effect of Pd coverage on the rate of TCBPA dechlorination 89

Figure 62 Correlation between the rate constant (k_{obs}) of TCBPA dechlorination and the Pd dosage 90
Figure 63 Importance of each variable in prediction model..... 103
Figure 64 Correlation between Q_X^+ and the observed logk_{obs}..... 105
Figure 65 Calculated charges of each bromine atoms for tri-BBPA..... 108
Figure 66 Predicted debromination pathway for TBBPA 108
Figure 67 Calculated charges of each chlorine atoms for tri-CBPA..... 109
Figure 68 Predicted dechlorination pathway for TCBPA 109

1 Chapter 1 Introduction

1.1 Polyhalogenated compounds pollution

Polyhalogenated compounds (PHCs), are an important chemical group because of their environmental persistence, high hydrophobicity, and bioaccumulation in humans (Takigami et al., 2009). PHCs are used in a wide array of manufactured products, including dry cleaning, metal degreasing (halogenated solvents), and fire resistant coatings (polybrominated diphenyl ethers or PBDEs). It is estimated that in the peak of their production, hundreds of millions of pounds of halogenated solvents were produced in the United States alone (Pankow, 1996).

Because of their wide application and chemical inertness, PHCs are found in groundwater, soil and the atmosphere. In fact, 10 of the 25 most frequently encountered pollutants in groundwater today are halogenated organic compounds (National Research Council, 1994), many of which are now suspected carcinogens (Klaassen, 1999). Remediation of PHC contaminated sites is one of the most important environmental goals specified by the United States Environmental Protection Agency (USEPA, 2001).

1.2 Remediation technologies for PHCs polluted groundwater

The United States faces a very large groundwater contamination problem. Although the total number of contaminated sites is unknown, estimates where groundwater and soil may be contaminated range from approximately 300,000 to 400,000 (National Reseach Council, 1994). Recent estimates of the total cost of cleaning up these sites over the next 30 years have ranged as high as $1 trillion (National Research Council, 1994).

Pump-and-treat systems are the most common technology for groundwater cleanup in the United States (National Research Council, 1994). Established pump-and-treat groundwater remediation is criticized for being too expensive and time-consuming, especially when cleanup standards are set at very low levels, e.g., < 10 parts per billion (ppb) (Hoffman, 1993).

Besides pump and treat systems, *insitu* remediation of polyhalogenated compounds can be generalized into two main categories: (1) natural attenuation and biological systems, and (2) physical-chemical treatments. Biological systems utilized include plantations (e.g. barley, poplar, etc. (Susarla et al., 2002)) and active microbial populations under aerobic (Alvarez-Cohen and Speitel, 2001; Clement et al., 2000; Semprini, 1997) and anaerobic (Aulenta et al., 2006; Ellis et al., 2000; Ferguson and Pietari, 2000; Witt et al., 2002) environments. However, *insitu* bioremediation has some disadvantages including the risk of toxic intermediates, adverse impacts on secondary water quality objectives and clogging of the subsurface due to uncontrolled (Interstate Technology & Regulatory Council, 2005). On the other hand, physical-chemical treatment technologies have been used to achieve immediate and effective degradation of toxic compounds and are extensively documented by the National Research Council (1994; 1997; 1999b). *Insitu* chemical oxidation (Li and Schwartz, 2004; Liang et al., 2004), soil vapor extraction (Boudouch et al., 2009; Nobre and Nobre, 2004) and permeable reactive barriers (PRBs, Figure 1) (Muegge and Hadley, 2009; Quinn, 2005; Vogan et al., 1999) have received successful results in the field and earned their spots in the groundwater/soil remediation technologies repertoire.

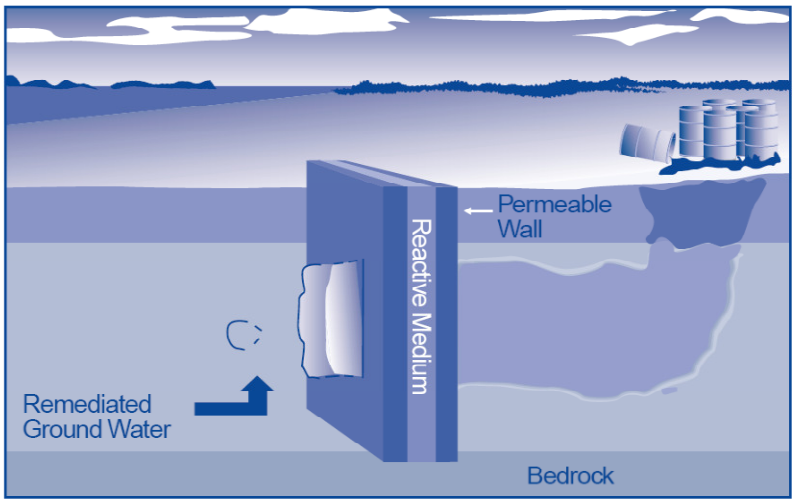

Figure 1 Permeable Reactive Barriers (Interstate Technology & Regulatory Council, 1999a)

Since the first implementation in the early 1990s, more than 200 PRB systems have been installed (Interstate Technology & Regulatory Council, 2011). The most common material used for PRB construction is zero valent iron (ZVI). Due to its relatively low cost and negligible metal toxicity, ZVI based systems have been receiving much attention. ZVI PRBs have been installed and performing in place for 15 years in a variety of geochemical environments (Interstate Technology & Regulatory Council, 2011a). Even though promising reaction kinetics have been reported by many (Agrawal and Tratnyek, 1995; Gillham and O'Hannesin, 1994; Sayles et al., 1997; Su and Puls, 1998; Tratnyek et al., 1997), dehalogenation by zero-valent metals also produce measurable amounts of less chlorinated intermediates and by-products such as dichloroethylenes and vinyl chloride (Arnold and Roberts, 2000; McMahon et al., 1999).

1.3 Nano-sized ZVI and bimetallic reductants/ particles

In the search for more complete dehalogenation and faster reaction rates, recent efforts are directed to synthesizing nano-sized ZVI (nZVI) or bimetallic reductants. Nano-sized systems with

higher surface area per unit volume as compared to the bulk particles have been synthesized and analyzed for the degradation of PHCs (He et al., 2010; Liu et al., 2005; Nyer and Vance, 2001; Wang and Zhang, 1997). Higher surface area of nano-sized particles will increase the availability of surface reaction sites for degradation process. However, due to a lack of suitable data, evaluations of the most serious criteria of environmental concern (i.e. persistency, bioaccumulation, toxicity) of nano-sized particles are largely unknown at this time (Grieger et al., 2010). This may seriously limit the application of nano-sized ZVI in groundwater remediation. Table 1 compares the injection of nZVI with a conventional PRB and two other *in situ* methods (thermal and chemical oxidation).

The so called bimetallic reductants/particles are iron based grains on which a second more noble metal is deposited. Most often these materials are generated by immersing iron granules into a metal salt solution, and allowing the iron to reduce the metal onto the iron surface. The use of bimetallic systems as reported in the literature for the remediation of PHCs include Ni/Fe (De Jong and Louw, 2004; Xu et al., 2009), Pd/Fe (Grittini et al., 1995; Liu et al., 2001; Nagpal et al., 2010), Pt/Fe (Zhang, 2003; Zhang et al., 1998), Ag/Fe (Li et al., 2006b), and Cu/Fe (Bransfield et al., 2006; Kim and Carraway, 2000; Kim and Carraway, 2003; Yuan et al., 2010a).

Table 1 Comparison of four in-situ methods: nZVI, conventional PRB, thermal treatment and chemical oxidation, adapted from Müller (2010).

	NZVI	PRB	Soil Vapor Extraction (Thermal)	Chemical oxidation
Material	nanoscale iron	granular iron	steam (heat)	oxidizing agents (e.g. permanganate)
Material reactivity	high	low	-	very high
Material mobility belowground	limited (max. a few meters)	not mobile (passive treatment)	limited – depending on thermal conductivity	fairly mobile
Material longevity (treatment time)	up to a few months	years	restricted to the duration of the application	hours (Fenton's reagent) to months (permanganate)
Material costs	high	low	high energy costs for stream/ heat production	moderate
Material toxicity	uncertainty about environmental impact of nanoparticles	low	non-toxic	substantial
Installation costs	moderate	expensive (especially if contaminant at greater depth)	moderate (high technical expertise and sophisticated equipment necessary)	inexpensive
Operation and maintenance costs	low to moderate	inexpensive	expensive	moderate
Requirements regarding site access	possible underneath buildings	open access for machinery necessary	possible underneath buildings	possible underneath buildings
Plume vs. source treatment	source and plume treatment; rebound possible if source is not completely eliminated	plume treatment only	source treatment; rebound possible if source is not completely eliminated	source and plume treatment; rebound possible if source is not completely eliminated
Formation of by-products	possible (e.g. NH_3, H_2)	possible (e.g. H_2)	possible (hydrolysis-products of chlorinated compound, uncontrolled condensation of contaminants)	possible (reactive oxygen species, solubilization of heavy metals, e.g. Cr)
Environmental effects	more reducing conditions- temporal change in microbiology	more reducing conditions- temporal change in microbiology	increase in temperature- temporal change in microbiology	oxidation of reducing environment- temporal change in microbiology

1.4 **Research objectives**

The first objective of this study is to synthesize different kinds of micro scale bimetallic particles and to subsequently investigate the dehalogenation potentials of these particles. It is expected that such investigations will lead to the development of more stable and more effective dehalogenation reductants.

The second objective of the work reported here is to compare reaction rates of structurally similar halogenated solvents and construct a quantitative structure-activity relationship (QSAR) model. The investigation will provide insight into the mechanisms involved in the iron-mediated transformation process.

The third objective is to assess whether the synthesized bimetallic particles are able to dehalogentate a new group of compounds (tetrabromobisphenol A and tetrachlorobisphenol A). This investigation will identify the optimal conditions (such as pH and noble metal loading) for dehalogenation of the above mentioned compounds.

2 Chapter 2 Literature Review

In this chapter, background information relating to the subject is presented and the subject area is defined more explicitly than in Chapter 1.

In particular, the historical development and current application of zero valent iron (ZVI) and ZVI based bimetallic particles for contaminant degradation is explored.

2.1 Historical development of ZVI for environmental remediation

2.1.1 History of ZVI-mediated reduction

Zero-valence state metals (such as Fe^0, Zn^0, Sn^0 and Al^0) are surprisingly effective agents for the remediation of contaminated groundwater (Powell et al., 1995; Warren et al., 1995). Zero-valent iron (ZVI) in particular has been the subject of numerous studies over the last 10 years and ZVI based permeable reactive barriers (PRBs) are becoming an increasingly popular choice for remediation of contaminated sites.

To our best knowledge, the earliest report recording the use of zero valent state metal to remove organic contaminants was in 1972. In the patent literature, iron was first recognized as a chlorinated pesticide degrader (Sweeny, 1972). Later in 1981, Sweeny (Sweeny, 1981a; Sweeny, 1981b) reported that catalyzed metallic iron powder was able to degrade a wide range of halogenated organic contaminants. Though the results were promising, the work of Sweeny was largely overlooked by the research community since the results were not published in refereed journals. Senzaki (1988) considered the use of iron powder for removal of trichloroethylene (TCE) from wastewater in the late 1980s. However, little focused work on the application of ZVI to remediation of polluted groundwater was reported until the early 1990s (Gillham RW, 1992;

Reynolds et al., 1990). These authors proposed the use of metals for both *insitu* and aboveground treatment of groundwater contaminated by halocarbons.

The success of laboratory studies led to the first field application of ZVI for *insitu* remediation of TCE-contaminated groundwater at a Canadian air force base in Ontario in 1991(Gillham RW, 1992). In 1993, a patent with the name "Cleaning halogenated contaminants from groundwater" (Gillham, 1993) was lodged by the University of Waterloo for using zero valent iron for treating contaminated groundwater *insitu*, demonstrating the identification of zero valent iron as a remediation constituent. Based on the success of the Canadian field demonstration, the first commercial ZVI PRB was installed at an industrial site in California for the removal of chlorinated hydrocarbons in groundwater in 1995 (Muegge and Hadley, 2009).

At present, ZVI has been used for the degradation of a wide range of groundwater contaminants (**Table 2**).

Table 2 Groundwater contaminants treated by ZVI[b]

Contaminants	Scale	Contaminants	Scale
Chlorinated ethenes, ethanes	F[a]	Cationic metals (e.g., Cu, Ni, Zn)	L
Nitrobenzene	P	Arsenic	F
Energetics	P	Chromium(VI)	F
Uranium	F	Selenium	L

[a]: F = full-scale application, L = laboratory evaluation, P = pilot-scale application. b: adapted from Table 4-1 (Interstate Technology & Regulatory Council, 2011)

2.1.2 History of ZVI based bimetallic particles mediated reduction

However, the use of zero-valent iron often results in only partial dechlorination in which the reaction products are sometimes more toxic than the reactants (Grittini et al., 1995). Recognizing the positive results and the potential problems associated with ZVI, researchers started to develop

new materials based on ZVI for remediation of a wide range of groundwater contaminants. The so called bimetallic reductants/particles are iron based grains on which a second more noble metal is deposited. Most often these materials are generated by immersing iron granules into a metal salt solution, and allowing the iron to reduce the metal onto the iron surface.

In 1995, Grittini (Grittini et al., 1995) demonstrated the rapid and complete dechlorination of polychlorinated biphenyls (PCBs) with Pd/Fe particles synthesized in the lab. Since then researchers have synthesized a wide array of ZVI based bimetallic particles, including Cu/Fe (Casey et al., 2000; Elsner et al., 2007; Fennelly and Roberts, 1998; Liou et al., 2005; Yuan et al., 2010a), Ni/Fe (De Jong and Louw, 2004; Schrick et al., 2002; Xu et al., 2009), Pt/Fe (Choi et al., 2008; Lin et al., 2004b), and Ag/Fe (Rivero-Huguet and Marshall, 2009; Wu et al., 2008; Wu et al., 2006). Bimetallic reductants have also been shown to reduce the yield of partially chlorinated reduction products (Bransfield et al., 2006; Cwiertny et al., 2006).

Due to their increased reactivity, bimetallic particles have been field tested as a practical alternative to subsurface granular iron for treating contaminant "hot spots" (Elliott and Zhang, 2001). At present, bimetallic particles are extensively used in the USA but they have not yet been applied in Europe (Mueller et al., 2012).

2.2 Zero valent iron mediated degradation

2.2.1 Reductive transformation of inorganic contaminants

- Reductive precipitation of hexavalent chromium

The key mechanisms for Cr(VI) removal using ZVI involve reduction to trivalent chromium [Cr(III)], followed by the precipitation of sparingly soluble chromium hydroxides and oxides,

such as $Cr(OH)_3$ and Cr_2O_3, respectively (Interstate Technology & Regulatory Council, 2011). The reaction sequence that leads to the precipitation of a mixed Cr(III)-Fe(III) oxyhydroxide (Blowes et al., 2000) can be described as follows:

$$CrO_4^{2-}{}_{(aq)} + Fe^0{}_{(s)} + 8H^+{}_{(aq)} \longrightarrow Fe^{3+}{}_{(aq)} + Cr^{3+}{}_{(aq)} + 4H_2O_{(l)} \quad \textbf{Equation 1}$$

$$(1-x)Fe^{3+}{}_{(aq)} + (x)Cr^{3+}{}_{(aq)} + 2H_2O \longrightarrow Fe_{(1-x)}Cr_xOOH_{(s)} + 3H^+{}_{(aq)} \quad \textbf{Equation 2}$$

- Reduction, sorption, and precipitation of redox-sensitive oxyanions

Laboratory bench-scale studies and field demonstrations have evaluated the potential of elemental iron for remediation of redox-sensitive oxyanions, such as selenium (Zhang et al., 2008; Zhang et al., 2005), technetium (Ding et al., 2001; Roh et al., 2000), and radioactive uranium (Noubactep et al., 2005; Wang and Salvage, 2005; Yi et al., 2009). The treatment mechanisms for these contaminants take advantage of their lower solubility in their more reduced state with removal through sorption and/or precipitation (Interstate Technology & Regulatory Council, 2011) .

- Removal of cationic metals

Reductive precipitation of metals is a potential treatment mechanism for metals with a standard potential much higher than that of ZVI(Interstate Technology & Regulatory Council, 2011) . For example, ZVI has been shown to reduce divalent copper [Cu(II)] to zero-valent copper, resulting in the precipitation of Cu(0) and Cu_2O (Rangsivek and Jekel, 2005). Li and Zhang (Li and Zhang, 2007) presented a model summarizing the potential mechanisms for metal removal using nanoscale ZVI (nZVI).

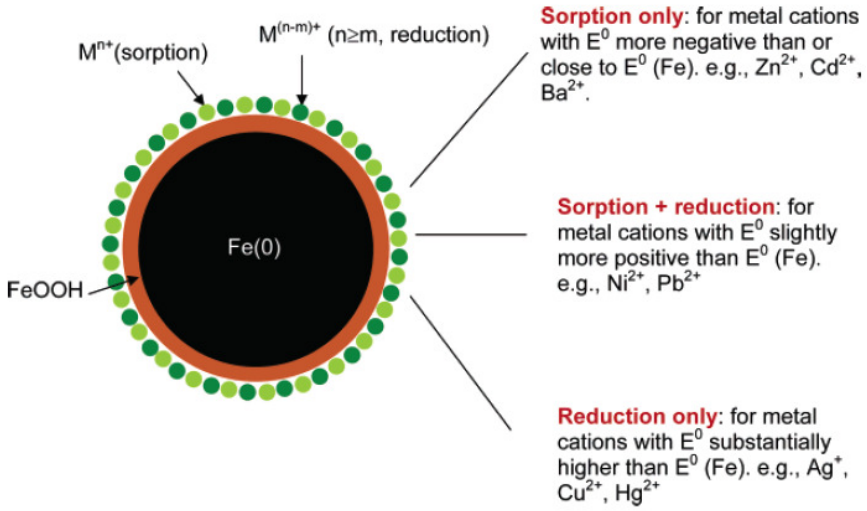

Figure 2 A conceptual model for metal removal with nZVI (Li and Zhang, 2007)

2.2.2 Reductive degradation of organic compounds

PHCs are in an oxidized state because of the presence of halogen (Cl, Br, and F). Iron is a strong reducing agent with a standard reduction potential of -0.44 volts (Hans Stroo, 2010). This makes ZVI a reducing agent relative to many redox-labile substances, including PHCs. There are three possible mechanisms for reductive removal of halogen from PHCs as indicated in Figure 3.

Pathway A: Direct reduction at the ZVI surface

Fe^0 provides electrons to the adsorbed halocarbon (RX) at the metal-water interface, which results in dehalogenation of halocarbon and production of Fe^{2+}.

$$Fe^0 + RX + H^+ \longrightarrow Fe^{2+} + RH + X^- \qquad \textbf{Equation 3}$$

Pathway B: Reduction by ferrous iron

Fe^{2+} resulting from corrosion of Fe^0 may dehalogenate RX, thereby producing Fe^{3+}.

$$Fe^{2+} \longrightarrow Fe^{3+} + e^- \qquad \textbf{Equation 4}$$

Pathway C: Reduction by hydrogen with catalysis

Hydrogen (H_2) formed in the anaerobic corrosion of Fe^{2+} might react with RX if an effective catalyst is present (e.g., Pd).

$$Fe^0 + 2H_2O \longrightarrow Fe^{2+} + H_2 + 2OH^- \qquad \textbf{Equation 5}$$

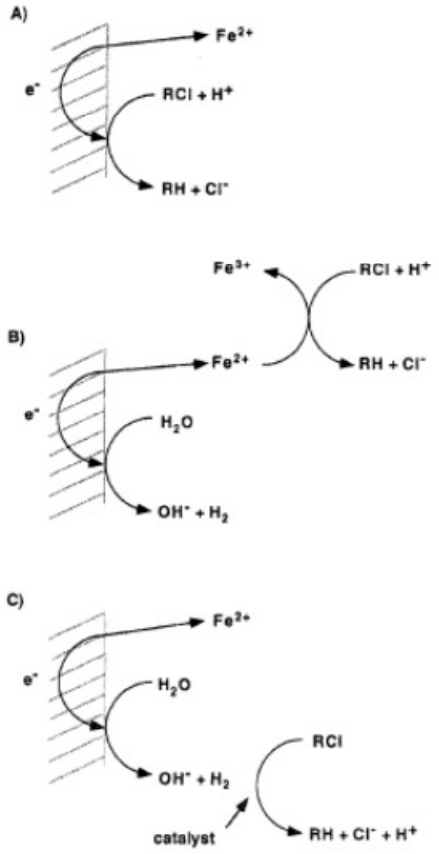

Figure 3 Schematic of possible pathways for the reductive degradation of halocarbon (Matheson and Tratnyek, 1994)

Since our study focuses on the reductive dehalogenation of PHCs, **Table 3** provides a summary of major bimetallic particle mediated reductive dehalogenation in the literature.

Table 3 Bimetallic particles mediated reductive dehalogenation of PHCs

Ref #	Citation	Materials	Scale	Particle Loading	Target Compound(s)	Results
1	(Grittini et al., 1995)	Pd/Fe	<10 µm	400 g/L	PCBs (Polychlorinated Biphenyls)	All PCB congeners in Aroclor 1260 and Aroclor 1254 were dechlorinated in approximately 5-10 min by reacting a methanol/water/acetone solution (1:3:1 volume ratio) with a 0.05% w/w Pd/Fe bimetallic system. The only reaction products were biphenyl and chloride ions.
2	(Liu et al., 2001)	Pd/Fe	>200 mesh(74µm); 0.25-1.5 m^2/g	<333 g/L	2-chlorophenol; 3-chlorophenol; 4-chlorophenol	Almost complete dechlorination was achieved within 5 h by pseudo-first-order reaction. The reduction product for all the three isomers was phenol. For conditions with 0.048% Pd/Fe, the rate constants were 0.0215, 0.0155 and 0.0112 min^{-1} for o-, m-, p-chlorophenol, respectively.
3	(Xu et al., 2005c)(a)	Pd/Fe	>200 mesh (74µm); 0.62 m^2/g	53.5 g/L	1,2-Dichlorobenzene	A pseudo-first-order reduction reaction regarding the *o*-DCB removal efficiency; reaction rate constants (*k*) were determined as 0.0032, 0.0092, 0.0237 and 0.0610 min^{-1}, for particles with Pd/Fe weight ratio of 0.002, 0.005, 0.020 and 0.026%, respectively.
4	(Xu et al., 2005b)(b)	Pd/Fe	>200 mesh (74µm); 0.62 m2/g	53.5 g/L	1,2-Dichlorobenzene; 1,3- Dichlorobenzene; 1,4- Dichlorobenzene	The dechlorination reaction took place via a pseudo-first-order kinetics, and resulted in benzene as the final reduction product. The reaction rate constant for o-, m- and p-DCBs in the presence of 0.020% (w/w) Pd/Fe at 25 °C was determined to be 0.0213, 0.0223, and 0.0254 min−1, respectively. The order of the tendency of the dechlorination was p-DCB > m-DCB > o-DCB.
5	(Xu et al., 2006)	Pd/Fe	>200 mesh (74µm); 0.62 m2/g	40 g/L	1,4-Chloronitrobenzene	100% of p-NCB was removed in 30 min with Pd/Fe particles with 0.03% Pd coating. p-NCB removal efficiency and the subsequent dechlorination rate increased with the increase of bulk loading of palladium and the increase of temperature as well. No other intermediates were generated besides Cl^-, p-chloroaniline and aniline.
6	(Zhu and Lim, 2007)	Pd/Fe	nanoscale	0.71 g/L	1,2,4-trichlorobenzene; 1,2-Dichlorobenzene; 1,3- Dichlorobenzene; 1,4- Dichlorobenzene;	Chlorinated benzenes could be completely reduced by the Pd/Fe to benzene and the reaction followed the pseudo-first-order kinetics within an hour. The reaction rates followed the order TCB < DCBs < MCB, while among

Ref #	Citation	Materials	Scale	Particle Loading	Target Compound(s)	Results
					chlorobenzene	the DCBs the order was 1,4-dichlorobenzene > 1,3-dichlorobenzene ≥ 1,2-dichlorobenzene.
7	(Ghauch and Tuqan, 2009)	Pd/Fe; Ru/Fe; Ag/Fe	325 mesh (44 μm)	40 g/L	2,2′-methylenebis(4-chlorophenol) (DCP)	(i) Total dechlorination with Pd/Fe, (ii) partial dechlorination (40%) with Fe/Ru, and no reaction with Fe/Ag. DCP vanished completely after 90 min of contact with Pd/Fe following a first order kinetic. The observed degradation rate k_{obs} was $(3.98 \pm 0.10) \times 10^{-2}$ min^{-1}, the calculated half-life $t_{1/2}$ about 17.4 ± 0.9 min and a t_{50} about 10.1 ± 0.5 min.
8	(Nagpal et al., 2010)	Pd/Fe	nanoscale	0.5 g/L	lindane (γ-hexachlorocyclohexane)	5 mg/L of lindane was completely dechlorinated within 5 min at a Pd/Fe loading of 0.5 g/L. The degradation process followed first-order kinetics. GC–MS analysis in corroboration with GC-ECD results showed the presence of cyclohexane as the final degradation product.
9	(Smuleac et al., 2011)	Pd/Fe on membrane	nanoscale	N/A	TCE (trichloroethylene)	Dechlorination of TCE was conducted by cutting PAA/PVDF membranes containing Fe or Fe/Pd nanoparticles into small pieces and immersing them in 20 mL sealed vials containing TCE (30 mg/L) solution. The surface normalized rate constant (*k*SA) of Pd/Fe was 0.008 L/m^2 h.
10	(Shih et al., 2011)	Pd/Fe	nanoscale	12.5 g/L	PCP (pentachlorophenol)	Freshly prepared Pd/Fe nanoparticles (12.5 g/L) were added to bottles containing 5 mg/L PCP in methanol – water (1: 200, v/v). The rate constant and degradation efficiency within 100 min of PCP by Pd/Fe nanoparticles were 0.083 min^{-1} and 97%.
11	(Schrick et al., 2002)	Ni/Fe	nanoscale	2.5 g/L	TCE (trichloroethylene)	Ni-Fe (0.1 g) nanoparticles reduced TCE from a 40-mL saturated aqueous solution (24 ppm) to <6 ppb in 120 min. The toxic dehalogenation products vinyl chloride (VC), 1,1-dichloroethylene (1,1-DCE), cis-dichloroethylene (cis-DCE), and trans-dichloroethylene (trans-DCE) formed only in trace amounts and did not persist.

Ref #	Citation	Materials	Scale	Particle Loading	Target Compound(s)	Results
12	(Xu et al., 2009)	Ni/Fe	nanoscale	6g/L	*p-NCB (para-*nitrochlorobenzene)	100% dechlorination efficiency was achieved for particles with 2.0% Ni at the Ni/Fe nanoparticles mass concentration of 6 g/L used after 300 min reaction. The *p*-NCB was quickly reduced to *p*-chloroaniline (*p*-CAN) and aniline (AN), and *p*-CAN was detected as an intermediate.
13	(Zhu et al., 2011)	Ni/Fe	nanoscale	2.5 g/L	PCBs (Polychlorinated Biphenyls)	Batch experiments showed that nanoscale Ni/Fe particles could more quickly and effectively dechlorinate PCBs stepwise as compared to nanoscale zerovalent iron (n-ZVI) and nano-Ni^0. The dechlorination products were much more centralized in the presence of Ni/Fe than other particles, and biphenyl, cyclohexyl-benzene and 1-alkyl-benzenes were the main products.
14	(Fennelly and Roberts, 1998)	Cu/Fe Ni/Fe	100 mesh (149 µm)	8g/L	1,1,1-TCA (1,1,1-trichloroethane)	1,1,1-TCA reacted with Ni/Fe at a significantly faster rate than with iron. As for Cu/Fe, a substantial increase in yield was observed for ethylene, while a decrease in 1,1-DCA (30 ± 1% yield) and cis-2-butene formation was obtained relative to Ni/Fe.
15	(Elsner et al., 2007)	Cu/Fe	100 mesh (149 µm)	8g/L	1,1,2,2-TeCA (1,1,2,2-tetrachloroethane)	In reactions of 1,1,2,2-TeCA with Cr(II) and Fe(0), cis-DCE and trans-DCE were formed in a relatively consistent proportion of about 2.5, whereas in the reaction with Cu/Fe the ratio was 3.5 to 4.0. The results showed that a high cis- to trans-DCE product ratio was not necessarily characteristic of an Fe(0) surface-catalyzed reaction but, in this case, appeared to result from the presence of Cu as an additional metal at the granular iron surface.
16	(Yuan et al., 2010b)	Cu/Fe	<100 mesh (149 µm)	40g/L	Various polychlorinated benzenes	Results showed that the reduction rates of CBs increased with the increase in chlorination. The rate constants were closely correlated to their lowest unoccupied molecular orbital (LUMO) energies and logarithmic octanol – water partition coefficients (Log K_{ow}). Lower LUMO energy and larger Log K_{ow} value led to higher rate constant.

Ref #	Citation	Materials	Scale	Particle Loading	Target Compound(s)	Results
17	(Zhu et al., 2010)	Cu/Fe	nanoscale	40g/L	HCB (hexachlorobenzene)	Near complete reduction of HCB was obtained by nanoscale Cu/Fe for 48 h treatment. HCB was quickly dechlorinated to PeCB, TeCBs, TCBs and DCBs without selectivity via a stepwise process. The reduction rate and dechlorination extent were much higher compared with microscale Cu/Fe.
18	(Xu and Zhang, 2000)	Ag/Fe	<0.1 µm	25g/L	HCB (hexachlorobenzene)	Hexachlorobenzene (HCB) (4 mg/L) was dechlorinated to tetra-, tri-, and dichlorobenzenes (TeCB, TCB, and DCB, respectively) within 24 h at a metal loading of 25 g/L. Principal degradation products included 1,2,4,5-TeCB, 1,2,4-TCB, and 1,4-DCB. The rate of dechlorination was positively correlated to the silver loading of the bimetallic particles.
19	(Wu et al., 2006)	Ag/Fe	microscale	N/A	CF(trichloromethane), CT tetrachloromethane, 1, 1, 1-TCA (1, 1,1-trichloroethane), 1,1,2,2-TeCA (1,1,2,2-tetrachloroethane), HCA(hexachloroethane), TCE (trichloroethylene), (PCE) perchloroethylene.	Results show that the existence of Ag on Fe can enhance the dechlorination rate of chlorinated hydrocarbons. The dechlorination rate constant of CF, CT, 1, 1, 1-TCA, 1, 1, 2, 2-TeCA, HCA, TCE, PCE were up to 1.850 h(-1), 9.504 h(-1), 1.624 h(-1), 1.778 h(-1), 2.842 h(-1), 0.463 h(-1), 1.251 h(-1) by Ag/Fe.
20	(Luo et al., 2010)	Ag/Fe	nanoscale	0.4g/L	TBBPA (Tetrabromobisphenol A)	Batch studies demonstrated that the TBBPA (2 mg/L) was completely degraded in 20 min over Ag/Fe nanoparticles, which had higher degradation efficiency than Fe^0 nanoparticles under ultrasonic radiation. The major intermediates identified by LC – MS technique were tri-BBPA, di-BBPA, mono-BBPA and BPA.

2.3 ZVI applications

2.3.1 Permeable Reactive Barrier

The primary application of ZVI-catalyzed degradation is its use in permeable reactive barriers (PRBs, Figure 4) in order to decontaminate groundwater. There are many advantages of using passive reactive barriers compared to existing *exsitu* treatment technology. First, the *insitu* approach requires no above-ground treatment facilities and the space can be returned to its original use. Second, at chlorinated solvent–contaminated sites, a passive technology that requires almost no annual energy or labor input (except for site monitoring) has obvious advantages over conventional groundwater treatment systems (Interstate Technology & Regulatory Council, 1999a). There is no need for expensive above-ground treatment, storage, transport, or disposal. In fact, the economic benefits of permeable reactive barriers have been driving the interest in the technology. Third, although the installation of a PRB requires a higher initial capital investment, there are little or no operation and maintenance costs. After construction, PRB technology fits the concept of green and sustainable technology (Interstate Technology & Regulatory Council, 2011b). Since the first implementation in the early 1990s, more than 200 PRB systems have been installed in different parts of the world (Interstate Technology & Regulatory Council, 2011b). However, it is worth pointing out that not all PRBs are made with ZVI, and not all environmental applications of ZVI involve PRBs (Figure 5).

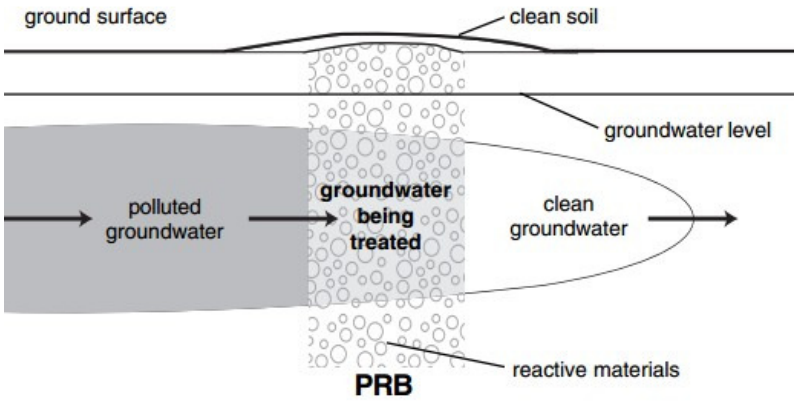

Figure 4 Permeable reactive barrier for groundwater plume remediation (USEPA, 2001)

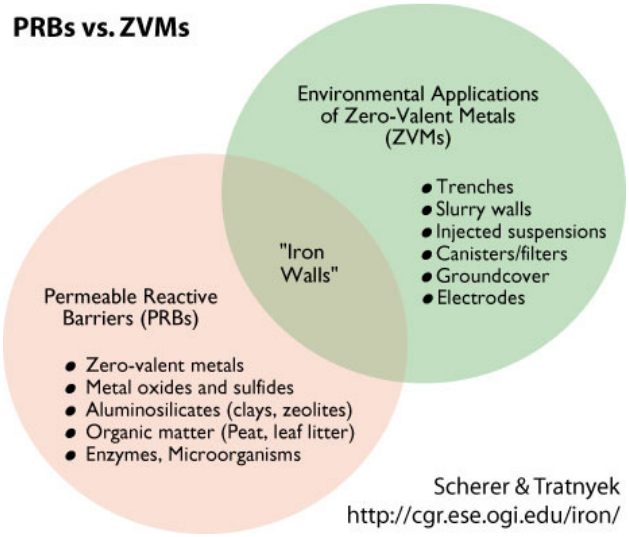

Figure 5 PRBs and zero-valent metals

One major issue associated with the application of PRBs in groundwater remediation is longevity. Longevity refers to the ability of a PRB to sustain its functions (hydraulic capture, residence time, and reactivity) in the years and decades following installation (Klausen et al., 2003). A number of native dissolved constituents in groundwater have the potential to reduce the hydraulic and reactive performance of PRBs over time through a variety of processes that may include corrosion, precipitation, gas production, and microbial metabolism (Interstate Technology &

Regulatory Council, 2011b). The resulting surface passivation and/or pore-space reduction in the ZVI media leads to the gradual loss of performance seen in some laboratory and field PRB systems (Kohn et al., 2005). The degree and speed with which these processes have affected the long-term field performance of ZVI PRBs are varied (Interstate Technology & Regulatory Council, 2011b). Calcium, carbonate, sulfate, and silicate are common groundwater constituents that precipitate out on ZVI surfaces, while nitrate and dissolved oxygen oxidize the reactive iron surface. Both processes lead to gradual loss of performance (Interstate Technology & Regulatory Council, 2011b). Therefore, differences in groundwater chemistry should be considered in the PRB design process.

2.3.2 *Insitu* injection methods

When field conditions make installation of conventional PRBs impossible (e.g., existing buildings or utilities), or contaminant depth requires deeper depths than can be cost-effectively achieved with trenching, *insitu* injection methods (Figure 6) are preferable to conventional PRBs. (USEPA, 2008). Advantages of injection borings include the following (Interstate Technology & Regulatory Council, 2011b):

- flexibility in their placement, including a single line of injection wells (similar to a traditional passive reactive barrier), multiple treatment lines, or a grid pattern
- the ability to install borings deeper than 100 feet, which is much deeper than possible using conventional trenching techniques
- the ability to address specific vertical contaminated intervals without excavation of overlying materials
- suitability for emplacement in urban settings, where surface structures and underground utilities may make surface trenching impractical

- less soil spoils generated—generally <0.5% of the volume of spoils generated during trenching construction.

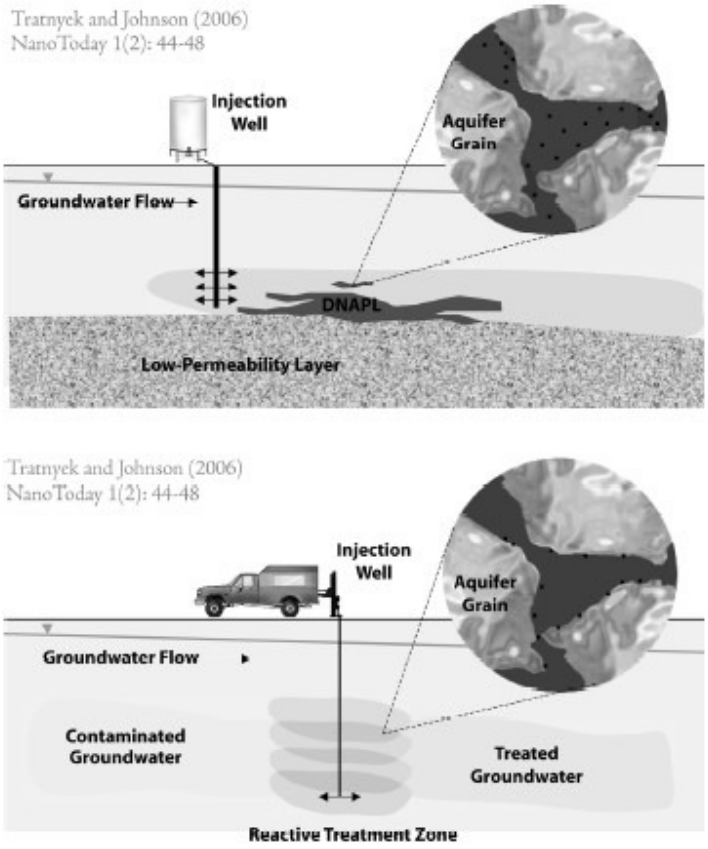

Figure 6 Schematic of two methods of groundwater remediation using *insitu* injection (Tratnyek and Johnson, 2006)

Also, *insitu* injection methods are the most direct route for *insitu* application of nanoscale ZVIs. Field tests have been conducted by researchers to test the effectiveness of target contaminant removal by nanoscale ZVIs (Bennett et al., 2010; He et al., 2010; Mueller et al., 2012; Phenrat et al., 2011; Taghavy et al., 2010; Yang et al., 2008).

However, the efficiency of nanoscale ZVI degradation process is substantially hindered by the rapid aggregation of the iron nanoparticles (Tratnyek and Johnson, 2006). Nanoscale zero-valent

iron particles are attracted to one another, which can cause them to agglomerate into larger micron-sized particles (Phenrat et al., 2007). Bennett found that after 13 hours in the aquifer, the nanoscale ZVI particles became essentially immobilized (Bennett et al., 2010). Agglomeration also reduces the exposed reactive surface area of the particles. The pH of the subsurface may also limit the effectiveness of nanoparticles because the sorption strength, agglomeration, and mobility of the particles are all affected by the pH of the groundwater (USEPA, 2007).

Passivation is another factor that may limit the effectiveness of iron nanoparticles (USEPA, 2008). If nanoscale ZVI is being used, improper handling can result in the iron becoming oxidized and passivated prior to reacting with the contaminants. As a rule, injection mechanisms should limit the volume of water injected along with the iron, to limit exposure to oxygen and other oxidants that could passivate the iron before and during injection (USEPA, 2008).

2.4 **Synthesis of ZVI based bimetallic particles**

- Pd/Fe bimetallic particles

One popular method for preparation of Pd/Fe particles is adding K_2PdCl_6 (potassium hexachloropalladate) water solution to dilute HCl washed iron particles (Muftikian et al., 1995). This synthesis method was employed by many other research groups with a little modification (Grittini et al., 1995; Liu et al., 2001; Morales et al., 2002b). Pd was coated on the iron particles as Pd^0.

$$2Fe^0 + PdCl_6^{2-} \rightarrow 2Fe^{2+} + Pd^0 + 6Cl^- \qquad \textbf{Equation 6}$$

In 1997, Wang and Zhang (1997) developed a recipe for synthesizing nanoscale iron particles and a new method for coating palladium on iron particles, which later gained popularity among many groups (Feng and Lim, 2005; He and Zhao, 2005). Borohydride reduction involves adding a

strong reductant into a metallic ion solution to reduce it to nanoscale metal particles. The most commonly used reductant is $NaBH_4$. Successful use of both ferric chloride ($FeCl_3.6H_2O$) and ferrous sulfate ($FeSO_4.7H_2O$) as the aqueous-phase iron solution has been reported (Li et al., 2006a). The reaction is described by the following equation.

$$Fe(H_2O)_6^{3+} + 3BH_4^- + 3H_2O \rightarrow Fe^0 \downarrow + 3B(OH)_3 + 10.5H_2 \qquad \textbf{Equation 7}$$

The freshly prepared nano iron particles were then saturated with an ethanol solution of $[Pd(C_2H_3O_2)_2]_3$, and Pd was reduced and deposited on the iron surface through the following reaction.

$$Pd^{2+} + Fe^0 \rightarrow Pd^0 \downarrow + Fe^{2+} \qquad \textbf{Equation 8}$$

- Other ZVI based bimetallic particles

The preparation methods of other ZVI based bimetallic particles are similar, usually involving the reductive deposition of a second metal (Pt, Cu, Ag, Ru, Au, Co, Cu, Pd) on the processed surface (either freshly prepared or cleaned after multiple solvents) of the ZVI (microscale and nanoscale). Chemicals containing the second metal are usually the salts of the metal (e.g., $AgSO_4$, $CuCl_2$) or acetate (e.g., $[Pd(C_2H_3O_2)_2]_3$).

2.5 **Summary**

The literature review presented above has shown that zero valent iron is an effective material for groundwater remediation because of its intrinsic reductive property, its low cost and high effectiveness. It has been used as the active medium in permeable reactive barriers and demonstrated promising field performance results.

The reductive dehalogenation ability of zero valent iron is well documented. Besides organic contaminants, zero valent iron is able to transform inorganic contaminants, including hexavalent chromium, selenium, technetium, uranium and many cationic metals.

The application of nZVI, however, faces major problems – the particles lose reactivity very quickly due to rapid aggregation and passivation. Increased reaction rates and less formation of intermediates can be achieved by modifying zero valent iron through reductive deposition of a second noble metal (so called bimetallic particles).

3 Chapter 3 Methodology

In order to both examine the reactivity of different bimetallic particles and to gain insight into the underlying mechanism(s) of reaction, a series of experiments have been undertaken over a range of different conditions. The reagents and chemicals used in these studies are described in this chapter, as are details of experimental setup and analytical techniques.

3.1 Chemicals and reagents

All chemicals were reagent grade and used as received without further treatment (Table 4). Stock solutions were prepared by dissolution of the received chemicals to the specified concentration. Glassware and plasticware was soaked in dilute detergent solution overnight, then rinsed 3 times with tap water, 3 times with distilled water and 3 times with Milli-Q water prior to use. After preparation, all stock solutions were stored in the refrigerator.

Table 4 Received chemicals

Manufacturer	Chemical
Alfa Aesar, Ward Hill, MA	Iron powder, spherical, <10 micron, 99.9+%
Alfa Aesar	1,2,4-Tribromobenzene, 95%; 1,2-Dibromobenzene, 98% ; 1,3-Dibromobenzene, 97+%; 1,4-Dibromobenzene, 98% ; Bromobenzene, 99%
Alfa Aesar	1,2,4-Trichlorobenzene, 98+%; 1,2-Dichlorobenzene, 98%; 1,3-Dichlorobenzene, 98%; 1,4-Dichlorobenzene, 98%; Chlorobenzene, 98%
Alfa Aesar	1,2,4-Trifluorobenzene, 98+% ; 1,2-Difluorobenzene, 98+%; 1,3-Difluorobenzene, 99% ; 1,4-Difluorobenzene, 99%; Fluorobenzene, 99%
Alfa Aesar	Palladium (II) Acetate, trimer,99.98% (metals basis), Pd 47% min
Sigma, St. Louis, MO	Tetrabromobisphenol A, 98+%; Bisphenol A, 98+%
Sigma	Hexane, Acetone, Methanol, HPLC grade
Sigma	KCl, KH_2PO_4, K_2HPO_4, 98+%
Sigma	$NiCl_2$, $CuCl_2$, $AgNO_3$, 98+%

3.2 **Solution phase synthesis of ZVI based bimetallic particles**

Zero valent iron based bimetallic particles were synthesized in an anaerobic chamber filled with hydrogen (0.5%) and nitrogen (99.5%), following a procedure described in Fennelly and Roberts (1998), Wang and Zhang (1997) and Wang et al. (2010) with modification (Figure 7). Prior to reductive deposition of the second metal, surfaces of the zero-valent iron particles were cleaned with 0.4M hydrochloric acid for 2 minutes to remove any surface oxides present. The acid-washed iron was rinsed 3 times with deoxygenated Milli-Q water, and once with acetone. Then a dilute acetone solution of $C_4H_6O_4Pd$, $NiCl_2$, $CuCl_2$ or $AgNO_3$ was added to the acid-washed iron with agitating. This caused the reduction and subsequent deposition of the second metal on the Fe surface through the following reaction:

$$Pd^{2+} + Fe^{0} \longrightarrow Pd^{0} + Fe^{2+} \qquad \textbf{Equation 9}$$

$$Ni^{2+} + Fe^{0} \longrightarrow Ni^{0} + Fe^{2+} \qquad \textbf{Equation 10}$$

$$Cu^{2+} + Fe^{0} \longrightarrow Cu^{0} + Fe^{2+} \qquad \textbf{Equation 11}$$

$$2Ag^{+} + Fe^{0} \longrightarrow 2Ag^{0} + Fe^{2+} \qquad \textbf{Equation 12}$$

Once the acetone solution containing the second metal had been added, the mixture was agitated for an additional 20 minutes until the color of the solution became clear. The mixture was then rinsed with deoxygenated Milli-Q water. After depositing and rinsing, the metals were removed from the anaerobic chamber and freeze-dried with a Labconco® FreeZone vacuum freeze dry system. The bimetallic particles were dark gray in color with no visual evidence of oxide formation. For palladium, three different amounts of palladium acetate were added. For nickel, copper and silver, two different amounts of each metal salt were added. Assuming all of the catalytic metal was reductively precipitated onto the iron base metal, the content of the Pd in the bimetallic reductant was calculated as 0.011 %, 0.022 % and 0.044 % (wt/wt). The content of

nickel, copper and silver was calculated as 0.1% and 1% (wt/wt). Iron particles with 0% metal loading was also made following the same procedure. Freeze-dried particles were placed in PTFE-sealed screw cap glass vials and stored in the refrigerator.

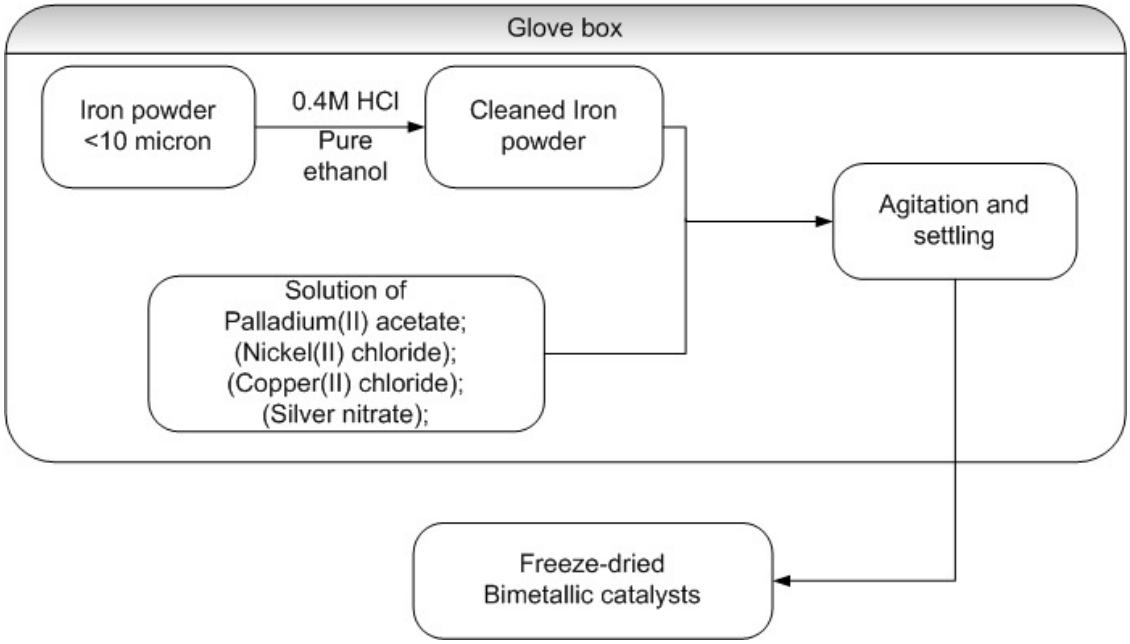

Figure 7 Solution phase synthesis of ZVI based bimetallic particles

3.3 ZVI based bimetallic particles characterization

3.3.1 Brunauer, Emmett, and Teller (BET) surface area analysis

Surface area is an important parameter for particle characterization. A Micromeritics ASAP 2020M Surface Area and Porosimetry System (Norcross, GA) was used to determine the surface area of untreated zero valent iron particles as well as synthesized bimetallic particles. The instrument provided single point, BET (Brunauer-Emmet-Teller) and Langmuir surface area at the same time. However, since most surface area normalized reaction rate constants reported in

the literature are based on the BET surface area, our reaction rate constants are also normalized to the BET surface area.

3.3.2 Scanning electron microscopy analysis

Scanning electron microscope (SEM) images were obtained through a FEI QUANTA 400 (Hillsboro, OR) microscope. SEM images can reveal information about the sample including external morphology (texture), chemical composition, and crystalline structure and orientation of materials making up the sample.

3.3.3 X-ray photoelectron spectroscopy analysis

X-ray photoelectron spectroscopy (XPS) analysis was performed using a PHI 5600 XPS (Bend, OR) system, with a magnesium anode X-ray source operated at a power of 300 W. XPS is a surface analysis technique with a sampling volume that extends from the surface to a depth of approximately 50-70 Angstroms (Wagner et al., 1979). XPS analysis can determine quantitative atomic composition and chemistry of the particles tested.

3.4 Batch degradation study

3.4.1 1, 2, 4-Trichlorobenzene, dichlorobenzenes and chlorobenzene

Batch experiments for dechlorination of 1,2,4-trichlorobenzene (TCB) with untreated iron particles and bimetallic particles (Pd/Fe, Ni/Fe, Cu/Fe and Ag/Fe) were conducted in 20 mL serum glass bottles (Figure 8). In each serum bottle, 0.05 gram bimetallic particles were added to 10 mL buffer solution (0.1M NaCl+ KH_2PO_4 + K_2HPO_4, pH= 7.2) spiked with TCB stock solution. The initial concentration of TCB was 2 ppm, or 11 µmol/L. The serum bottles were sealed with Teflon-lined silicon septa and aluminum cap, placed in a cardboard box and put on a G10 Gyrotory (Enfield, CT) shaker at 120 rpm throughout the duration of the experiment. Control

experiments without any particles were also performed. Table 5 lists basic property data for 1,2,4-TCB, DCBs, MCB and benzene.

Table 5 Basic property data for 1,2,4-TCB, DCBs, MCB and Benzene at 25°C *

Chemical	Molecular weight	Structure	Water solubility (mg/L)	Log K_{OW} (octanol-water)	Henry's law coefficient (atm-m^3/mole)
1,2,4-trichlorobenzene	181	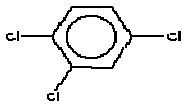	49	4.02	0.00142
1,2-dichlorobenzene	147	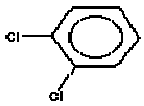	156	3.43	0.00192
1,3-dichlorobenzene	147	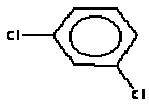	125	3.53	0.00263
1,4-dichlorobenzene	147		81.3	3.44	0.00241
chlorobenzene	113	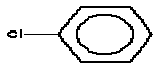	498	2.84	0.00311
benzene	78		1790	2.13	0.00555

*Data from SRC Physprop database (SRC, 2012)

Reaction time was recorded from the start of mixing. At designated times, triplicate reactors were taken out from the shaker, and 5 mL hexane containing p-xylene as surrogate standard was added immediately to each reactor by a glass syringe through the septum. The reactors were then placed back on the shaker for 10 minutes to extract the reactant and the products from both the aqueous and the solid phases. After mixing, the reactors were centrifuged (Beckman Coulter® Allegra

25R, Danvers MA) at 3000 rpm for 3 minutes, and 1 mL of the hexane solution was transferred immediately from each reactor to a gas chromatography (GC) vial using a disposable volumetric pipette. Internal standard (n-pentadecane) was added to the GC vials right before analysis on the GC-mass spectrometer (MS). Preliminary tests showed that the extraction efficiencies for the target chemicals exceeded 90%.

Batch experiments for dechlorination of dichlorobenzenes (1,2-dichlorobenzene;1,3-dichlorobenzene and 1,4-dichlorobenzene) and monochlorobenzene with Pd/Fe bimetallic particles were also conducted. The same standard operating procedure was followed as described above. The initial concentration of dichlorobenzenes and monochlorobenzene was 10 µmol/L.

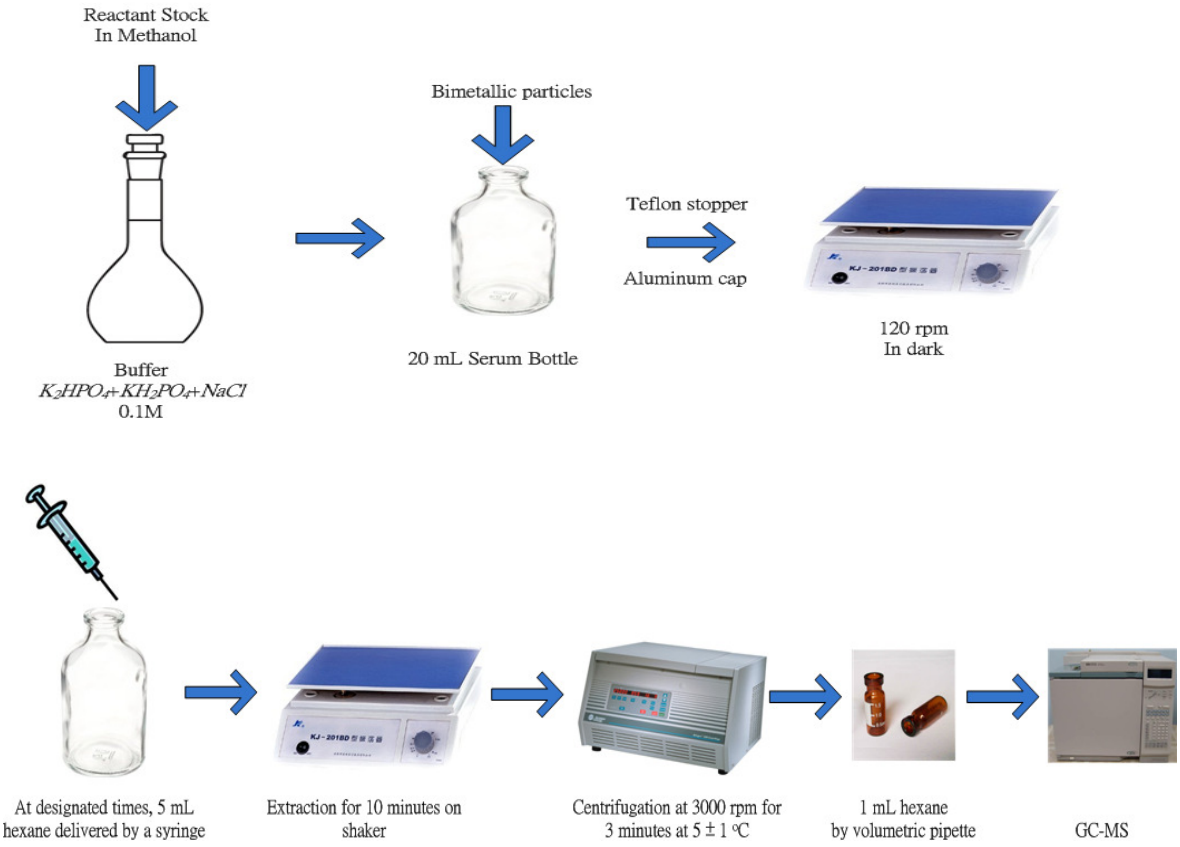

Figure 8 Major steps of batch degradation study for halogenated benzenes

3.4.2 1, 2, 4-Tribromobenzene, dibromobenzenes and bromobenzene

Batch experiments for debromination of 1,2,4-tribromobenzene (TBB) with untreated iron particles and bimetallic particles (Pd/Fe, Ni/Fe, Cu/Fe and Ag/Fe) were conducted in the same way. Table 6 lists basic property data for 1,2,4-TBB, DBBs and MBB.

Table 6 Basic property data for 1,2,4-TBB, DBBs and MBB at 25°C *

Chemical	Molecular weight	Structure	Water solubility (mg/L)	Log K_{OW} (octanol-water)	Henry's law coefficient (atm-m^3/mole)
1,2,4-tribromobenzene	315	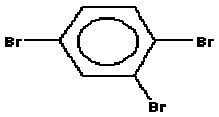	4.9	4.66	0.000341
1,2-dibromobenzene	236	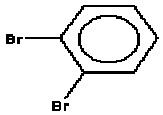	74.6	3.64	0.000855
1,3-dibromobenzene	236	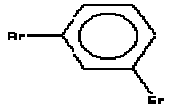	67.5	3.75	0.00124
1,4-dibromobenzene	236	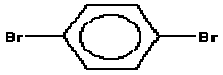	20	3.79	0.000893
Bromobenzene	157	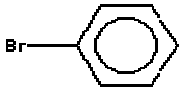	446	2.99	0.00247

*Data from SRC Physprop database (SRC, 2012)

Batch experiments for dechlorination of dibromobenzenes (1,2-dibromobenzene;1,3-dibromobenzene and 1,4-dibromobenzene) and monobromobenzene with Pd/Fe bimetallic particles were also conducted. The same standard operating procedure was followed as described above. The initial concentration of dibromobenzenes and monobromobenzene was 10 μmol/L.

3.4.3 1, 2, 4-Trifluorobenzene

Batch experiments for dehalogenation of 1,2,4-trifluorobenzene (TFB) with untreated iron particles and Pd/Fe bimetallic particles were conducted in the same way. The initial concentration of TFB was 10 µmol/L. Table 7 lists basic property data for 1,2,4-TFB, DFBs and MFB.

Table 7 Basic property data for 1,2,4-TFB, DFBs and MFB at 25°C *

Chemical	Molecular weight	Structure	Water solubility (mg/L)	Log K_{OW} (octanol-water)	Henry's law coefficient (atm-m^3/mole)
1,2,4-trifluorobenene	132	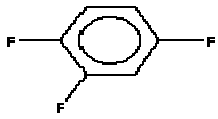	636	2.52	0.00856
1,2-difluorobenene	114	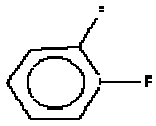	1140	2.37	0.00734
1,3-difluorobenene	114	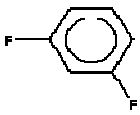	1140	2.21	0.00734
1,4-difluorobenene	114		1220	2.13	0.00734
Fluorobenzene	96	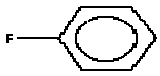	1540	2.27	0.00625

*Data from SRC Physprop database (SRC, 2012)

3.4.4 Tetrabromobisphenol A

The rates of TBBPA (Table 8) transformation in the presence of Pd/Fe bimetallic particles were measured at 25°C under anoxic and different pH conditions. Glass vials with Teflon lined caps were used as reactors. Each reactor contained a predetermined amount of Pd/Fe bimetallic

particles and 5 mL reaction solution with an initial TBBPA concentration of 27.6 μmol L^{-1}. The reaction solution was prepared in an anaerobic chamber by dissolving a predetermined amount of neat TBBPA in methanol, followed by dilution with 0.1 M phosphate buffer solution that contained 30% methanol by volume. The reactors were then placed on a shaker preset at 200 rpm (Figure 9).

Table 8 Basic property data for TBBPA and BPA at 25°C*

Chemical	Molecular weight	Structure	Water solubility (mg/L)	Log K_{OW} (octanol-water)	pKa Dissociation Constant
Tetrabromobisphenol A	544	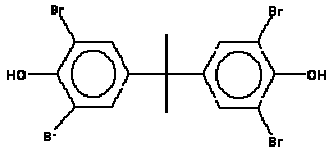	0.001	7.20	9.40 (ACCBFRIP, 2004)
Bisphenol A	228	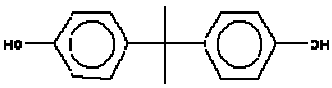	120	3.32	9.59-11.30 (Cousins et al., 2002)

* Data from SRC Physprop database (SRC, 2012)

Three sets of experiments were conducted to examine the effects of Pd coverage, particle dosage, and solution pH on reaction rates (Table 9). The first set of tests was conducted at pH 7.2 and a solids dosage of 4 g L^{-1} Pd/Fe bimetallic particles with Pd coverage of 0, 0.011, 0.022, and 0.044 wt%. The second set of tests was conducted at pH 7.2 and solids dosages of 2, 3 and 4 g L^{-1} Pd/Fe bimetallic particles with 0.022 wt% Pd coverage. The third set of tests was performed at four different pH values (4.2, 5.2, 6.2 and 7.2) and a solids dosage of 4 g L^{-1} Pd/Fe bimetallic particles with 0.022 wt% Pd coverage. The solution pH was buffered by KH_2PO_4 and K_2HPO_4 and adjusted by dilute hydrochloric acid. At each designated time, triplicate reactors were removed from the shaker and centrifuged at 4000 rpm for 5 min at 5 ± 1 °C. The lower

temperature was set to quench the reaction as the expected reaction rate was substantially lower. After centrifugation, the supernatant was sampled from each reactor and analyzed by HPLC for the concentrations of TBBPA, intermediate and final products.

Table 9 TBBPA experimental sets

Experiment set	pH	Pd/Fe dosage (g/L)	Pd coverage on Pd/Fe (wt%)
#1	7.2	4	0, 0.011, 0.022, 0.044
#2	7.2	2, 3, 4	0.022
#3	4.2, 5.2, 6.2 ,7.2	4	0.022

In all tests, control reactors containing no particles were run simultaneously. Results showed that the aqueous TBBPA concentrations in those control reactors after mixing for 24 hrs were within 98-102% of the initial concentrations, indicating no loss of the reactant from the solution phase.

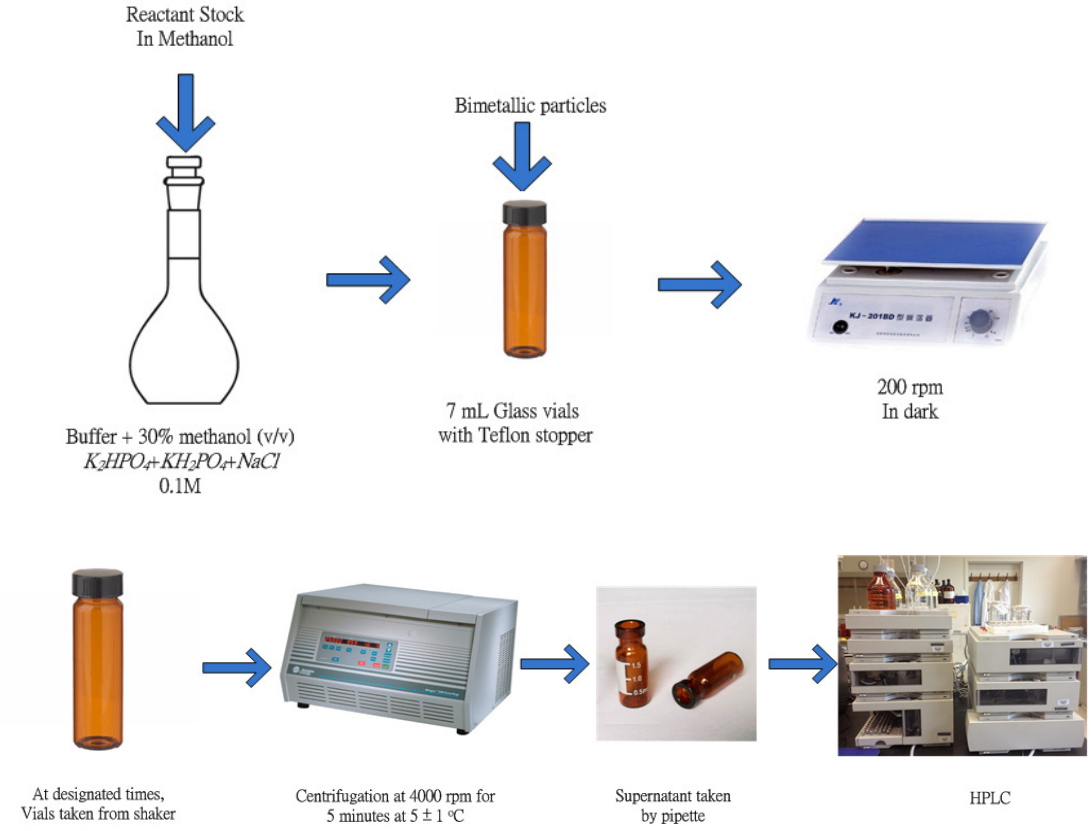

Figure 9 Major steps of batch degradation study for TBBPA/TCBPA

3.4.5 Tetrachlorobisphenol A

The rates of tetrachlorobisphenol A (TCBPA, Table 10) transformation in the presence of Pd/Fe bimetallic particles were measured at 25°C under anoxic conditions. Glass vials with Teflon lined caps were used as reactors. Each reactor contained a predetermined amount of Pd/Fe bimetallic particles and 5 mL reaction solution with an initial TCBPA concentration of 20 μmol L^{-1}. The reaction solution was prepared in an anaerobic chamber by dissolving a predetermined amount of neat TCBPA in methanol, followed by dilution with 0.1 M phosphate buffer solution which contained 30% methanol by volume. The reactors were then placed on a shaker preset at 200 rpm (Figure 9).

Table 10 Basic property data for TCBPA at 25°C*

Chemical	Molecular weight	Structure	Water solubility (mg/L)	Log K_{OW} (octanol -water)	pKa Dissociation Constant
Tetrachlorobisphenol A	366	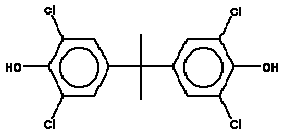	0.0916	6.22	N/A

* Data from SRC Physprop database (SRC, 2012)

Three sets of experiments were conducted to examine the effects of Pd coverage, particle dosage, and initial concentration on reaction rates (Table 11). The first set of tests was conducted at pH 4.0, solids dosages of 2, 3, 4 and 5 g L^{-1} Pd/Fe bimetallic particles with Pd coverage of 0.044 wt%, and 20 μmol L^{-1} initial concentrations of TCBPA. The second set of tests was conducted at pH 4.0, a solids dosage of 5 g L^{-1} Pd/Fe bimetallic particles with 0.044 wt% Pd coverage and 5, 10, 15, 20 and 25 μmol L^{-1} initial concentrations of TCBPA. The third set of tests was performed at pH 4.0, a solids dosage of 5 g L^{-1} Pd/Fe bimetallic particles with 0.0055, 0.011, 0.022 and 0.044 wt% Pd coverage and 20 μmol L^{-1} initial concentrations of TCBPA. The solution pH was

buffered by KH_2PO_4 and K_2HPO_4 and adjusted by dilute hydrochloric acid. At each designated time, triplicate reactors were removed from the shaker and centrifuged at 4000 rpm for 5 min at 5 ± 1 ^oC. The lower temperature was set to quench the reaction as the expected reaction rate was substantially lower. After centrifugation, the supernatant was sampled from each reactor and analyzed with HPLC for the concentrations of TCBPA, intermediate and final products.

Table 11 TCBPA experimental sets

Experiment set	Pd/Fe dosage (g/L)	Initial concentration of TCBPA (μM)	Pd coverage on Pd/Fe (wt%)	pH
#1	2, 3, 4, 5	20	0.044	4.0
#2	5	5, 10, 15, 20, 25	0.044	4.0
#3	5	20	0.0055, 0.011, 0.022	4.0

In all tests, control reactors containing no particles were run simultaneously. Results showed that the aqueous TCBPA concentrations in those control reactors after mixing for 24 hrs were within 98-102% of the initial concentrations, indicating no loss of the reactant from the solution phase.

3.5 **Method of analysis**

3.5.1 GC-MS

Analysis of all chlorobenzenes, bromobenzenes and fluorobenzenes were done on an Agilent® gas chromatograph 6890 (Santa Clara, CA) with a mass spectrometer detector 5973. The GC column used was a 60-meter DB-5 column (0.25 μm film thickness, 0.32 mm internal diameter) with Helium as the carrier gas. Injector temperature was set at 200°C (splitless mode). The temperature program of the gas chromatograph was as followed: start at 50°C for 2 minutes, ramp 8°C/min to 220ºC, then hold at 220°C for 5 minutes.

Quantification of each target chemical was performed using the internal standard method. This method eliminates errors due to variation in the sample injection, and is independent of the final extract volume (Totten, 2004). The internal standard used n-pentadecane, was added to each sample before GC analysis at a concentration similar to the sample components. Relative response factors relative to the internal standard (RRF) were calculated according to the following equation (Totten, 2004):

$$RRF = \left(\frac{Mass\ Chemical}{Area\ Chemical}\right)_{std} \div \left(\frac{Mass\ istd}{Area\ istd}\right)_{std} \qquad \textbf{Equation 13}$$

Target chemical concentrations were calculated from the average RRF and the internal standard response in the sample, by the following equations (Totten, 2004):

$$(mass\ chemical)_{sample} = (area\ chemical)_{sample} \quad X \quad RRF_{std} \quad X \quad \left(\frac{mass\ istd}{area\ istd}\right)_{sample} \qquad \textbf{Equation 14}$$

3.5.2 HPLC

All tetrabromobisphenol A (TBBPA) / tetrachlorobisphenol A (TCBPA) and its daughter products were measured by HPLC (Agilent® HPLC 1100 series) on a C18 reversed-phase column (250 x 2.0 mm, 5 μm). Both diode array detector (at 208 nm) and fluorescence detector (emission at 313 nm and excitation at 275 nm) were used. The mobile phase was a methanol/water (73:27 (v/v)) mixture at a flowrate of 0.34 mL min^{-1}. The water phase contained 0.1% (v/v) glacial acetic acid. The injection volume was 20 μL.

External standards of seven concentration levels ranging from 0.3 to 30 μmol L^{-1} were used for quantification of TBBPA/TCBPA and BPA. The retention times were 3.18, 3.87, 5.16, 7.31 and 10.88 min for BPA, mono-BBPA, di-BBPA, tri-BBPA and TBBPA, respectively. The retention times were 3.75, 4.18, 5.60, 8.05 and 11.57 min for BPA, mono-CBPA, di-CBPA, tri-CBPA and TCBPA, respectively. Since there are no commercially available standards for mono-BBPA/mono-CBPA, di-BBPA/di-CBPA and tri-BBPA/tri-CBPA, their aqueous phase

concentrations were estimated from their peak areas of the chromatogram based on the standard curves of TBBPA/TCBPA and BPA on a molar basis with compensation for the number of bromine/chlorine atoms.

4 Chapter 4 Results and Discussion

4.1 Characterization of bimetallic particles

4.1.1 Surface area analysis

Table 12 lists the surfaces areas of untreated iron and four bimetallic particles. Assuming a spherical particle of iron powder (mean diameter = *D*, in the unit of μm), the surface area per unit mass (m^2/g) is calculated to be 0.762/*D* (Liao et al., 2003), based on a specific iron density of 7.87 g/cm^3 (Alfa Aesar). In other words, the specific surface area is proportional to 1/*D*. In the case of an Fe^0 size of 10 μm, the surface area is approximately 0.0762 m^2/g. The iron particles we purchased were less than 10 μm in diameter. Theoretically our particles are expected to have a surface area larger than 0.0762 m^2/g. However, BET surface areas of five tested particles were in the range of 0.0159 to 0.2256 m^2/g. This indicates that our particles were not uniform in size.

Table 12 Surface areas of bimetallic particles and commercial iron particles

Particles	Single point Surface area (m^2/g)	BET Surface area (m^2/g)	Langmuir Surface Area(m^2/g)
Commercial iron particles (<10μm)	0.0255	0.0216	0.0242
Pd/Fe	0.2314	0.2256	0.3192
Ni/Fe	0.0494	0.0451	0.0548
Cu/Fe	0.1014	0.0720	0.0794
Ag/Fe	0.0176	0.0159	0.0185

4.1.2 Scanning electron microscopy analysis

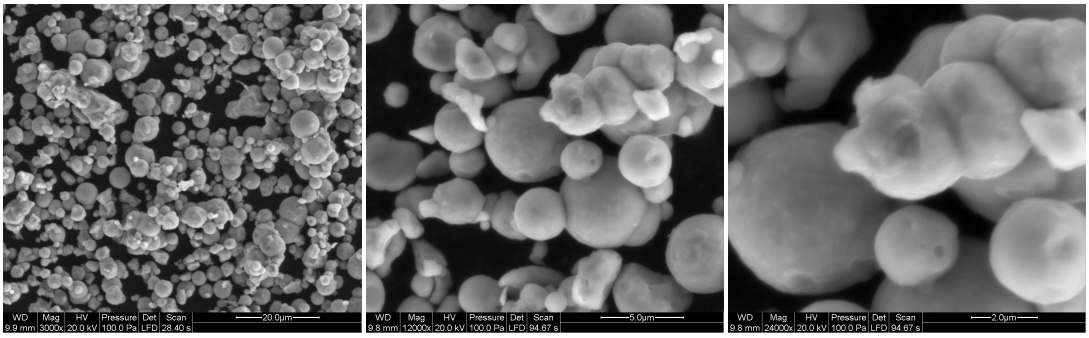

Figure 10 Pd/Fe SEM images, from left to right: 20 µm, 5 µm and 2 µm

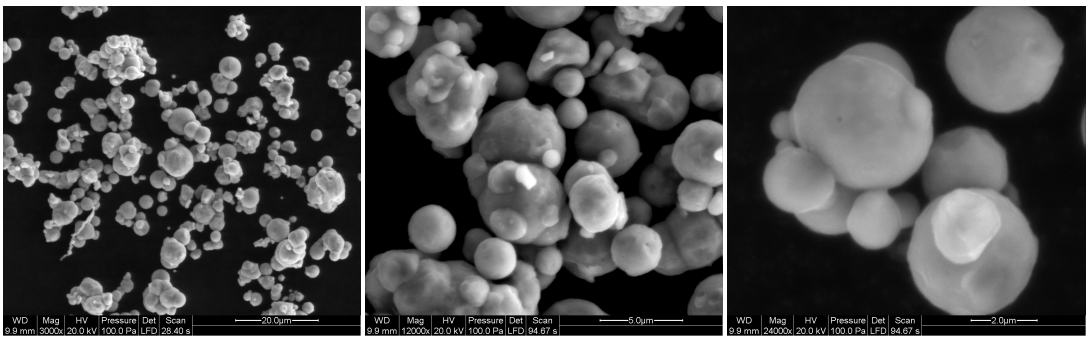

Figure 11 Ni/Fe SEM images, from left to right: 20 µm, 5 µm and 2 µm

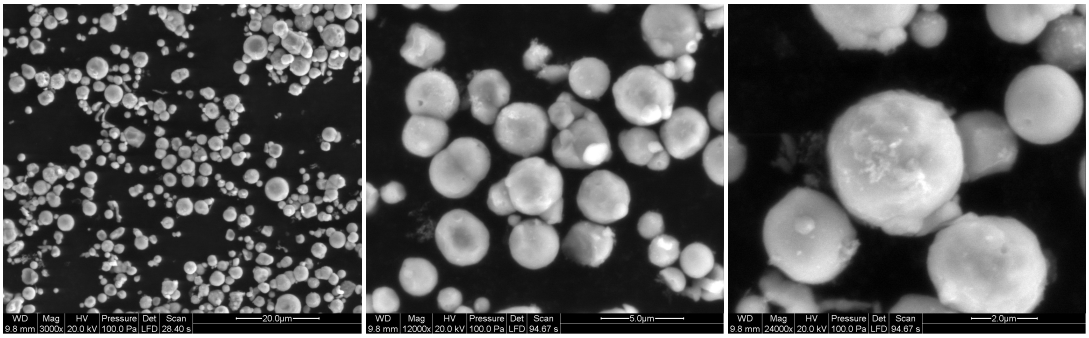

Figure 12 Cu/Fe SEM images, from left to right: 20 µm, 5 µm and 2 µm

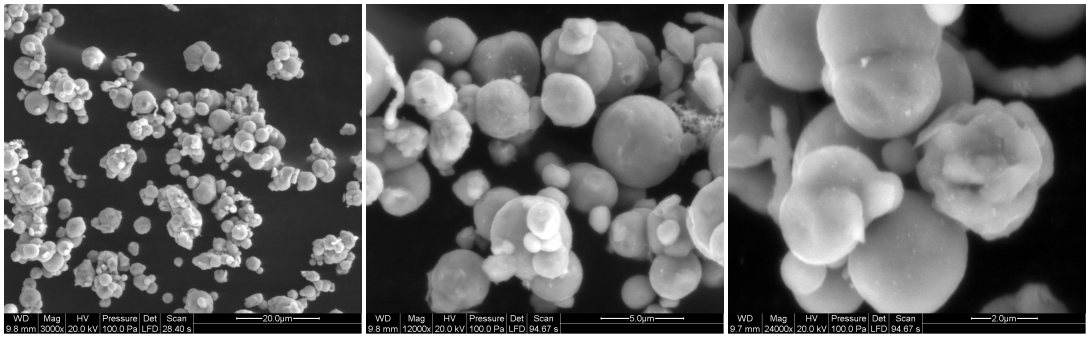

Figure 13 Ag/Fe SEM images, from left to right: 20 µm, 5 µm and 2 µm

The morphology and structure of bimetallic Pd/Fe, Ni/Fe, Cu/Fe and Ag/Fe particles are shown in Figure 10 to 13 by SEM (scanning electron microscopy). Unlike nanosized particles that form chains of beads due to magnetic interactions between the primary iron particles (Shih et al., 2009), these particles appeared to be in small clusters.

A size distribution curve (Figure 14) was produced by measuring the particle sizes in the SEM images, assuming spherical particle shape. The majority of the particles are less than 4 µm in diameter.

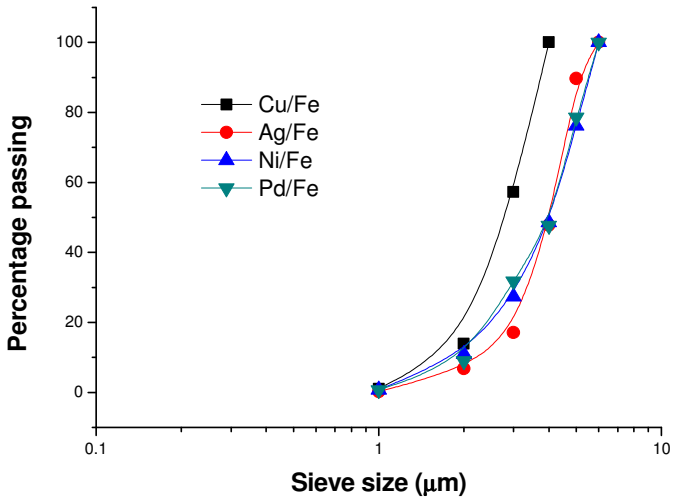

Figure 14 Size distribution curve for 4 bimetallic particles

4.1.3 X-ray photoelectron spectroscopy analysis

X-ray photoelectron spectroscopy (XPS) provides information on elemental composition and chemical oxidation state (Hu et al., 2010). Seven particles were tested and the resulting surface images are presented in Figure 15 to 21. It is shown clearly that the Pd peak area at 336 eV increased with increasing Pd loading (Figure 16 to 18). The appearance of oxygen (530eV) in the elemental analyses is probably due to the oxidation reaction when the particles were exposed to air.

Element analysis of the second metal (Figure 22 to 25) confirmed that the second metal was successfully deposited on the surface of iron as zero valent metal.

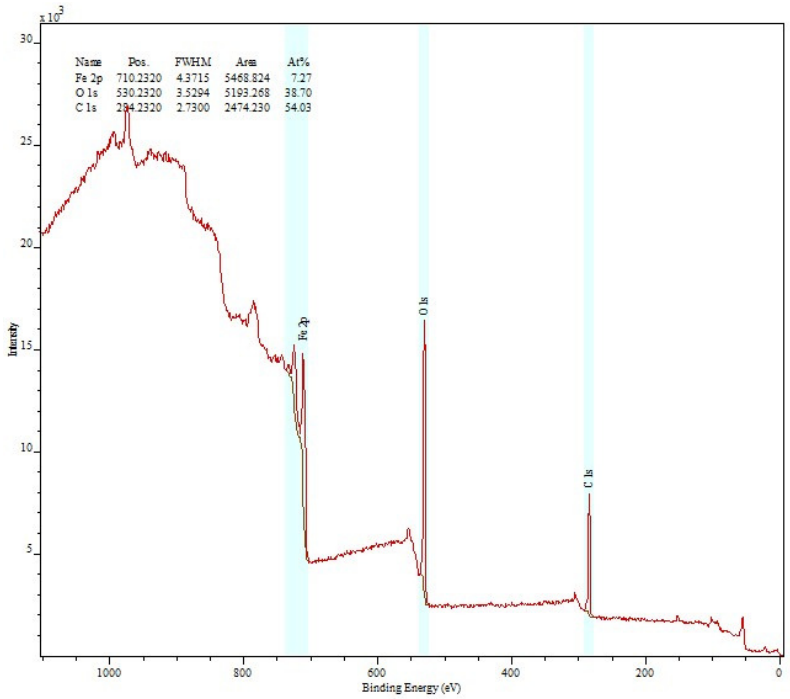

Figure 15 XPS spectra of commercial iron particles

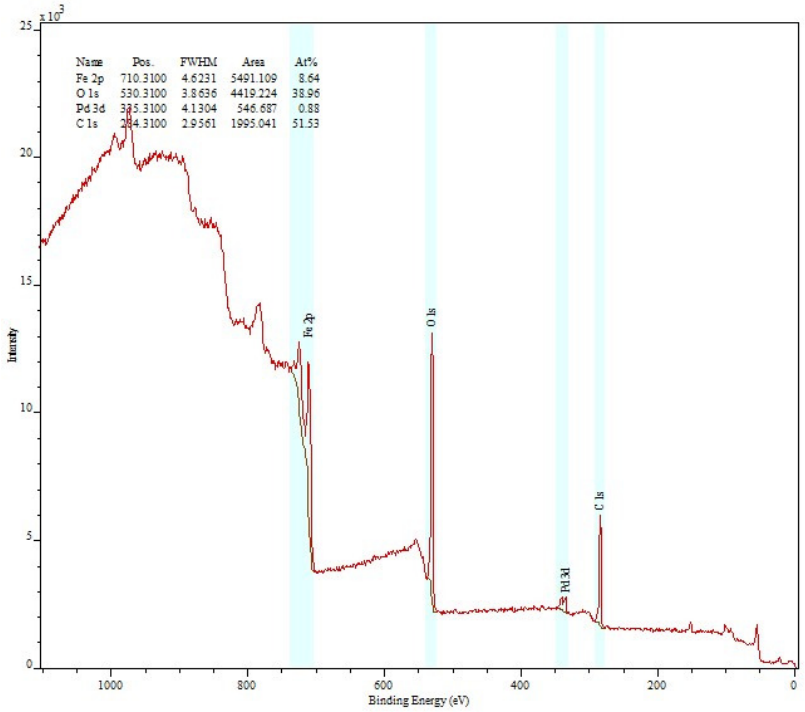

Figure 16 XPS spectra of Pd/Fe 0.011 wt %

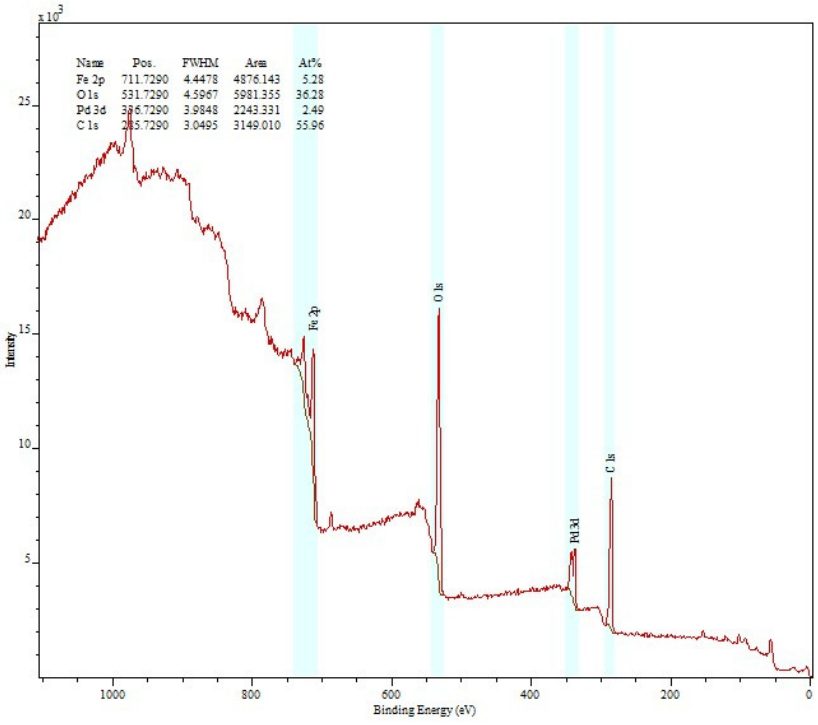

Figure 17 XPS spectra of Pd/Fe 0.022 wt %

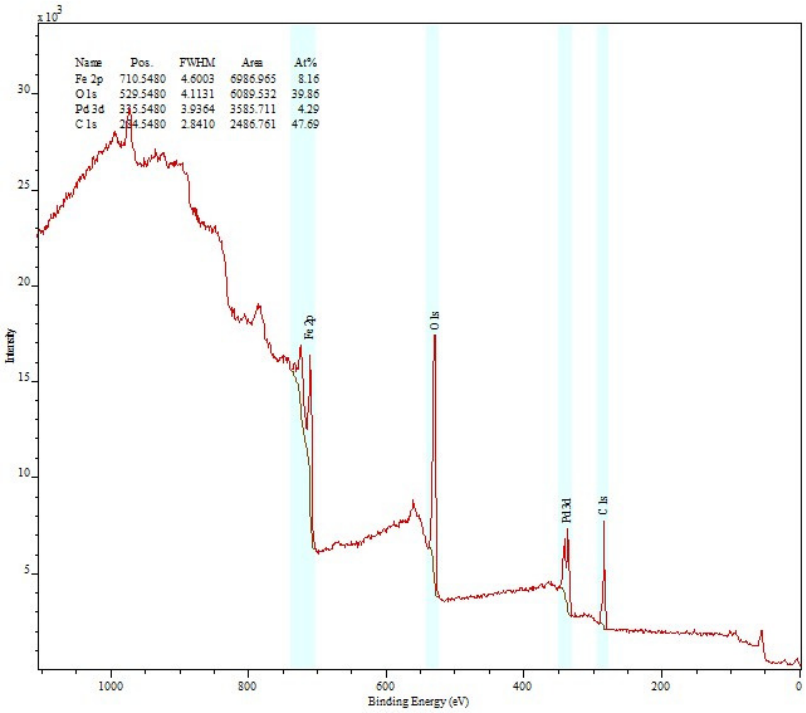

Figure 18 XPS spectra of Pd/Fe 0.044 wt %

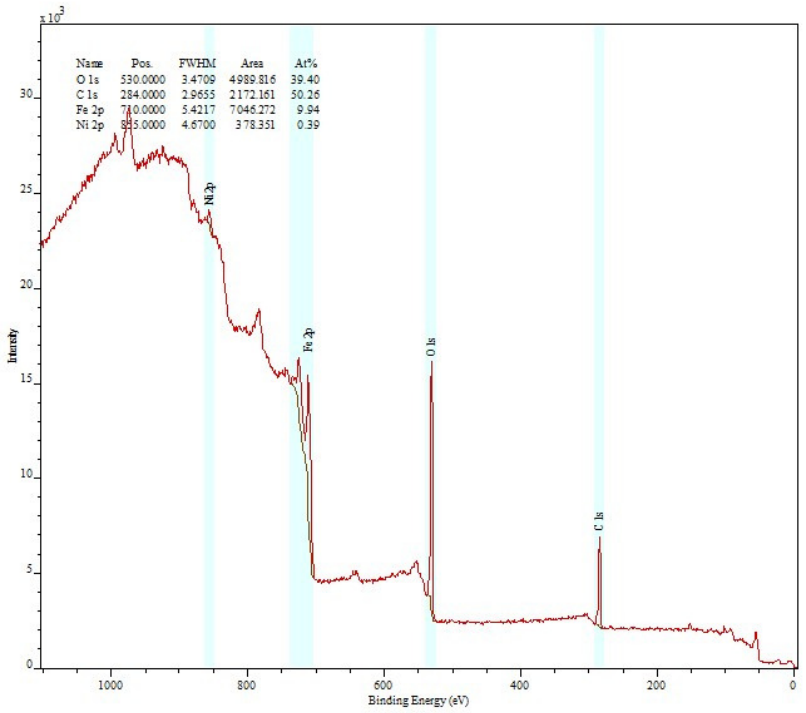

Figure 19 XPS spectra of Ni/Fe 1 wt%

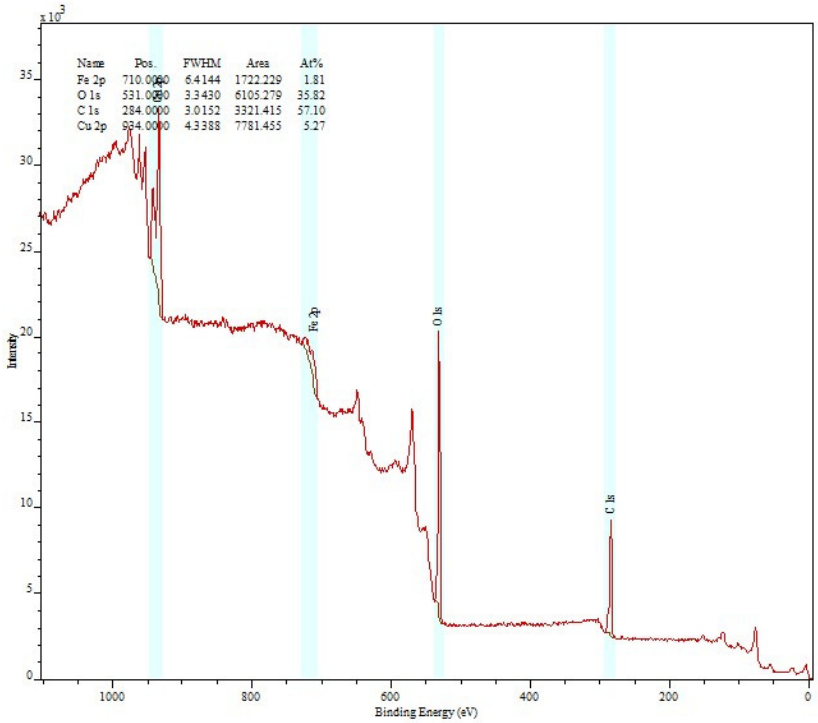

Figure 20 XPS spectra of Cu/Fe 1 wt%

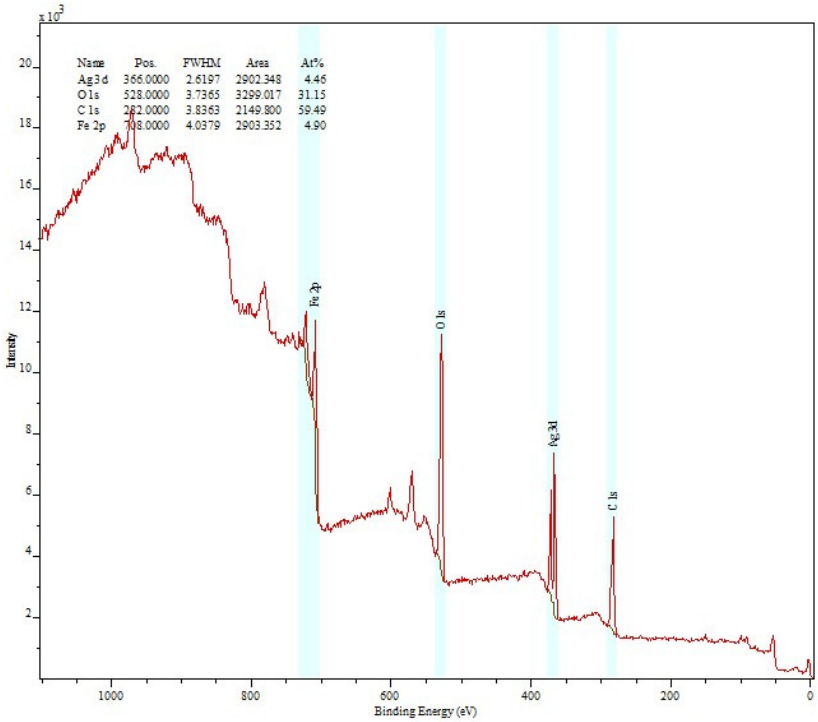

Figure 21 XPS spectra of Ag/Fe 1 wt%

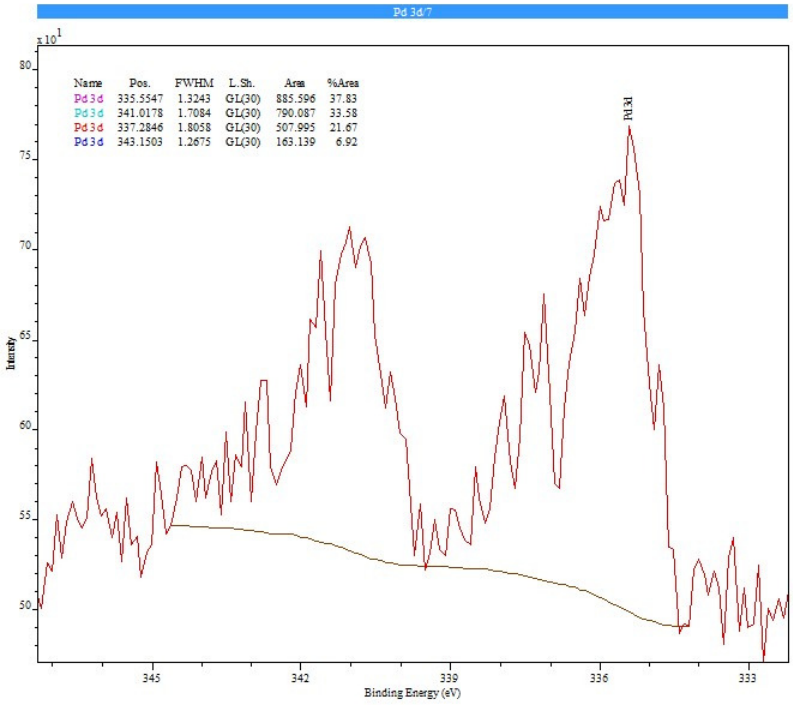

Figure 22 Pd on the surface of Pd/Fe, 0.011 wt %

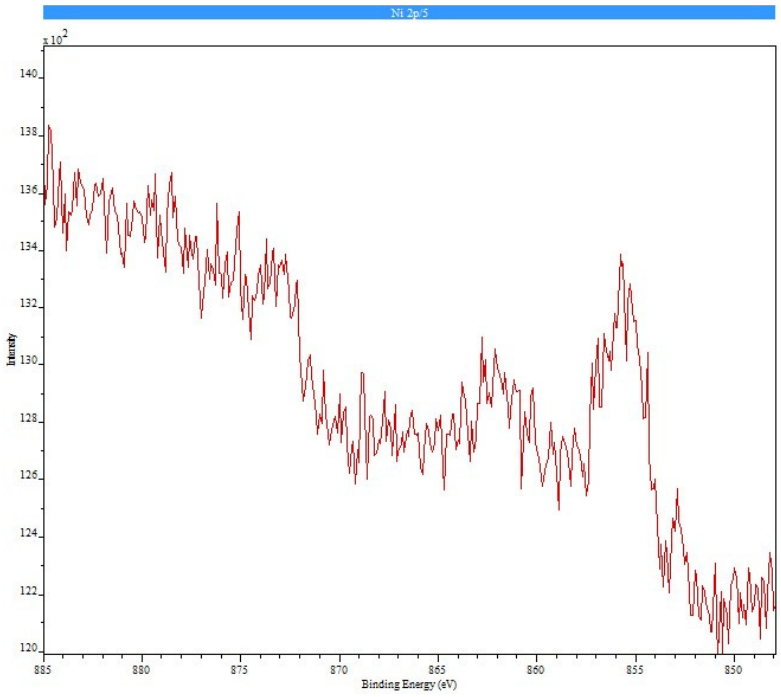

Figure 23 Ni on the surface of Ni/Fe

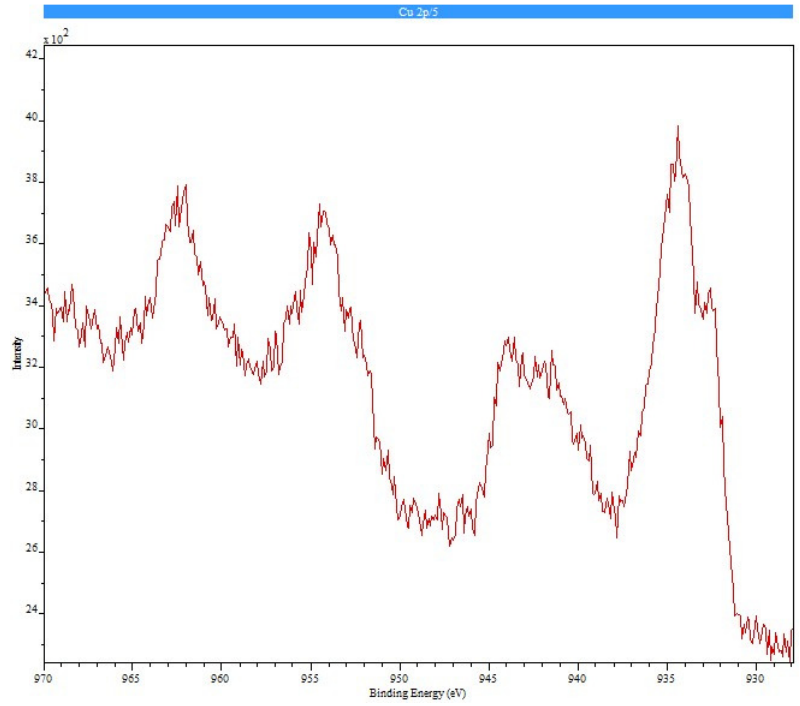

Figure 24 Cu on the surface of Cu/Fe

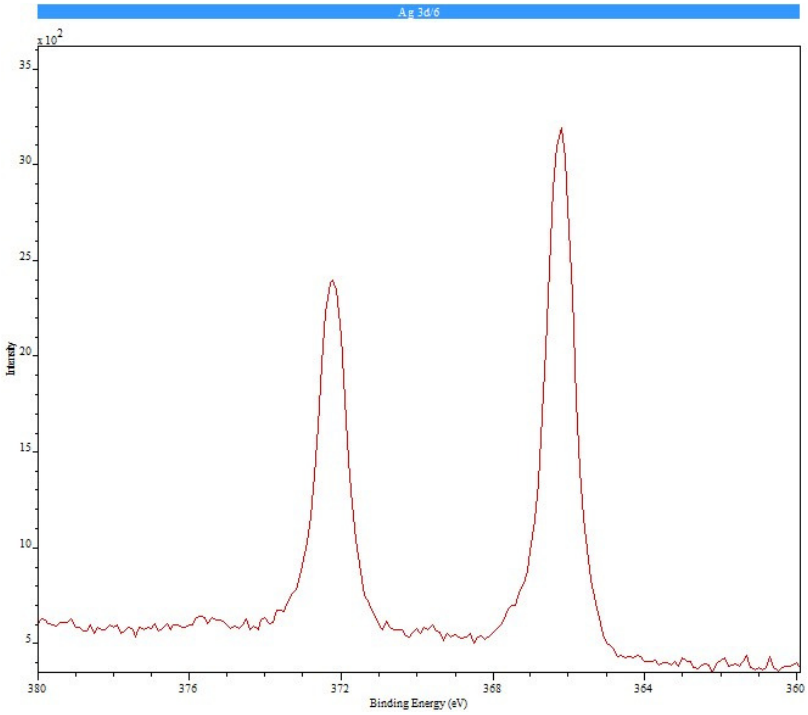

Figure 25 Ag on the surface of Ag/Fe

4.2 Dechlorination of 1, 2, 4-trichlorobenzene, dichlorobenzenes and chlorobenzene by Pd/Fe

A batch dechlorination experiment of 124-TCB with 5 g/L of 0.011% Pd/Fe was initially run for 96 hours (4 days). The starting concentration of 124-TCB was 2 mg/L (11 µmol/L). It was found that more than 90% of the 124-TCB was dechlorinated within the first 8 hours of reaction. The dechlorination experiment was then re-run for 8 hours, with more sampling taking place within the first 2 hours. Benzene was the major dechlorination product detected by GC-MS. Among the intermediates detected, 12-DCB was the major one (Figure 26), following the order of 12-DCB > 14-DCB > 13-DCB. Error bars represent standard deviation for triplicates. The amounts of 124-TCB in the blank experiments remained relatively constant during the reaction time, which indicated minimal leakage or sorption to the glass wall of the serum bottle.

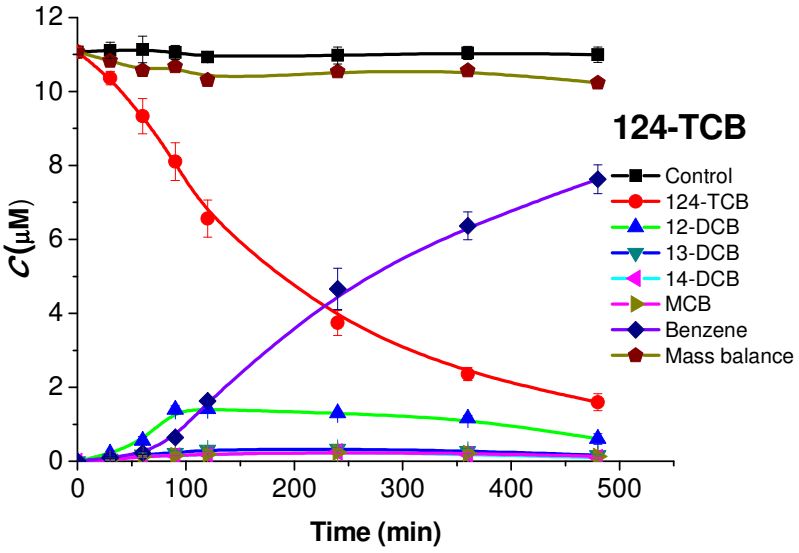

Figure 26 Reaction of 5 g/L of 0.011% Pd/Fe with 1,2,4-trichlorobenzene

Dechlorination experiments for monochlorobenzene (MCB) and dichlorobenzenes were conducted with 0.011% Pd/Fe for 8 hours. MCB was rapidly dechlorinated and benzene was the sole product detected (Figure 27). No other products (such as cyclohexane) were observed. This indicates the resonance energy of the benzene ring was not sufficiently lowered as a result of substitution of H for Cl, and the aromatic ring remained intact (Zhu and Lim, 2007). However, Morales (Morales et al., 2002a) found cyclohexanol and cyclohexanone as their dechlorination products for pentachlorophenol using Pd/Mg particles as reductant.

With the 0.011% Pd/Fe, the three DCBs were dechlorinated to half of their initial concentrations within 3 hours (Figures 28-30). The corresponding rate constants and reaction half times are listed in Table 13. The order of dechlorination rates among DCBs was 14-DCB ≥ 13-DCB ≥ 12-DCB. The order was consistent with the results reported by Zhu and Lim (2007) on dechlorination of chlorobenzenes with Pd/Fe nanoparticles. The order was also consistent with the results reported by Keane et al. (2004) on gas-phase catalytic hydrodechlorination of DCBs over Ni/SiO_2.

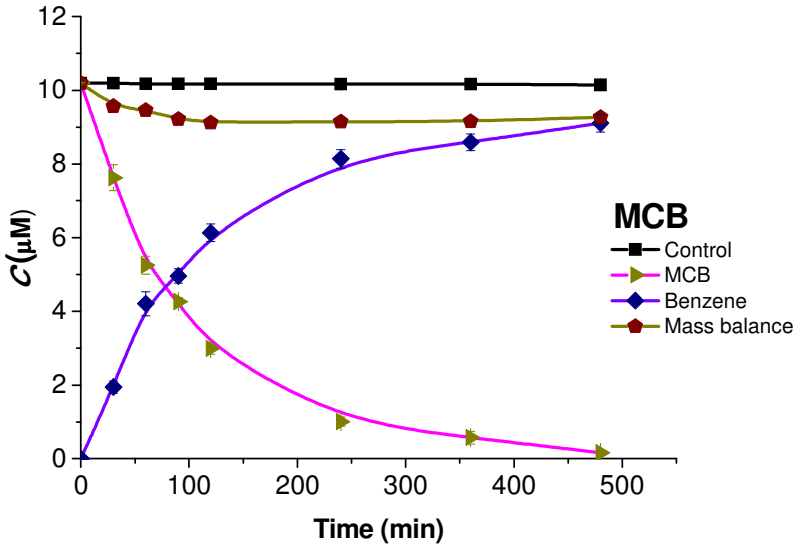

Figure 27 Reaction of 5 g/L of 0.011% Pd/Fe with chlorobenzene

Pseudo-first-order kinetics generally has been used to describe the reductive dehalogenation of organics (Gillham and O'Hannesin, 1994; Klausen et al., 2003; Matheson and Tratnyek, 1994; Xu et al., 2005a). In this study, the plotted results confirm the validity of this kinetic model for 124-TCB, DCBs and MCB reductive dechlorination, with R^2 (correlation of determination) of linear plots higher than 0.99 (Table 13).

Table 13 Rate constants and half-lives for MCB, DCBs and 124-TCB dechlorination with 5 g/L of 0.011% Pd/Fe

Parameters	MCB	12-DCB	13-DCB	14-DCB	124-TCB
k_{obs} ($10^{-3}min^{-1}$) [a]	8.3±0.8[b]	4.9±0.3	5.2±0.3	5.8±0.3	4.2±0.3
$t_{1/2}$ (min)[c]	84	141	133	119	165
R^2	0.991[d]	0.996	0.997	0.997	0.993

[a] Pseudo-first-order kinetic rate constant for dechlorination of the parent compounds. [b] ±95% confidence level. [c] the half-life period of the parent compounds. [d] coefficient of determination from the overall regression analysis.

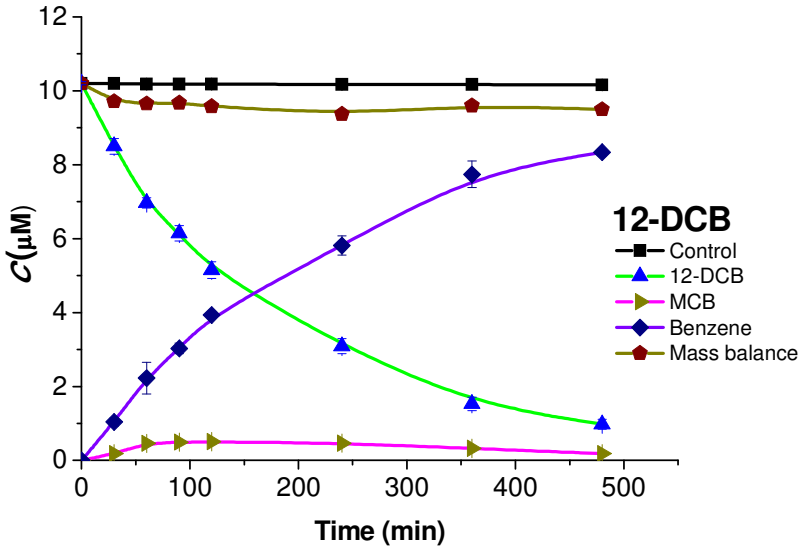

Figure 28 Reaction of 5 g/L of 0.011% Pd/Fe with 1,2-dichlorobenzene

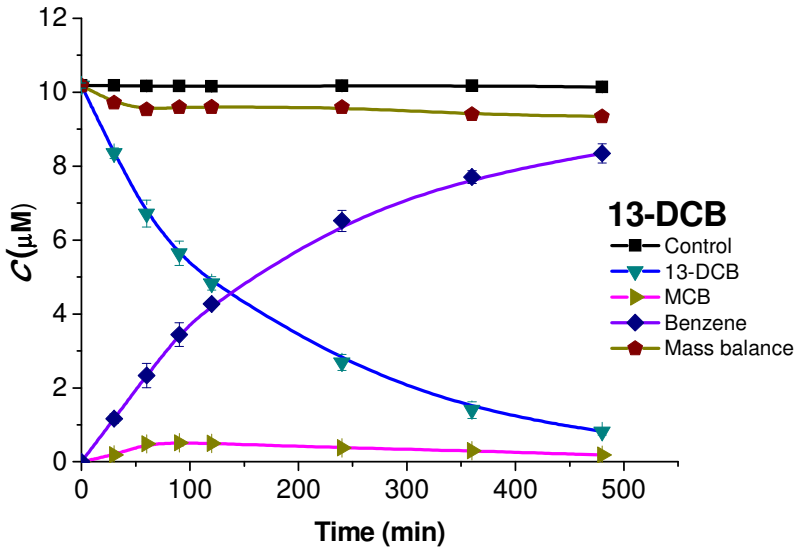

Figure 29 Reaction of 5 g/L of 0.011% Pd/Fe with 1,3-dichlorobenzene

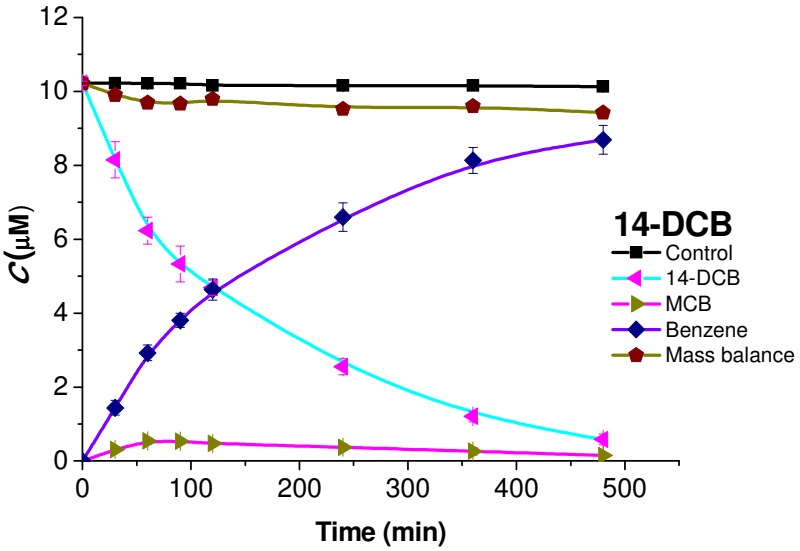

Figure 30 Reaction of 5 g/L of 0.011% Pd/Fe with 1,4-dichlorobenzene

4.3 **Dechlorination of 1, 2, 4-trichlorobenzene by Ni/Fe, Cu/Fe and Ag/Fe**

Bimetallic particles other than Pd/Fe were synthesized to test their dechlorination performance of 124-TCB. Ni/Fe, Cu/Fe and Ag/Fe were synthesized by depositing the metal containing salts on ZVI particles. Reactions of 124-TCB with Ni/Fe particles in a batch system are shown in Figure 31. Only 40% of the 124-TCB were dechlorinated within the first two days of reaction. A gradual accumulation of less chlorinated benzenes was observed after 1 day. 12-DCB was the most abundant intermediate among the DCBs, accounting for 10% of the total mass. Benzene was the final dechlorination product. Summation of the total molar concentrations for the reactant and products remained above 90% for the reaction system.

Reaction of 1% Cu/Fe with 124-TCB is shown in Figure 32. The reaction time was set as 12 days. The 124-TCB was slowly converted to less chlorinated benzenes after 4 days. Only 20% 124-TCB was transformed at the end of the reaction period. No benzene was detected in the batch system. 12-DCB was the most abundant intermediate among all products, accounting for less than 10% of the total mass.

Among all the bimetallic particles tested in this study, Ag/Fe was the least effective as shown in Figure 33. Less than 10% of the initial 124-TCB was dechlorinated at the end of the reaction period. No monochlorobenzene or benzene was detected. A small amount of DCB was found as products, accounting for less than 5% of the total mass.

Table 14 lists the observed rate constants and half lives for 124-TCB dechlorination by Pd/Fe, Ni/Fe, Cu/Fe and Ag/Fe bimetallic particles.

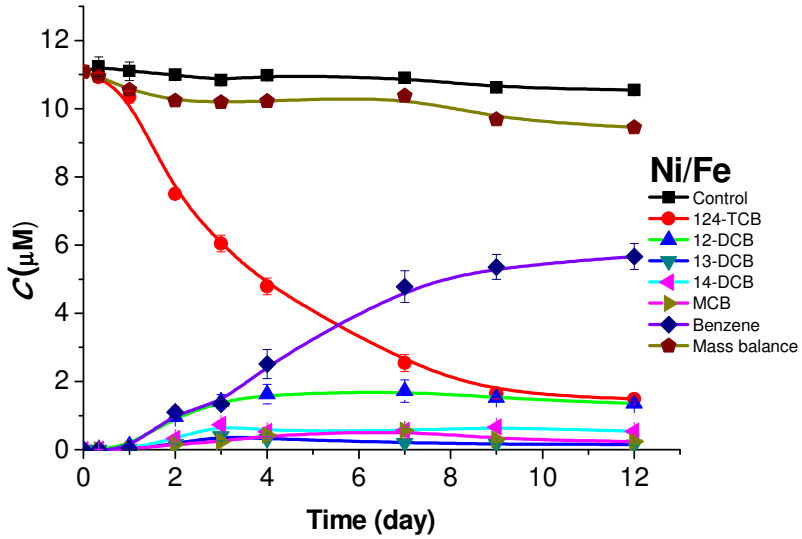

Figure 31 Reaction of 5 g/L of 1% Ni/Fe with 1,2,4-trichlorobenzene

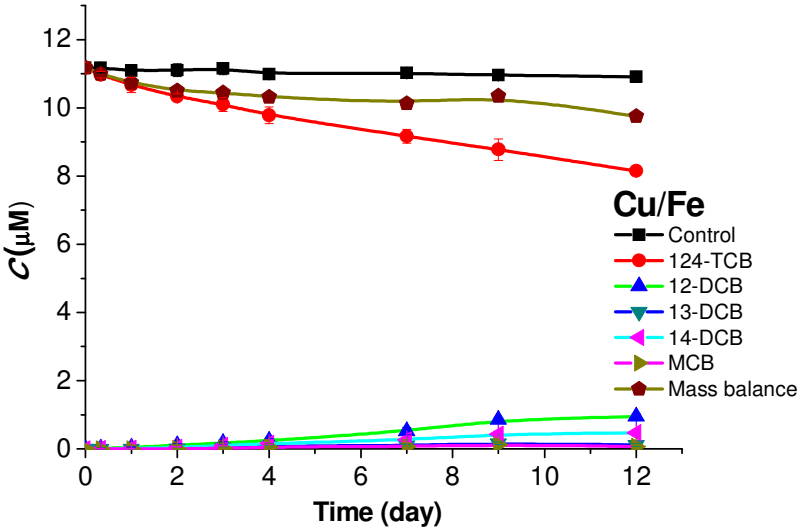

Figure 32 Reaction of 5 g/L of 1% Cu/Fe with 1,2,4-trichlorobenzene

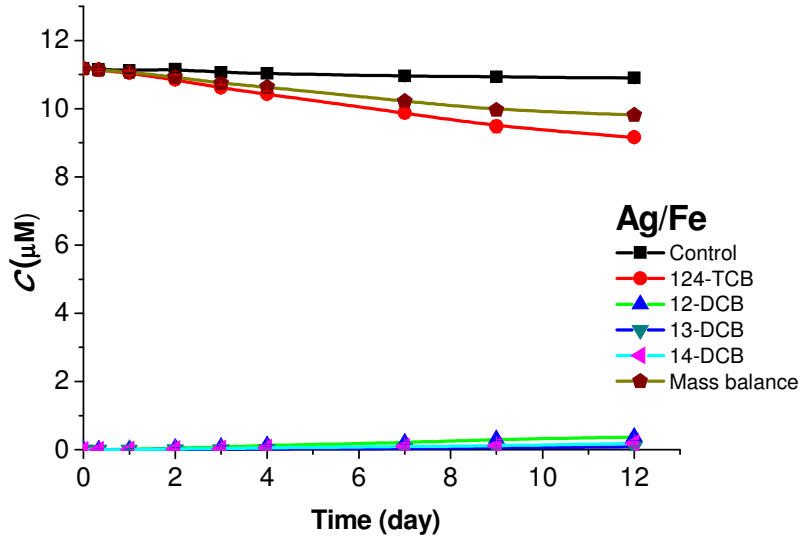

Figure 33 Reaction of 5 g/L of 1% Ag/Fe with 1,2,4-trichlorobenzene

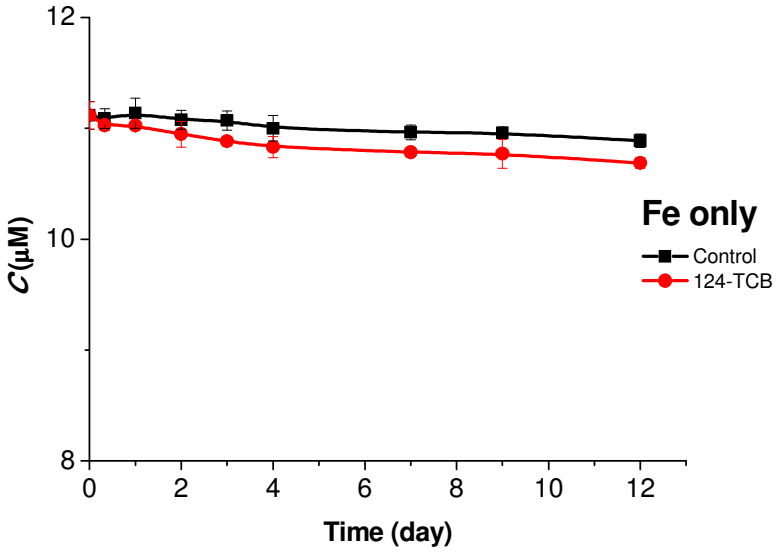

Figure 34 Reaction of 5 g/L of Fe^0 with 1,2,4-trichlorobenzene

Table 14 Rate constants and half-lives for 124-TCB dechlorination by Pd/Fe, Ni/Fe, Cu/Fe and Ag/Fe

Parameters	Pd/Fe	Ni/Fe	Cu/Fe	Ag/Fe[e]
k_{obs} (10^{-2} day^{-1})[a]	610±49[b]	18.8±3.0	2.53±0.22	1.74±0.11
$t_{1/2}$ (day)[c]	0.11	3.7	27.4	39.7
Surface coverage of the second metal (wt%)	0.011	1.0	1.0	1.0
R^2	0.994[d]	0.969	0.991	0.995

[a] Pseudo-first-order kinetic rate constant for dechlorination of 124-TCB. [b] ±95% confidence level. [c] the half-life period. [d] coefficient of determination from the overall regression analysis. [e] solids dosage of all bimetallic particles = 5 g/L.

The results showed the following reactivity trend for 124-TCB: Pd/Fe>> Ni/Fe> Cu/Fe > Ag/Fe ≈ Fe (Figure 34). This finding is consistent with several other studies (Cwiertny et al., 2006; Elliott and Zhang, 2001; He and Zhao, 2008; Kim and Carraway, 2000; Kim and Carraway, 2003; Lin et al., 2004a; Zhang et al., 1998). This trend indicates that the reactivity enhancement of bimetallic particles is sensitive to the chemical identity of the transition metal additive (Cwiertny et al., 2006).

There are two popular hypotheses on the enhanced dehalogenation rates by ZVI based bimetallic particles. One is that surface additives increase reactivity by enhancing the oxidation rate of iron through the formation of a galvanic couple (Lien and Zhang, 2002; Schrick et al., 2002). Table 15 lists standard reduction potentials for Fe, Pd, Ni, Cu and Ag. The standard potentials for the four galvanic cells (ΔE°) were plotted against the $\ln k_{obs}$ for 1,2,4-TCB as shown in Figure 35. There was no obvious correlation between the two parameters. If the galvanic couple hypothesis stands, the catalytic effect of the second metal should be in the order of Pd> Ag > Cu > Ni. However, this is not consistent with what we observed.

Table 15 Standard reduction Potentials at 25°C

Half-reaction	E°(V)
$Fe^{2+} + 2e^- \rightleftharpoons Fe(s)$	-0.44^a
$Pd^{2+} + 2e^- \rightleftharpoons Pd(s)$	$+0.99^b$
$Ni^{2+} + 2e^- \rightleftharpoons Ni(s)$	-0.27^b
$Cu^{2+} + 2e^- \rightleftharpoons Cu(s)$	$+0.34^c$
$Ag^+ + e^- \rightleftharpoons Ag(s)$	$+0.80^d$

[a] Atkins, (1997), [b] Hayes, (1993), [c] Bard,(1985), [d] Vanýsek, (2007)

Another hypothesis is that atomic hydrogen adsorbed in the additive represents a reactive species involved in the reductive dehalogenation process, while others have speculated that the beneficial effects of transition metal additives can be correlated with their ability to generate surface-bound atomic hydrogen (Lien and Zhang, 2002; Lin et al., 2004b). As shown in Figure 36, hydrogen can be adsorbed on the surface of Pd through physisorption and chemisorption. Hydrogen can also be absorbed into the bulk of Pd. The heat of hydrogen solution, ΔH_{sol}, is an indicator for hydrogen absorption; whereas the heat of hydrogen chemisorption, ΔH_{chem}, is an indicator for hydrogen adsorption.

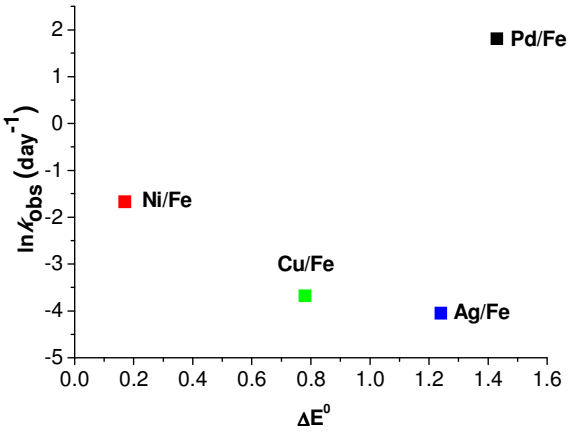

Figure 35 Reaction standard potential (ΔE°) vs lnk_{obs} for 1,2,4-TCB

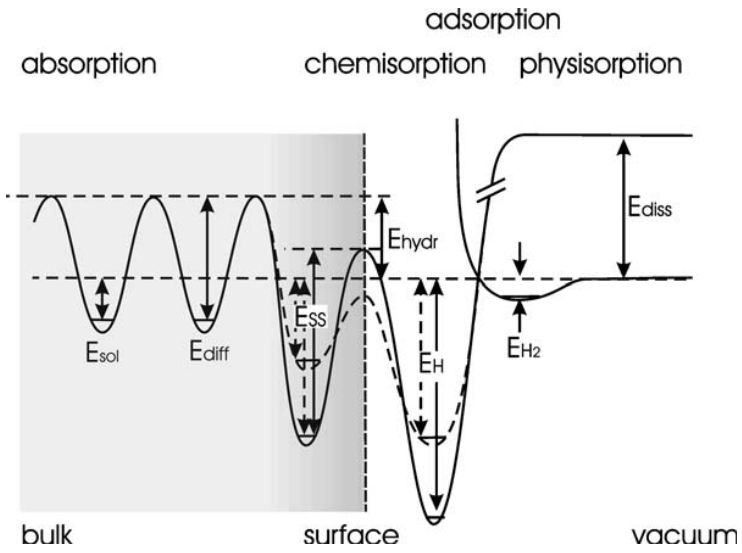

Figure 36 Schematic of the potential energy of a hydrogen atom at the surface of Pd (*left side*) and the immediate vacuum (*right side*), (Pundt and Kirchheim, 2006)

The energy is scaled to that of the hydrogen molecule H_2 (E_{H2}) far away from the surface. The various energy levels in the figure correspond to the expected values of the heat of solution (E_{sol}), the activation energy for diffusion (E_{diff}), the activation energy for hydrogen absorption (E_{hydr}), the desorption energy from a subsurface site (E_{SS}), and the desorption energy from a chemisorbed site (E_H), both for the original and reconstructed surfaces. The energy level for hydrogen molecule dissociation (E_{diss}) is also implemented. Adapted from (Behm RJ, 1983).

Borgschulte et al. (2006) measured hydrogen uptake rate R at 420K and hydrogen pressure of 2 bar for a 130-nm-thick yttrium indicator layer catalyzed by several noble and transition metals. They found a near linear correlation (Figure 37) between the hydrogen uptake rate R and the heat of hydrogen solution, ΔH_{sol} (Fukai, 1992) , and that the catalytic effect decreased in the order Pd, Ni, Pt, Cu, Au, Ag.

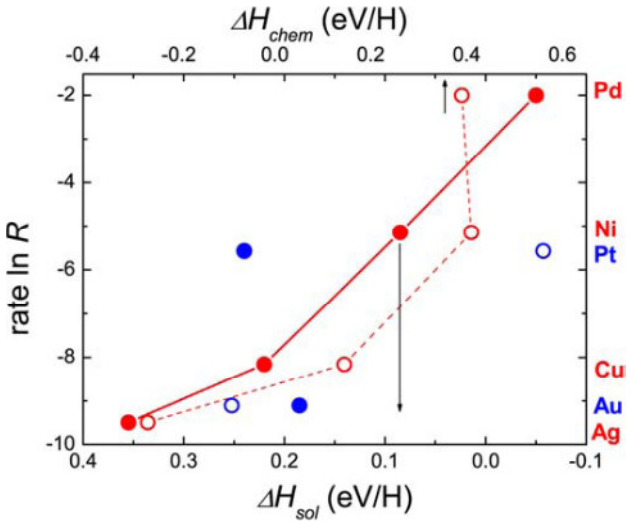

The film is covered with the noble metals Pd, Ni, Cu, and Ag (red points) and Au, Pt (blue points) with a thickness of 10 nm. The logarithmic uptake rate ln$R$ is compared to the heat of hydrogen solution ΔH_{sol} (full circles) and to the heat of chemisorption $-\Delta H_{chem}$ (empty circles). A nearly linear relation is found between ln$R$ and ΔH_{sol} (with the exception of Pt and Au (the lines are a guide to the eyes).

Figure 37 Hydrogen uptake rate *R* of a 130 nm thick yttrium film at 420 K and 2 bar hydrogen (Borgschulte et al., 2006).

Inspired by this correlation between ΔH_{sol} and the hydrogen uptake rate R, we plotted $1/k_{obs}$ (the observed rate constants) for 1,2,4-TCB dechlorination by different bimetallic particles against the heat of hydrogen solution (ΔH_{sol}) and found a near linear correlation as shown in Figure 38a. The heat of hydrogen chemisorption (ΔH_{chem}) was also plotted against $\ln k_{obs}$ for 1,2,4-TCB as shown in Figure 38b. The resulting correlation was not as obvious as that of ΔH_{sol}, which underlines the better correlation of the catalytic activity with the heat of solution than the heat of chemisorption.

The reactivity trend of four different bimetallic particles for 124-TCB identified in our study showed better correlation of the catalytic activity with the heat of solution than the heat of chemisorption. This indicated that the hydrogen absorbed inside the metal played a more important role than the hydrogen adsorbed on the surface in the catalytic activity of the second noble metal. Not only can palladium adsorb hydrogen at its surface at room temperature, it can also absorb hydrogen into its subsurface sites (Figure 36). In fact, palladium is the most effective metal in terms of the ability to absorb hydrogen into its lattice and to maintain a high surface concentration of hydrogen (Lawson et al., 1991).

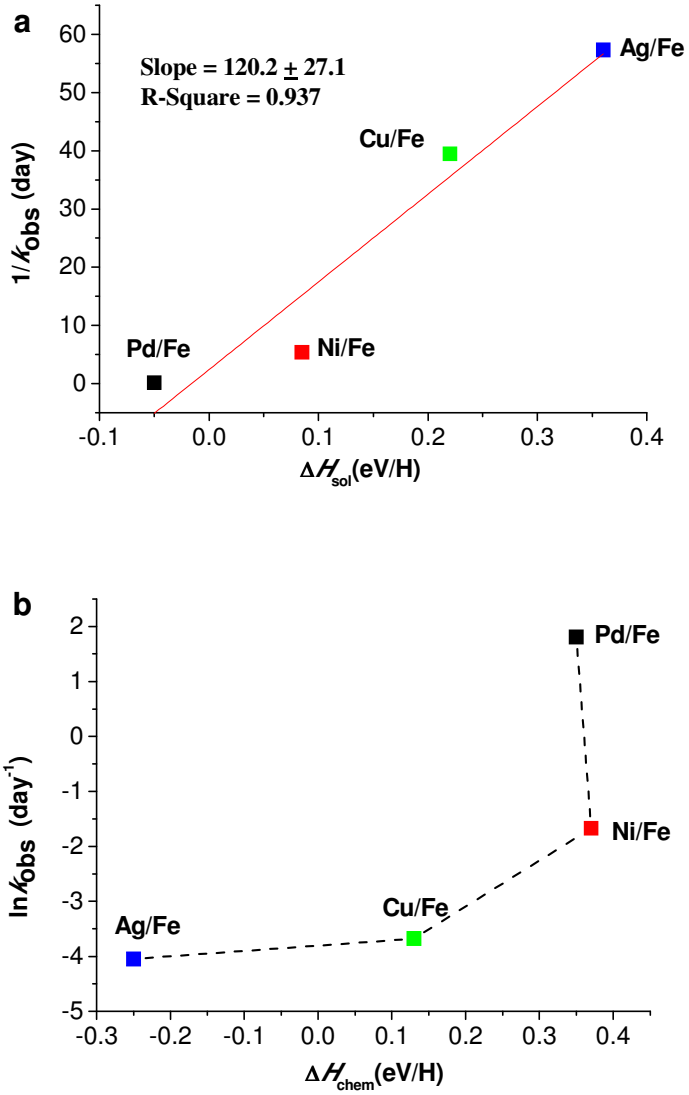

Figure 38 The heat of hydrogen solution ΔH_{sol} vs. $1/k_{obs}$ (the observed rate constants) (a) and the heat of hydrogen chemisorption ΔH_{chem} vs. $\ln k_{obs}$ (b) for 1,2,4-TCB

4.4 Debromination of 1, 2, 4-tribromobenzene, dibromobenzenes and bromobenzene by Pd/Fe

Figure 39 depicts 124-TBB transformation with 0.011% Pd/Fe. The concentrations of 124-TBB and its debromination daughter products at various reaction times were measured by GC-MS. Rapid debromination of 124-TBB was witnessed, with 90% of starting 124-TBB converted to benzene within 4 hours. The major intermediate observed was 12-DBB, reaching its peak concentration (about 10% of the initial concentration of 124-TBB) at about 1 hour into the reaction. Other intermediates detected were 13-DBB, 14-DBB and bromobenzene, all at lower concentrations compared to 12-DBB.

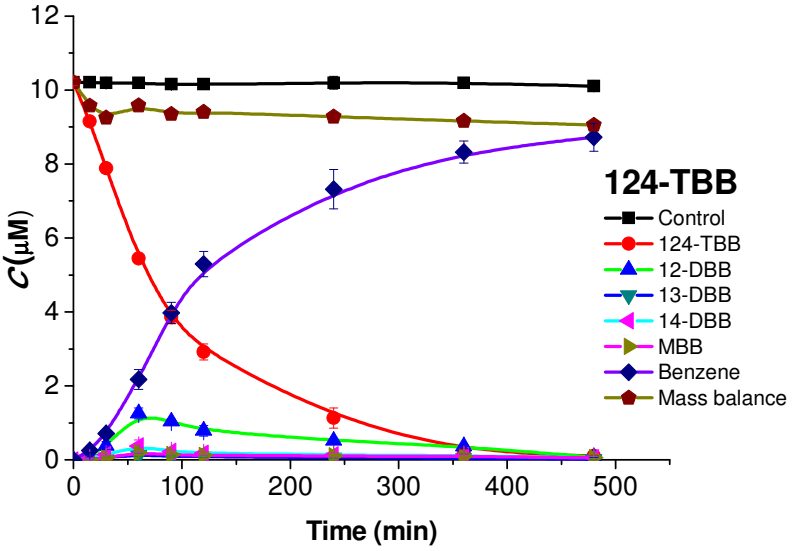

Figure 39 Reaction of 5 g/L 0.011% Pd/Fe with 1,2,4-tribromobenzene

Debromination experiments were also conducted for MBB and dibromobenzenes with 0.011% Pd/Fe (Figure 40 to 43). Debromination of MBB was rapid with a half-life of only 54 minutes (Table 16). Benzene was the sole debromination product identified by GC-MS.

The order of debromination rates among DBBs was 14-DBB ≥ 13-DBB ≥12-DBB. Debromination of DBBs followed the same pattern: benzene was the major product with bromobenzene as the intermediate (<10% of the initial concentration detected).

Table 16 Rate constants and half-lives for MBB, DBBs and 124-TBB debromination with 5 g/L 0.011% Pd/Fe

Parameters	MBB	12-DBB	13-DBB	14-DBB	124-TBB
k_{obs} (10^{-3}min^{-1}) [a]	12.9±1.1[b]	10.2±0.7	11.0±0.6	12.2±1.2	9.8±0.8
$t_{1/2}$ (min)[c]	54	68	63	57	71
R^2	0.991[d]	0.995	0.996	0.988	0.993

[a] Pseudo-first-order kinetic rate constant for debromination of the parent compounds. [b] ±95% confidence level. [c] the half-life period of the parent compounds. [d] coefficient of determination from the overall regression analysis.

Pseudo-first-order kinetic model was used to describe the debromination of 124-TBB, DBBs and bromobenzene by Pd/Fe. The plotted results confirmed the validity of this kinetic model with R^2 (correlation of determination) of linear plots generally higher than 0.98 (Table 16).

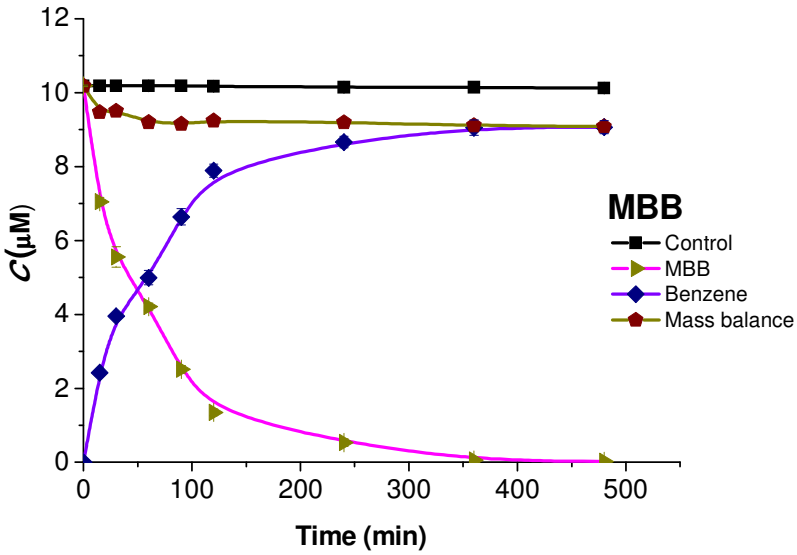

Figure 40 Reaction of 5 g/L 0.011% Pd/Fe with bromobenzene

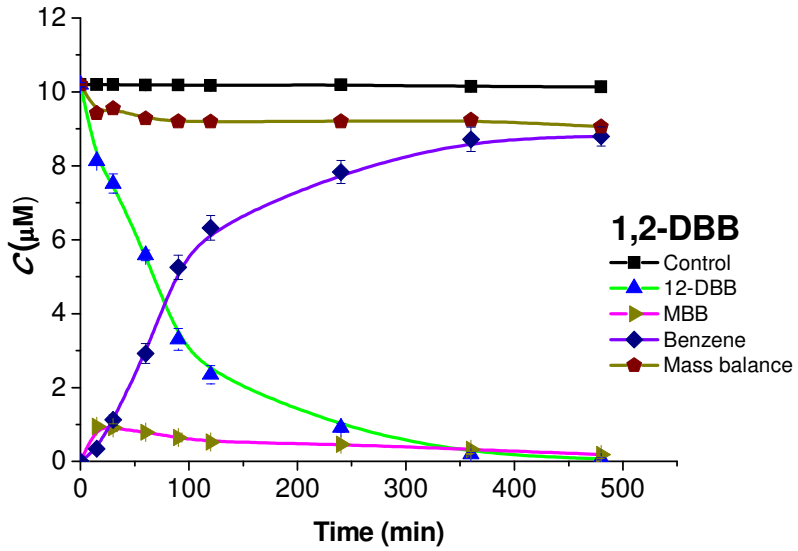

Figure 41 Reaction of 5 g/L 0.011% Pd/Fe with 1,2-dibromobenzene

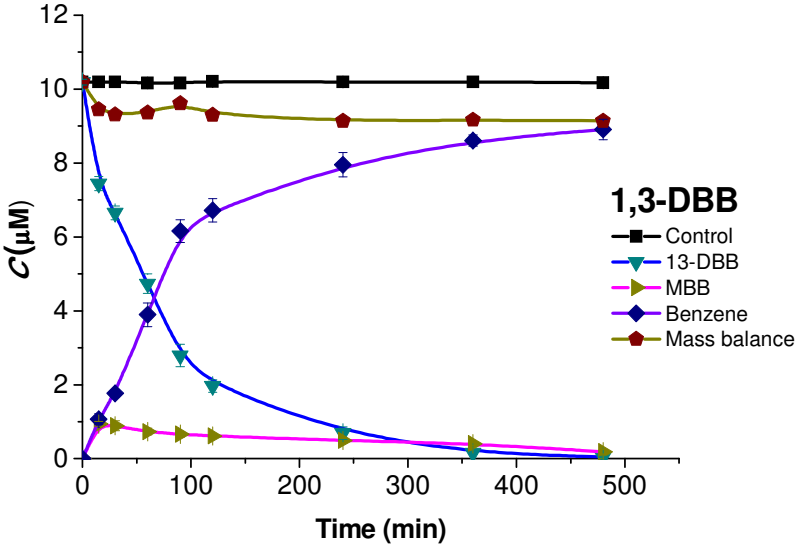

Figure 42 Reaction of 5 g/L 0.011% Pd/Fe with 1,3-dibromobenzene

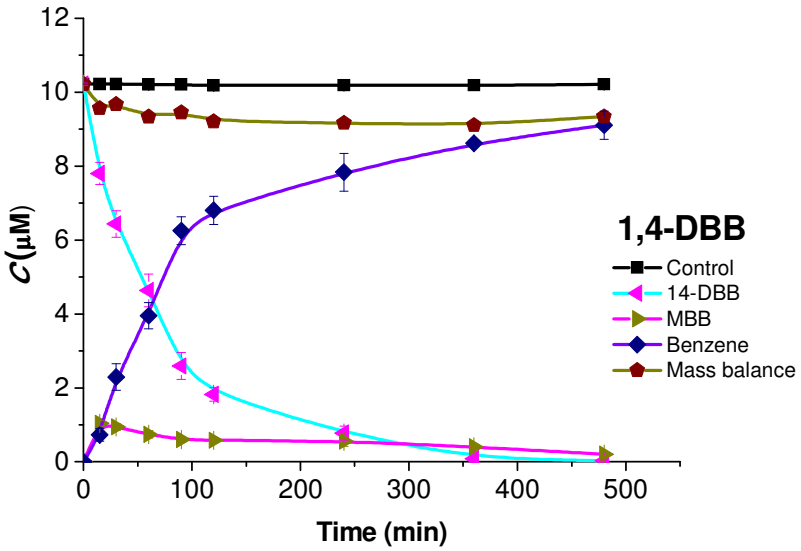

Figure 43 Reaction of 5 g/L 0.011% Pd/Fe with 1,4-dibromobenzene

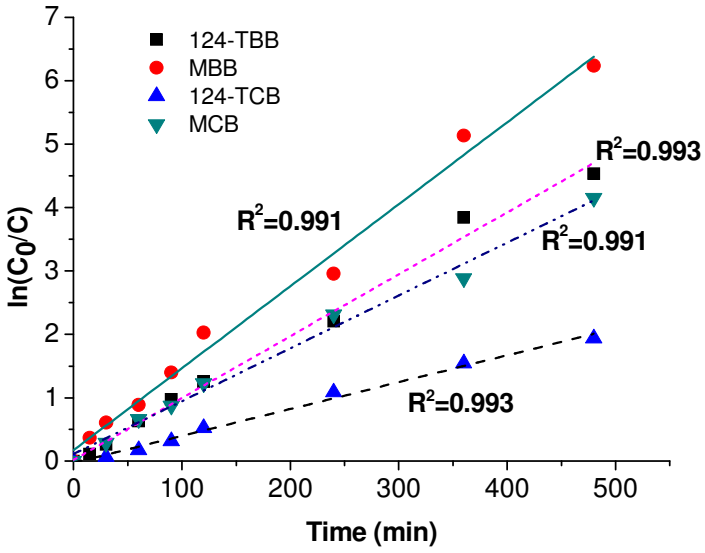

Figure 44 Coefficient of determination from the overall regression analysis

4.5 **Debromination of 1, 2, 4-tribromobenzene by Ni/Fe, Cu/Fe and Ag/Fe**

Batch debromination studies of 124-TBB were conducted with 1% Ni/Fe, 1% Cu/Fe and 1% Ag/Fe. Among the three bimetallic particles tested, Ni/Fe showed the most reactivity, although the reactivity was not of the same order of magnitude as that of Pd/Fe. The debromination of 124-TBB with 1% Ni/Fe is shown in Figure 45. About 60% of 124-TBB was converted to benzene in the course of 12 days reaction. Among the intermediates formed, 12-DBB was the most abundant, accounting for about 10% of the total mass, followed by 14-DBB, 13- DBB, and bromobenzene.

Figure 46 shows the conversion of 124-TBB with 1% Cu/Fe. About 25% of total 124-TBB was converted to intermediates and benzene. However, benzene accounts for less than 7% of the total mass.

The conversion of 124-TBB with 1% Ag/Fe is depicted in Figure 47. By the end of 12 days, still no benzene was produced. About 20% of the initial 124-TBB was converted to dibromobenzenes and bromobenzene.

Table 17 lists the observed rate constants and half lives for 124-TBB debromination by Pd/Fe, Ni/Fe, Cu/Fe and Ag/Fe bimetallic particles. Again, the results showed the following reactivity trend for 124-TBB: Pd/Fe>> Ni/Fe> Cu/Fe > Ag/Fe ≈ Fe (Figure 48). This is consistent with the reactivity trend found for 124-TCB.

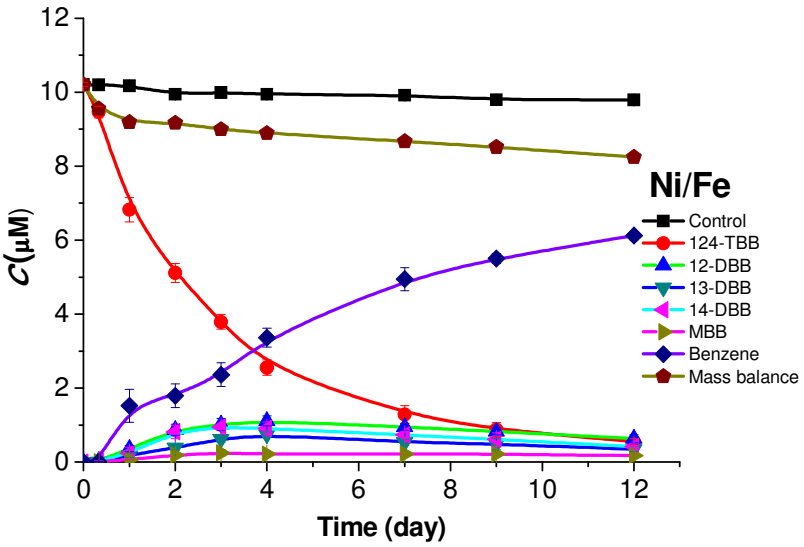

Figure 45 Reaction of 5 g/L 1% Ni/Fe with 1,2,4-tribromobenzene

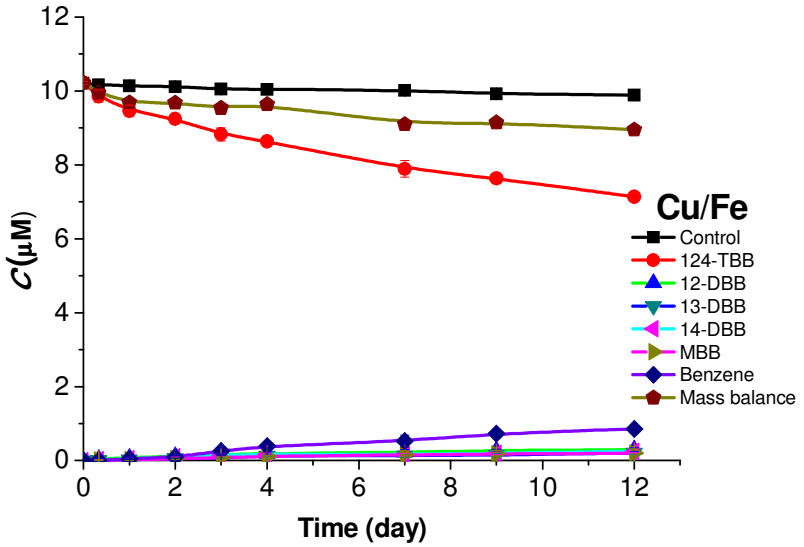

Figure 46 Reaction of 5 g/L 1% Cu/Fe with 1,2,4-tribromobenzene

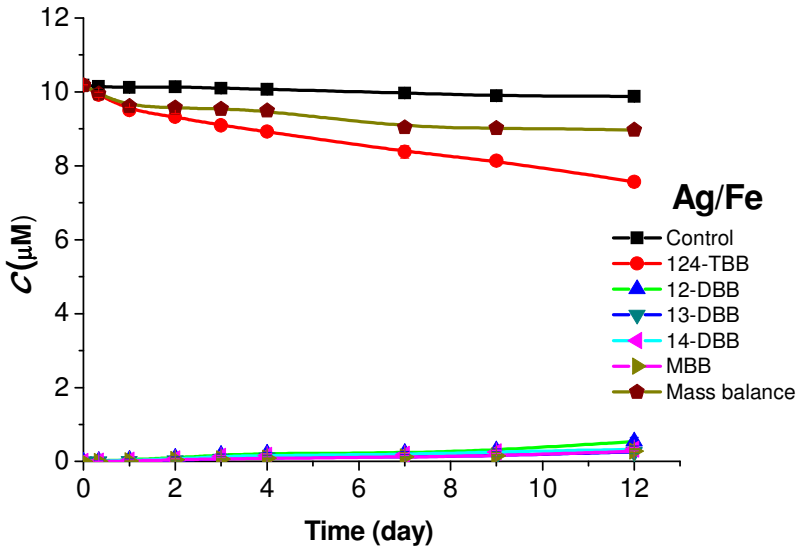

Figure 47 Reaction of 5 g/L 1% Ag/Fe with 1,2,4-tribromobenzene

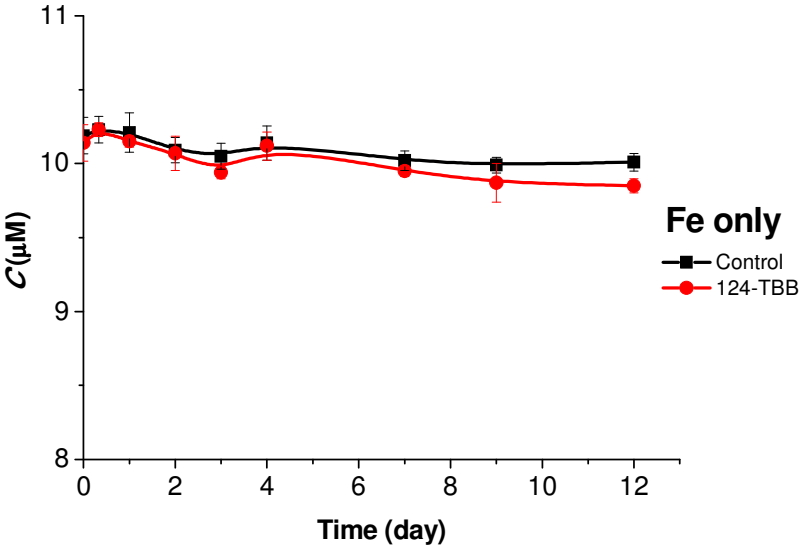

Figure 48 Reaction of 5 g/L Fe^0 with with 1,2,4-tribromobenzene

Table 17 Rate constants and half-lives for 124-TBB debromination by Pd/Fe, Ni/Fe, Cu/Fe and Ag/Fe

Parameters	Pd/Fe	Ni/Fe	Cu/Fe	Ag/Fe[e]
k_{obs} (10^{-2} day^{-1})[a]	1406±109[b]	27.7±3.2	3.01±0.43	2.26±0.34
$t_{1/2}$ (day)[c]	0.05	2.5	23	31
Surface coverage of the second metal (wt%)	0.011	1.0	1.0	1.0
R^2	0.993[d]	0.987	0.980	0.973

[a] Pseudo-first-order kinetic rate constant for debromination of 124-TBB. [b] ±95% confidence level. [c] the half-life period. [d] coefficient of determination from the overall regression analysis. [e] solids dosage of all bimetallic particles = 5 g/L

The reaction standard potentials calculated from Table 15 were plotted again the lnk_{obs} for 1,2,4-TCB dechlorination by different bimetallic particles (Figure 49). Similar to Figure 35, no obvious correlation was found between the two parameters. Contradictory observation was made for 124-TBB against the galvanic couple hypothesis.

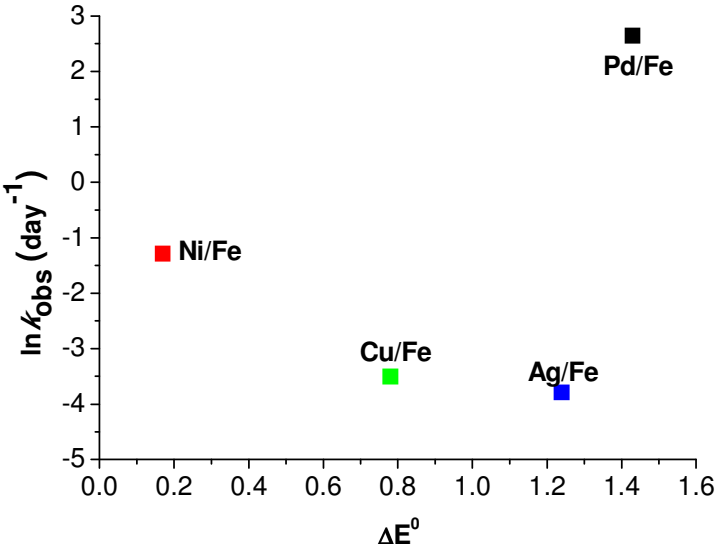

Figure 49 Reaction standard potential (ΔE°) vs lnk_{obs} for 1,2,4-TBB

The $1/k_{obs}$ (the observed rate constants) for 1,2,4-TBB debromination by different bimetallic particles were plotted against ΔH_{sol} and a nearly linear correlation (R^2=0.920) was found as shown in Figure 50a. No obvious correlation was identified between the heat of hydrogen chemisorption ΔH_{chem} and $\ln k_{obs}$ (Figure 50Figure 50b). This is consistent with our finding for 1,2,4-TCB dechlorination by different bimetallic particles. It demonstrates again that the catalytic effect of the second metal in the bimetallic particles has a strong correlation with their ability for hydrogen uptake.

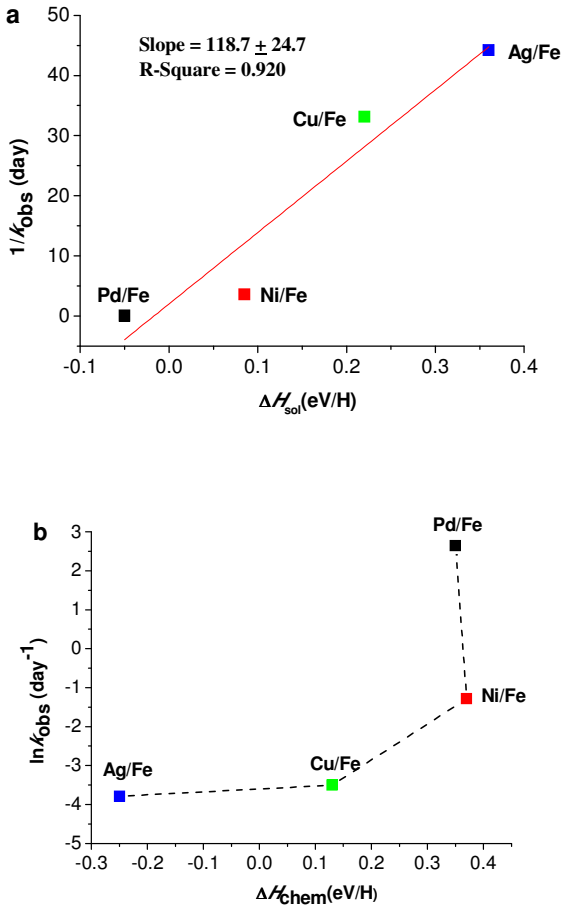

Figure 50 The heat of hydrogen solution ΔH_{sol} vs. $1/k_{obs}$ (the observed rate constants) (a) and the heat of hydrogen chemisorption ΔH_{chem} vs. $\ln k_{obs}$ (b) for 1,2,4-TBB

4.6 Reaction of 1, 2, 4-trifluorobenzene with Pd/Fe

The compound 1,2,4-trifluorobenzene (TFB) was subjected to the same batch experimental procedure with 0.011% Pd/Fe. However, the initial concentration of 124-TFB remained virtually unchanged throughout the reaction period (4 days). No daughter products were identified by GC-MS.

4.7 Debromination of tetrabromobisphenol A by Pd/Fe

4.7.1 Rates of debromination

Control experiments with only ZVI and TBBPA were run at pH 4.2 and pH 7.2 for 24 hours. No loss of TBBPA was detected, indicating no measurable debromination nor adsorption of TBBPA by micron-size ZVI particles. In the presence of Pd/Fe particles, TBBPA was rapidly debrominated in all reactors initiated at different solution pH and dosage conditions. Three intermediate products, tri-BBPA, di-BBPA, mono-BBPA, and one final product (BPA) were detected by HPLC. The summation of the molar concentrations for the reactant and products exceeded 96% of the initial TBBPA for all the reaction systems, suggesting that formation of other products was unlikely, consistent with the observations by Luo et al. (2010) for TBBPA transformation in the presence of Ag/Fe nanoparticles. Figure 51 shows rapid debromination of TBBPA with 4 g L^{-1} of 0.022% Pd/Fe and solution pH 6.2. As shown in the figure, the aqueous phase TBBPA concentration dropped by 85% within the first 2 minutes of the reaction. The reactant was not detected in the solution phase after 20 min, and all intermediate products were converted to BPA within 180 min.

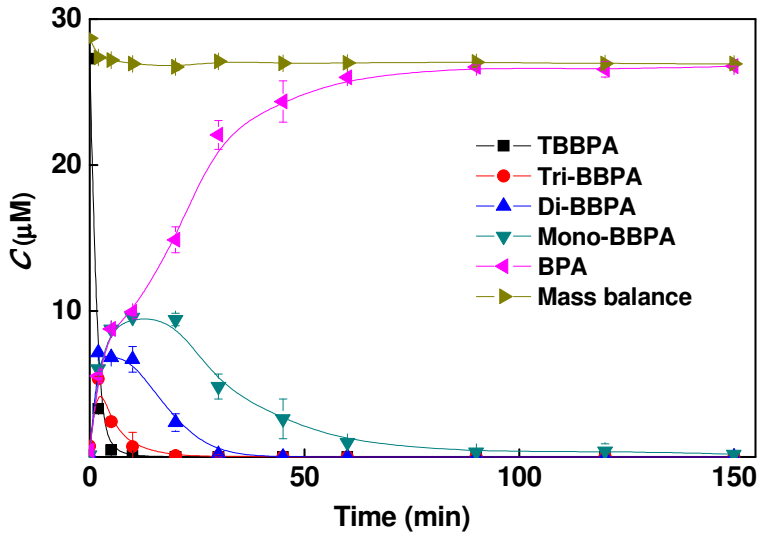

Figure 51 Debromination of TBBPA with 4 g L^{-1} of 0.022% Pd/Fe and solution pH 6.2

The apparent rates of TBBPA transformation could be quantified with a pseudo-first-order kinetic model:

$$\frac{dC}{dt} = -k_{obs}C = -k_{SA}a_sC \qquad \textbf{Equation 15}$$

where C is the aqueous phase TBBPA concentrations (μmol L^{-1}) at time *t* (min); k_{obs} and k_{SA} are the observed rate constant (min^{-1}) and the specific surface area normalized rate constant (L min^{-1} m^{-2}) , respectively; and a_s is the surface area of the bimetallic particles per unit volume of solution phase (m^2 L^{-1}). The integral form of the rate model was used to fit the rate data to obtain the k_{obs} value for TBBPA debromination with the Pd/Fe particles in a given reaction condition. The resulting rate constants, along with reaction conditions, are listed in Table 18. The effects of Pd coverage, Pd/Fe dosage and solution pH on the observed rates of TBBPA debromination are detailed hereinafter.

Table 18 Apparent rate constants of TBBPA debromination

Parameters	Pd loading (w/w) [f]			Pd/Fe dosage [g]			pH [h]			
	0.011%	0.022%	0.044%	2g/L	3g/L	4g/L	4.2	5.2	6.2	7.2
k_{obs} [a] ($\times 10^{-2}$ min^{-1})	0.880±0.053	7.57±0.63	18.0±0.8	1.85±0.25	4.54±0.31	6.45±0.50	264±3	144±9	55.9±5.1	7.72±0.52
$t_{1/2}$ [b] (min)	78.8	9.2	3.9	37.5	15.3	10.7	0.3	0.5	1.2	9.0
k_{SA} [c] (L min^{-1} m^{-2})	0.102	0.876	2.09	0.428	0.701	0.747	30.5	16.7	6.47	0.894
k_{Pd} [d] ($\times 10$ L min^{-1} g^{-1})	2.00	8.60	10.3	4.20	6.88	7.33	300	164	63.6	8.77
R^2 [e]	0.985	0.973	0.991	0.931	0.981	0.976	0.999	0.992	0.967	0.978

[a] Pseudo-first-order kinetic rate constant for debromination of the TBBPA under different reaction conditions. [b] The half-life of a reaction describes the time needed for half of the reactant to be depleted [c] k_{SA} is specific reduction rate constant; $k_{SA} = k_{obs}/\alpha_s$, where α_s is the surface area concentration of the metal particles (m^2 L^{-1}). [d] k_{Pd} represents the k_{obs} normalized by the Pd loading. [e] R^2 is coefficient of determination from the overall regression analysis. [f] at pH=7.2, with 4g L^{-1} Pd/Fe. [g] at pH=7.2, 0.022%Pd loading. [h] at 0.022% Pd loading, 4g L^{-1} Pd/Fe mass.

4.7.2 Effect of Pd coverage

The rate and the extent of reaction were highly dependent upon the relative amount of Pd loaded on the iron particles. Figure 52 shows the time-dependent concentration profiles for the three different Pd coverages at a bimetallic particle loading 4 g L^{-1}. For the system having the bimetallic particles at 0.011% Pd coverage (Figure 52a), 69% of the initial TBBPA was transformed after 240 min of reaction, and tri- and di-BBPAs were the dominant products, accounting for 33% and 23% of the total molar-based mass balance, respectively. Only 4% of BPA and 9% of mono-BBPA were produced. For the system having the bimetallic particles at 0.022% Pd coverage (Figure 52b), TBBPA was completely transformed after 60 min of reaction, and tri- and di-BBPAs increased initially and reached maxima, then decreased as a function of the reaction time. After 240 min of reaction, tri-BBPA was completely transformed, and di-BBPA, mono-BBPA and BPA accounted for 21%, 55% and 24% of the total mass balance, respectively. For the system having the bimetallic particles at 0.044% Pd coverage (Figure 52c), TBBPA was completely transformed within 20 min; tri-, di- and mono-BBPAs increased initially, reached maxima, then decreased as a function of reaction time. After 240 min of reaction, tri- and di-BBPAs were completely transformed; mono-BBPA and BPA accounted for 29% and 70% of the mass balance, respectively.

The k_{obs} values for the disappearance of TBBPA were 0.880 (±0.053), 7.57 (±0.63) and 18.0 (±0.8) $\times 10^{-2}$ min^{-1} for the bimetallic particles with 0.011%, 0.022% and 0.044% Pd coverage, respectively. Figure 53a shows a linear correlation between k_{obs} values versus the percentage of Pd coverage with a slope of 5.34±0.23 (R^2 = 0.993). Apparently, the debromination rate increased linearly as a function of surface coverage of Pd on the iron particles. This is generally consistent with prior studies of dehalogenation rate involving bimetallic particles including Pd/Fe and Ag/Fe nanoparticles (Luo et al., 2010; Wei et al., 2006; Zhu and Lim, 2007). For instance, Luo et al.

(2010) reported that the debromination rate constant of TBBPA increased with the Ag coverage and a maximal constant was found at the Ag coverage of approximately 3 wt%. They found that the rate constant decreased at Ag coverage greater than 3 wt%. In this study, the optimal Pd coverage was not observed.

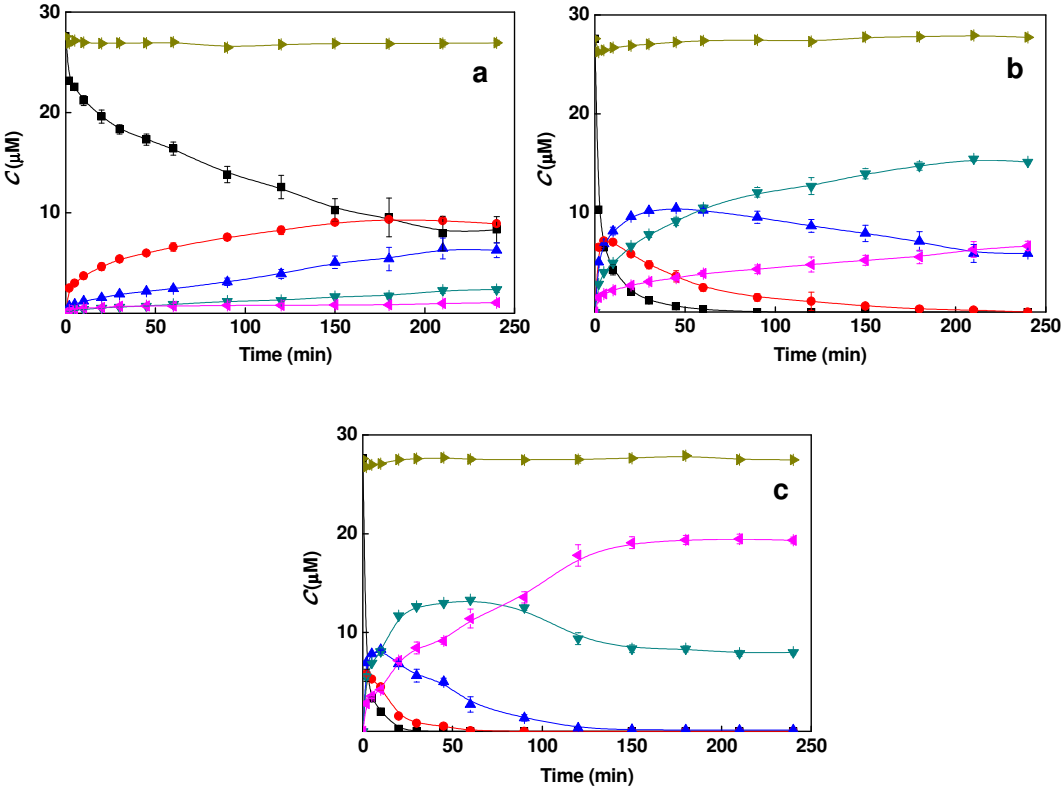

Figure 52 Effect of Pd coverage on TBBPA transformation rates

Experimental conditions: pH 7.2, 4 g L^{-1} of Pd/Fe particles, and Pd coverage of (a) 0.011%, (b) 0.022%, and (c) 0.044%. (Captions: TBBPA - ■ and black line; tri-BBPA - ● and red line; di-BBPA - ▲ and blue line; mono-BBPA - ▼ and dark cyan line; BPA - ◀ and magenta line; mass balance - ▶ and dark yellow line).

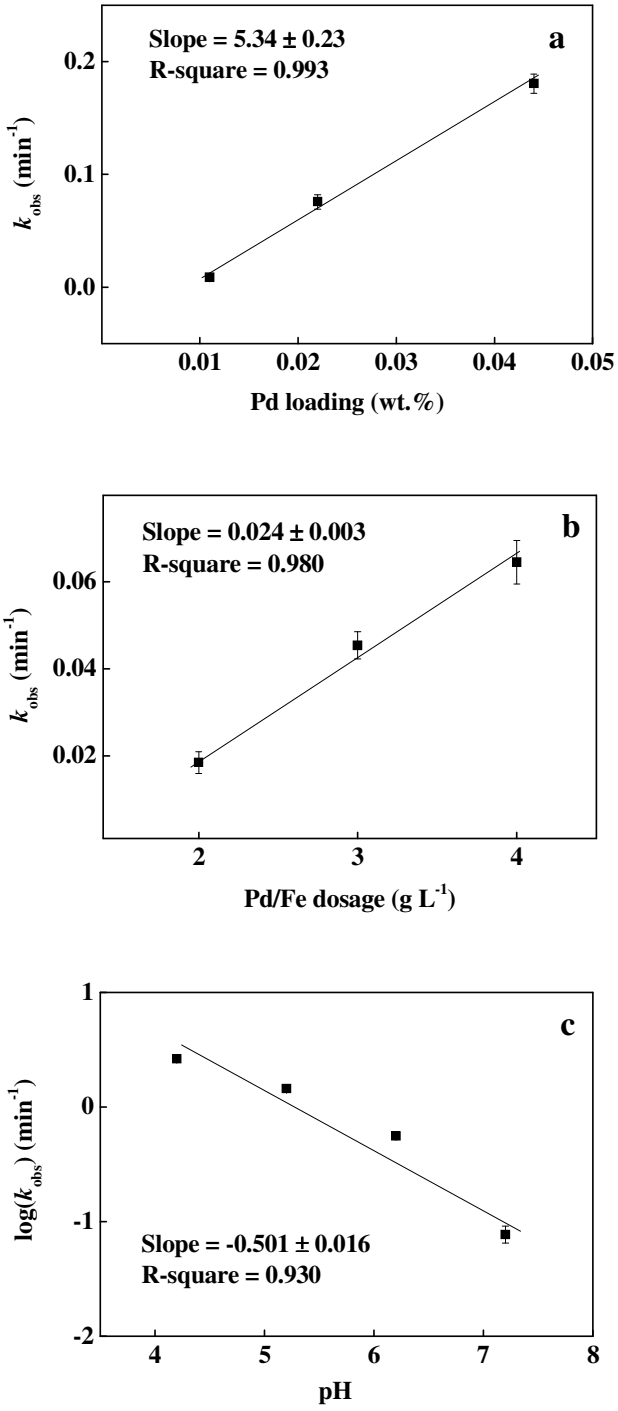

Figure 53 TBBPA: correlations between the rate constants (k_{obs}) and the Pd loading (a), k_{obs} and the Pd/Fe dosage (b), and log k_{obs} and the solution pH (c)

4.7.3 Effect of bimetallic particle dosage

The rate and extent of the reaction were also dependent upon the dosage of the Pd/Fe particles. Figure 54 shows three time dependent concentration profiles for the systems having loadings of 2, 3 and 4 g L^{-1} for the 0.022% Pd/Fe particles. For the system having the particle dosage at 2 g L^{-1} (Figure 54a), 74% of the initial TBBPA was transformed after 60 min of reaction, and the concentrations of the intermediate products increased slowly as reaction time increased. At 60 min, tri-, di-, mono- and BPA accounted for 29%, 24%, 13% and 7% of the total mass balance, respectively. For the system having the particle dosage at 3 g L^{-1} (Figure 54b), 93% of initial TBBPA was transformed after 60 min of reaction, and tri-BBPA increased initially and reached a maximum, then decreased as time proceeded. After 60 min of reaction, tri-BBPA, di-BBPA, mono-BBPA and BPA accounted for 23%, 32%, 25% and 14% of the mass balance, respectively. For the system with particle dosage at 4 g L^{-1} (Figure 54c), TBBPA was transformed completely within 60 min of reaction; tri- and di-BBPAs increased initially and reached a maximum, then decreased. After 60 min of reaction, tri-BBPA, di-BBPA, mono-BBPA and BPA accounted for 4%, 21%, 44% and 31% of the mass balance, respectively.

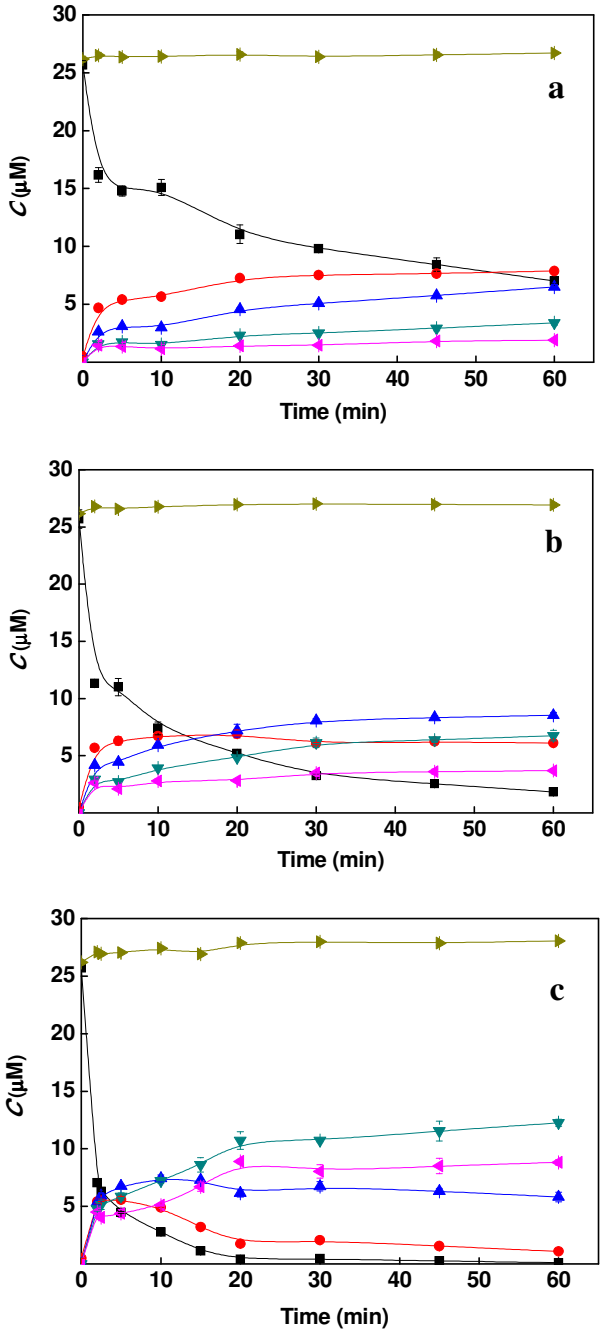

Figure 54 The effect of bimetallic particle dosage on the rate of TBBPA debromination (0.022% Pd/Fe and solution pH 7.2)

(a) 2 g L^{-1}, (b) 3 g L^{-1}, and (c) 4 g L^{-1} (captions: TBBPA - ■ and black line; tri-BBPA - ● and red line; di-BBPA - ▲ and blue line; mono-BBPA - ▼ and dark cyan line; BPA - ◀ and magenta line; mass balance - ▶ and dark yellow line).

The k_{obs} values for the disappearance of TBBPA were 1.85 (±0.25), 4.54 (±0.31) and 6.45 (±0.50) $\times 10^{-2}$ min^{-1} for the particle dosages with 2 g L^{-1}, 3 g L^{-1} and 4 g L^{-1}, respectively. Figure 53b shows a linear correlation between k_{obs} (min^{-1}) values versus the dosage (g L^{-1}) of Pd/Fe with a slope of 0.024±0.003 (R^2 = 0.980). The linear correlation between the initial particle dosage of Pd/Fe particles and TBBPA debromination rate constants (k_{obs}) was evident (Figure 53b). When the Pd/Fe particle loading increased from 2 g L^{-1} to 4 g L^{-1}, the k_{obs} value increased from 0.0185 to 0.0645 (min^{-1}) (Table 18). The surface area normalized k_{SA} values for the three systems ranged from 0.428 to 0.747 L min^{-1} m^{-2}, and the Pd normalized k_{Pd} value increased from 42 to 73.3 (L min^{-1} g^{-1}), indicating that the debromination rate of TBBPA was closely related to the total Pd site on ZVI surface.

4.7.4 Effect of solution pH

The rate and extent of the reaction were highly affected by the solution pH. Figure 55 shows the time dependent concentration profiles tested at four different solution pH conditions for the systems containing 4 g L^{-1} of 0.022% Pd/Fe. At solution pH 4.2 and 5.2 (Figure 55a and Figure 55b), TBBPA was completely transformed into BPA after 10 min of reaction and no other intermediate products were detected. At solution pH 6.2 (Figure 55c), TBBPA was completely transformed within 10 min of reaction. From 0 to 60 min., the concentrations of the three intermediate products increased initially and reached maxima, then decreased as reaction time proceeds. After 60 min of reaction, tri- and di-BBPA were all not-detected, and mono-BBPA and BPA accounted for 4% and 96% of the total molar based mass balance, respectively. At solution pH 7.2 (Figure 55d), 99% of initial TBBPA was transformed after 60 min of the reaction. From 0 to 60 min, tri-BBPA increased initially and reached a maximum, then decreased as the reaction time proceeds. After 60 min, tri-BBPA, di-BBPA, mono-BBPA and BPA accounted for 9%,

37%, 38% and 14% of the mass balance, respectively. Apparently, the lower solution pH favored faster rates and greater extent of debromination of both reactant and intermediate products.

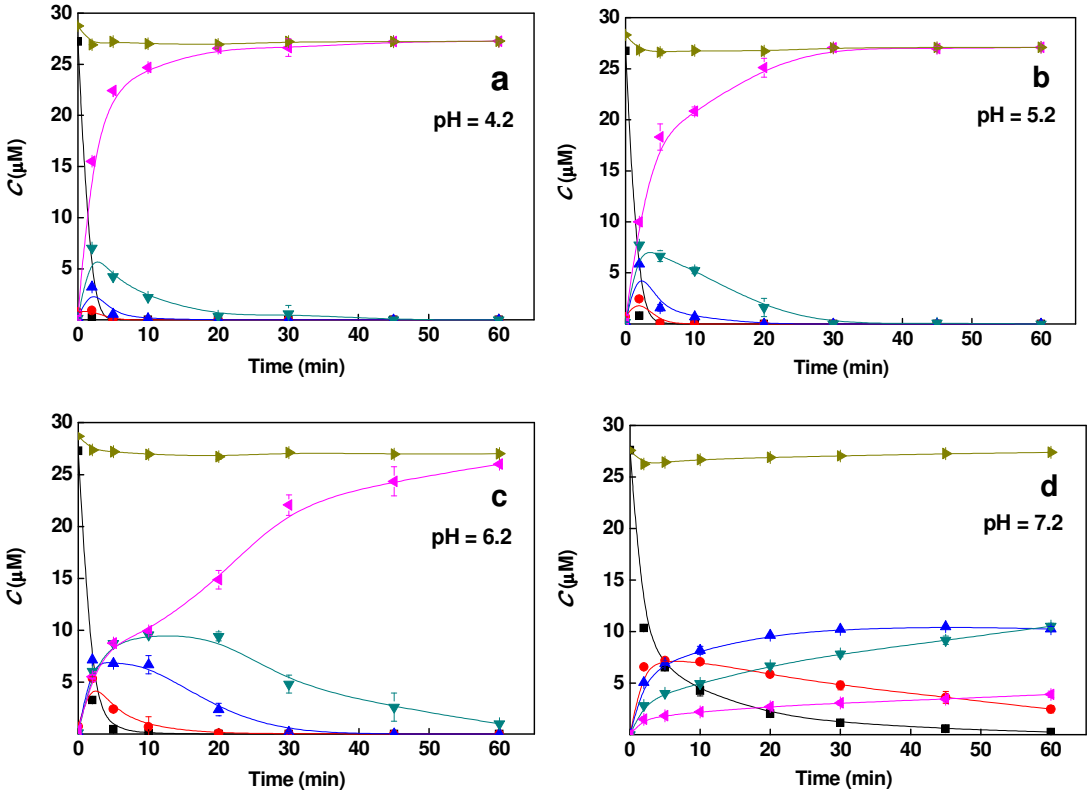

Figure 55 The effect of solution pH on the rate of TBBPA debromination (4 g L^{-1} of 0.022% Pd/Fe)

(Captions: TBBPA - ■ and black line; tri-BBPA - ● and red line; di-BBPA - ▲ and blue line; mono-BBPA - ▼ and dark cyan line; BPA - ◀ and magenta line; mass balance - ▶ and dark yellow line).

The best fit k_{obs} values for the disappearance of TBBPA were 264 (±3), 144 (±9), 55.9 (±5.1) and 7.72(±0.52) $\times 10^{-2}$ min^{-1} for the solution pH 4.2, 5.2, 6.2 and 7.2, respectively (Table 18). Figure 53c shows a linear correlation between logk_{obs} (min^{-1}) values versus the solution pH. The slope of the best fit shown in Figure 53c is -0.501±0.008 (R^2 = 0.930). It shows that the lower solution pH results in faster degradation rate of TBBPA, which is consistent with the reaction mechanisms summarized in the following section. Similar solution pH dependence of apparent reaction rates was reported in the literature. Fang and Al-Abed (2008) studied the dechlorination of 2-chlorobiphenyl by Pd/Fe bimetallic particles. We reprocessed their rate data and found a linear

correlation between log *k* values versus the solution pH (from 3-7) with slopes of -0.149 (R^2 = 0.812) and -0.075 (R^2 = 0.828). Xu et al. (2012) investigated 4-chlorophenol reduction by Ni/Fe bimetallic particles. According to our regression of their rate data, there existed a linear correlation between log k values and the solution pH (from 2-7) with a slope of -0.185 (R^2 = 0.912). Bokare et al. (2008) reported a linear correlation between log k values versus the solution pH (from 2-6) with a slope of -0.021 (R^2 = 0.987) for reductive degradation of azo dye Orange G by Ni/Fe bimetallic nanoparticles. However, completely opposite pH dependence also has been observed in dehalogenation reactions. Luo et al. (2010) found that the rate constant decreased with increasing solution pH (4-8) in debromination of TBBPA by Zn/Fe nanoparticles, yielding a positive linear correlation between log k values and the solution pH with a slope of 0.08 (R^2=0.895). Wang et al. (2009) suggested that the optimal pH value for the highest dechlorination efficiency of chlorinated methanes by Pd/Fe nanoparticles was 7, rather than at acidic conditions. They explained that at acidic conditions, the contact (or adsorption) between target pollutants and nanoparticles may be hindered by minute H_2 bubbles produced from rapid corrosion of iron.

Low solution pH contributes to faster debromination of TBBPA in two aspects, promoting iron corrosion and preventing formation of passivation layers on bimetallic particle surfaces. The reactions of Fe^0 with H_2O can be expressed with following equations:

$$Fe^0 + 2H^+ \rightarrow Fe^{2+} + H_2 \quad \text{(in acidic solution)} \qquad \text{Equation 16}$$

$$Fe^0 + 2H_2O \rightarrow Fe^{2+} + H_2 + 2OH^- \quad \text{(in neutral or alkaline solution)} \qquad \text{Equation 17}$$

Under acidic conditions, zero valent iron has greater reactivity in terms of hydrogen production. More hydrogen produced in the corrosion reaction of iron is adsorbed at the Pd surface and dissociated into atomic H* to accelerate the dehalogenation process of TBBPA. Besides, a lower solution pH favors higher solubility of iron species in water and slows formation of iron-based passivation layers on the surface of Fe or Pd/Fe.

4.7.5 Mechanisms

Based on findings of this work and also prior studies on Pd/Fe dehalogenation in the literature (Graham and Jovanovic, 1999; Jovanovic et al., 2005; Mackenzie et al., 2006), the mechanisms of dehalogenation by the Pd/Fe bimetals are delineated here. The Pd-catalyzed debromination reaction and the overall debromination reaction process can be represented by these equations below:

$$Fe^0 + 2H_2O \rightarrow Fe^{2+} + 2OH^- + H_2 \qquad \textbf{Equation 18}$$

$$H_2 \xrightarrow{Pd} 2H* \qquad \textbf{Equation 19}$$

$$Fe^0 \rightarrow Fe^{2+} + 2e^- \qquad \textbf{Equation 20}$$

$$2H^+ + 2e \xrightarrow{Pd} 2H* \qquad \textbf{Equation 21}$$

$$BPA\text{—}Br_n + 2H* \rightarrow BPA\text{—}Br_{n-1} + Br^- + H^+ \qquad \textbf{Equation 22}$$

where BPA–Br_n (n = 1, 2, 3, 4) is TBBPA and its debromination products. In this study, GC-MS analysis of intermediates and final products revealed the reductive transformation of the TBBPA to produce tri-BBPA, di-BBPA, mono-BBPA and BPA.

It is known that the reductive dehalogenation occurs at the surface of Pd/Fe particles (Grittini et al., 1995; Guasp and Wei, 2003; Mackenzie et al., 2006) and that the Pd on the iron surface acts as a collector of hydrogen gas produced by the reaction of iron corrosion in water. The molecular hydrogen on the surface then partially dissociates to H atoms (H*) (Eq. 19, 21), which are primary reactive species for reduction (Zhu and Lim, 2007). When TBBPA and its intermediate products are adsorbed on the surface of the bimetallic particles, the H* produced could then attack the organic molecules via electrophilic H addition to the double bond of the benzene ring, followed by the C-Br scission. The Pd/Fe bimetallic particles have high surface energy and activity that facilitate breakage of the C–Br bond.

During the debromination reaction, the total amount of Pd added to the reactor appeared to be the dominating factor. As summarized in prior sections, the higher Pd dosage led to more complete of TBBPA transformation to BPA. Moreover, linear correlations were observed between the k_{obs} values and Pd surface coverage (Figure 53a) and the Pd/Fe dosage (Figure 53b), indicating high dependence of the observed rates of TBBPA debromination on the amount of Pd in the reactors. As shown in Figure 56, the k_{obs} (min^{-1}) values measured at constant solution pH (7.2) for all the six reaction systems correlate linearly with the Pd dosage, with a slope of 126±5 (R^2 = 0.992). It shows that, regardless of Pd/Fe particle dosage or Pd surface coverage, the greater amount of Pd resulted in proportionally faster degradation rate of TBBPA. This is generally consistent with the results reported in previous studies (Liu et al., 2001; Wei et al., 2006; Zhu and Lim, 2007). In addition, our control experiments showed no measurable debromination of TBBPA with unpalladized ZVI at pH 7.2, suggesting Pd is likely the active site on the surface responsible for the reaction. As mentioned above, atomic hydrogen is likely responsible for the bimetallic reactivity and that the metals such as Pd on the iron particle surface serves as a collector of hydrogen gas that results from the corrosion of Fe. Palladium is the most effective metal in terms of the ability to absorb hydrogen into its lattice and to maintain a high surface concentration of hydrogen (Lawson et al., 1991).

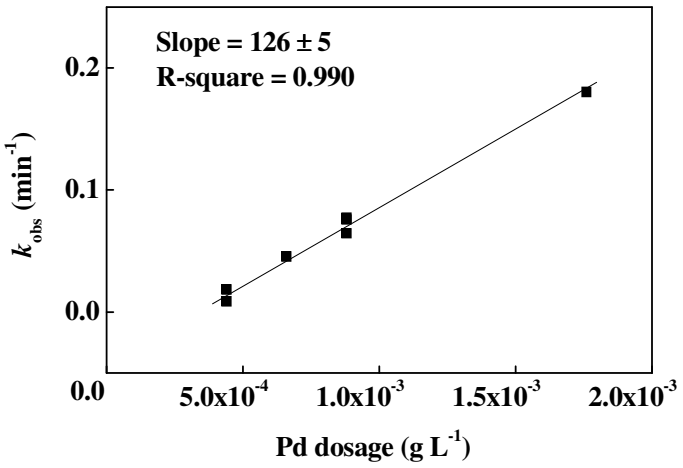

Figure 56 Correlation between the rate constant (k_{obs}) for TBBPA debromination and the Pd dosage.

4.8 Degradation of tetrachlorobisphenol A by Pd/Fe

4.8.1 Rates of dechlorination

Control experiments with only ZVI and TCBPA were run at pH 4.0 for 24 hours. No loss of TCBPA was detected, indicating no measurable dechlorination nor adsorption of TCBPA by micron-size ZVI particles. In the presence of Pd/Fe particles, TCBPA was quickly dechlorinated in the reactors initiated with different TCBPA concentrations and different dosage conditions. Three intermediate products, tri-CBPA, di-CBPA, mono-CBPA, and one final product (BPA) were detected by HPLC. The summation of the molar concentrations for the reactant and products exceeded 98% of the initial TCBPA for all the reaction systems, suggesting that formation of other products was unlikely. Figure 57 shows rapid dechlorination of TCBPA with 4 g L^{-1} of 0.044% Pd/Fe and solution pH 4.0. As shown in the figure, the aqueous phase TCBPA concentration dropped by 85% within the first 30 minutes of the reaction. The final product was BPA, accounting for 85% of the total mass at the end of the 90-minute reaction. The intermediates formed included tri-CBPA, di-CBPA and mono-CBPA.

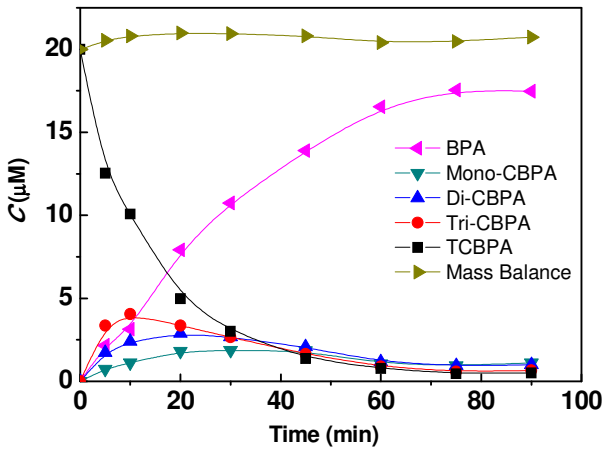

Figure 57 Dechlorination of TCBPA (20 μM) with 4 g L^{-1} of 0.044% Pd/Fe and solution pH 4.0

The apparent rates of TCBPA transformation could be quantified with a pseudo-first-order kinetic model:

$$\frac{dC}{dt} = -k_{obs}C = -k_{SA}a_s C \qquad \textbf{Equation 23}$$

where C is the aqueous phase TCBPA concentrations (μmol L^{-1}) at time *t* (min); k_{obs} and k_{SA} are the observed rate constant (min^{-1}) and the specific surface area normalized rate constant (L min^{-1} m^{-2}) , respectively; and a_s is the surface area of the bimetallic particles per unit volume of solution phase (m^2 L^{-1}). The integral form of the rate model was used to fit the rate data to obtain the k_{obs} value for TCBPA debromination with the Pd/Fe particles in a given reaction condition. The resulting rate constants, along with reaction conditions, are listed in Table 19. The effects of Pd coverage, Pd/Fe dosage and initial concentration of TCBPA on the observed rates of TCBPA dechlorination are detailed hereinafter.

Table 19 Apparent Rate Constants of TCBPA Dechlorination

Parameters	**Initial TCPBA concentration (μM)** [f]					**Pd/Fe dosage (gL^{-1})** [g]				**Pd loading (w/w)** [h]			
	5	10	15	20	25	2	3	4	5	0.0055%	0.011%	0.022%	0.044%
k_{obs} [a] ($\times 10^{-2}$ min^{-1})	13.1 ±1.3	11.5 ±7.1	6.66 ±1.61	5.55 ±0.49	3.89 ±0.63	0.669 ±0.085	2.15 ±0.24	4.13 ±0.97	5.55 ±0.49	0.0682 ±0.0168	0.141 ±0.032	0.622 ±0.211	5.55 ±0.49
k_{SA} [b] (L min^{-1} m^{-2})	1.52	1.33	0.772	0.643	0.451	0.078	0.249	0.479	0.643	0.008	0.016	0.072	0.643
k_{Pd} [c] (L min^{-1} g^{-1})	61.2 ±1.4	55.1 ±7.8	38.7 ±4.5	27.7 ±2.2	18.4 ±3.0	8.0 ±1.3	19.5 ±1.1	30.8 ±1.4	31.1 ±2.0	6.4±1.6	7.2±1.5	14.3±1.5	26.9±4.0
$t_{1/2}$ [d] (min)	5.27	6.00	10.4	12.5	17.8	104	32.2	17	12.5	1017	493	111	12.5
R^2 [e]	0.999	0.898	0.957	0.994	0.974	0.984	0.988	0.947	0.994	0.943	0.951	0.897	0.994

[a] Pseudo-first-order kinetic rate constant for dechlorination of the TCBPA under different reaction conditions. [b] k_{SA} is specific reduction rate constant; $k_{SA} = k_{obs}/\alpha_s$, where α_s is the surface area concentration of the metal particles (m^2 L^{-1}). [C] k_{Pd} represents the k_{obs} normalized by the Pd loading. [d] The half-life of a reaction describes the time needed for half of the reactant to be depleted. [e] R^2 is coefficient of determination from the overall regression analysis. [f] at pH=4.0, 0.044% Pd loading, 5g L^{-1} Pd/Fe mass. [g] at pH=4.0, 0.04%Pd loading, 20μM initial TCBPA. [h] at pH=4.0, with 5g L^{-1} Pd/Fe, 20μM initial TCBPA.

4.8.2 Effect of bimetallic particle dosage

Similar to the debromination of TBBPA, the rate and the extent of dechlorination of TCBPA were dependent on the dosage of the Pd/Fe particles. Figure 58 shows three time dependent concentration profiles for the systems having loadings of 2, 3, 4 and 5 g L^{-1} for the 0.044% Pd/Fe. For the system having the particle dosage at 2 g L^{-1} (Figure 58a), 52% of the initial TCBPA was transformed after 90 min of reaction, and the concentrations of the intermediate products increased slowly as reaction time increased. At 90 min, tri-, di-, mono- and BPA accounted for 25%, 15%, 7% and 11% of the total mass balance, respectively. For the system having the particle dosage at 3 g L^{-1} (Figure 58b), 89% of initial TCBPA was transformed after 90 min of reaction, and tri-CBPA increased initially and reached a maximum, then decreased as time proceeds. After 90 min of reaction, tri-CBPA, di-CBPA, mono-CBPA and BPA accounted for 12%, 13%, 11% and 59% of the mass balance, respectively. For the system with particle dosage at 4 g L^{-1} (Figure 58c), 97% TCBPA was transformed within 90 min of reaction; tri- and di-CBPAs increased initially and reached a maximum, then decreased as time proceeds. After 90 min of reaction, tri-CBPA, di-CBPA, mono-CBPA and BPA accounted for 3%, 5%, 6% and 87% of the mass balance, respectively. For the system having the particle dosage at 5 g L^{-1} (Figure 58d), 99% TCBPA was transformed within 90 min of reaction, tri- and di-CBPAs increased initially and reached a maximum, then decreased as time proceeds. After 90 min of reaction, tri-CBPA, di-CBPA, mono-CBPA and BPA accounted for 1%, 1%, 1% and 98% of the mass balance, respectively.

The k_{obs} values for the disappearance of TCBPA were 0.669 (±0.085), 2.15 (±0.24), 4.13 (±0.97) and 5.55 (±0.49) $\times 10^{-2}$ min^{-1} for the particle dosages with 2 g L^{-1}, 3 g L^{-1} 4 g L^{-1} and 5 g L^{-1} respectively. Figure 60a shows a linear correlation between k_{obs} (min^{-1}) values versus the dosage (g L^{-1}) of Pd/Fe with a slope of 0.0216±0.001 (R^2 = 0.980). The linear correlation between the particle dosage of Pd/Fe particles and TCBPA dechlorination rate constants (k_{obs}) was evident

(Figure 60a). When the Pd/Fe particle loading increased from 2 g L^{-1} to 5 g L^{-1}, the k_{obs} value increased from 0.669 to 5.55 (min^{-1}) (Table 19). The surface area normalized k_{SA} values for the four systems ranged from 0.078 to 0.643 L min^{-1} m^{-2}, and the Pd normalized k_{Pd} value increased from 8.0 to 31.1 (L min^{-1} g^{-1}), indicating that the dechlorination rate of TCBPA was closely related to the total Pd site on ZVI surface.

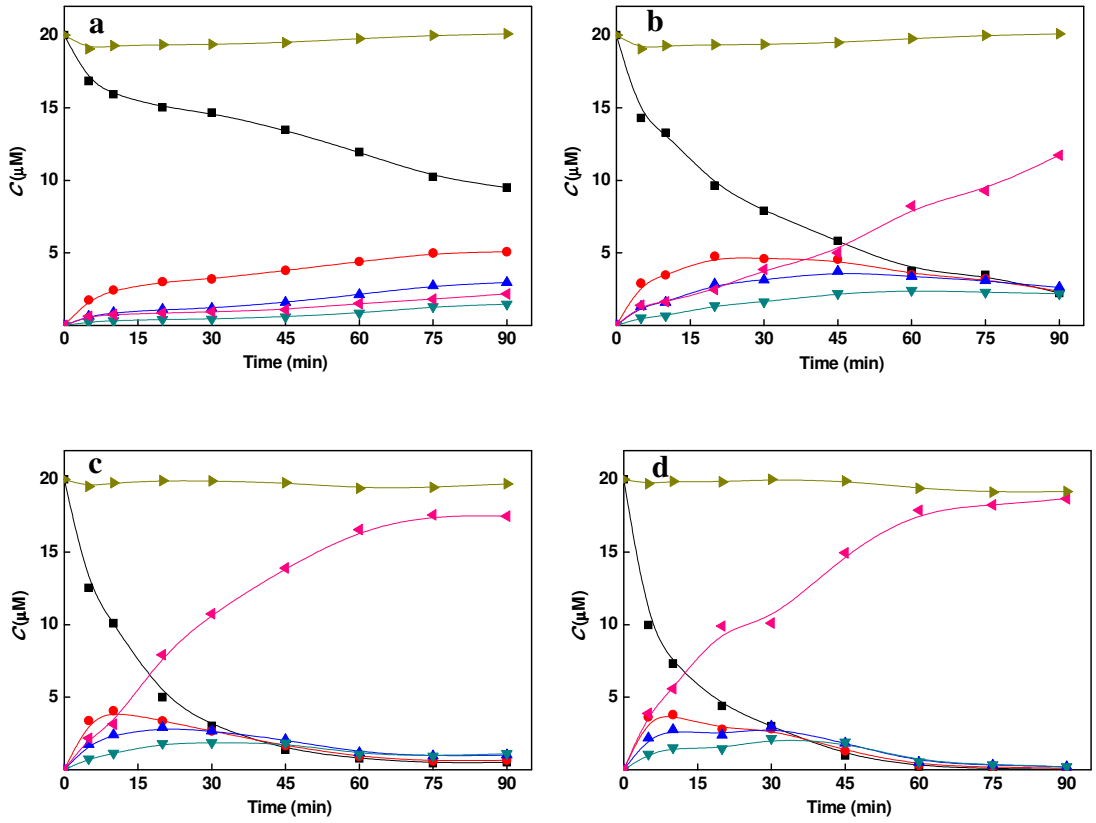

Figure 58 The effect of Pd/Fe dosage on TCBPA transformation rates.

Experimental conditions: pH 4.0, 0.044% Pd coverage, 20 μM initial concentration of TCBPA and Pd/Fe dosage of (a) 2g L^{-1}, (b) 3g L^{-1}, (c) 4g L^{-1} and (d) 5g L^{-1}. (captions: TCBPA - ■ and black line; tri-CBPA - ● and red line; di-CBPA - ▲ and blue line; mono-CBPA - ▼ and dark cyan line; BPA - ◀ and magenta line; mass balance - ▶ and dark yellow line).

4.8.3 Effect of initial concentration of TCBPA

It was found that the rate and the extent of dechlorination of TCBPA were dependent on the initial concentration of TCBPA in the reactor. Figure 59 shows five time-dependent concentration

profiles for the systems having 5 g L^{-1} of the 0.044% Pd/Fe with initial TCBPA concentrations of 5, 10, 15, 20 and 25 µmolL^{-1}.

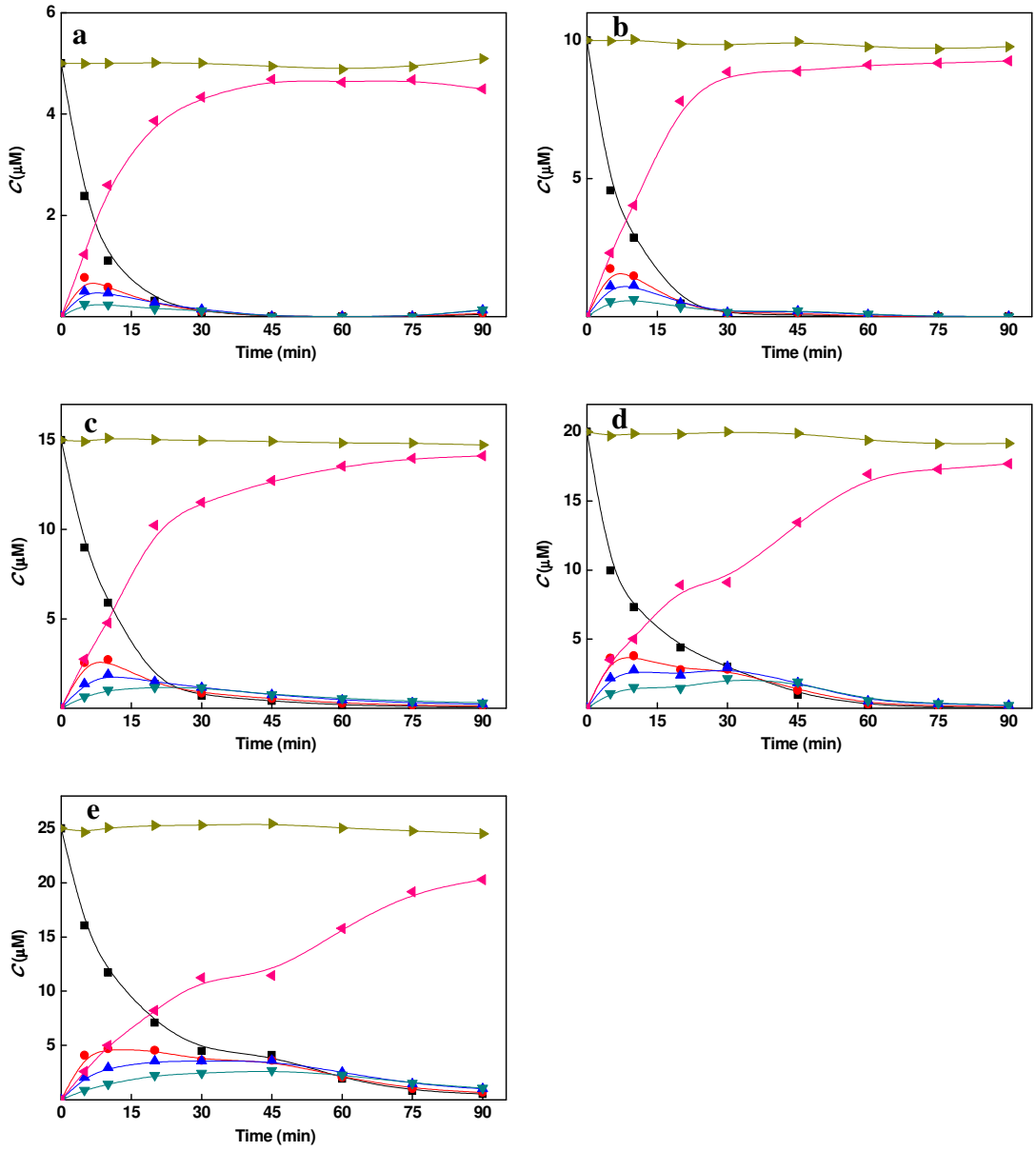

Figure 59 The effect of initial concentration on the rate of TCBPA dechlorination

Experimental conditions: pH 4.0, 0.044% Pd coverage, Pd/Fe dosage of 5g L^{-1} and initial concentration of TCBPA (a) 5 µM, (b) 10 µM, (c) 15 µM, (d) 20 µM and (e) 25 µM (captions: TBBPA - ■ and black line; Tri-BBPA - ● and red line; Di-BBPA - ▲ and blue line; mono-BBPA - ▼ and dark cyan line; BPA - ◀ and magenta line; mass balance - ▶ and dark yellow line).

The k_{obs} values for the disappearance of TCBPA were 13.1 (±1.3), 11.5 (±7.1), 6.66 (±1.61), 5.55 (±0.49), and 3.89 (±0.63) ×10^{-2} min^{-1} for the initial TCBPA concentration of 5, 10, 15, 20 and 25

μmolL^{-1}respectively. Figure 60b shows a linear correlation between k_{obs} (min^{-1}) values versus the initial TCBPA concentrations (μmolL^{-1}) with a slope of -0.0048±0.003 (R^2 = 0.997). The negative correlation indicates the higher the initial TCBPA concentration, the less percentage of TCBPA converted. This is consistent with the results on TCE dechlorination using nano-ZVI (Liu et al., 2007) and chlorophenol dechlorination by nano-ZVI (Cheng R, 2007).

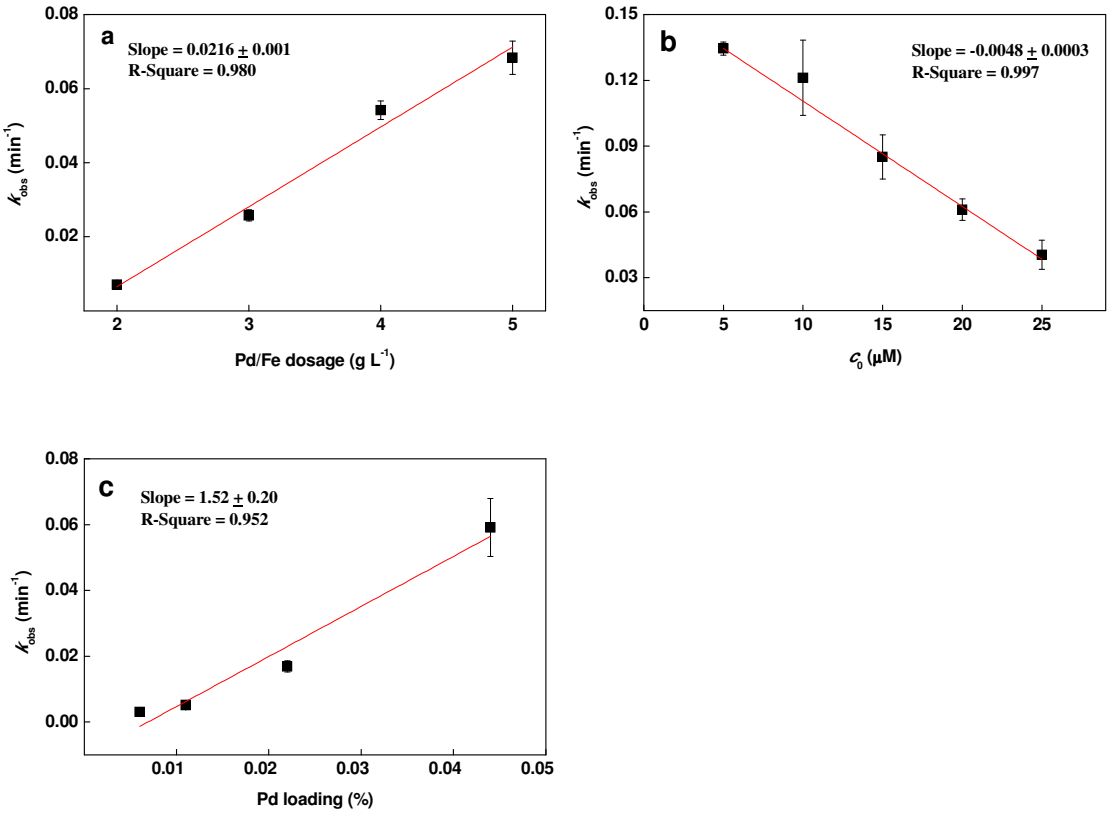

Figure 60 TCBPA: correlations between the rate constants (k_{obs}) and the Pd/Fe dosage (a), k_{obs} and initial TCBPA concentration (b), and k_{obs} and Pd loading (c)

4.8.4 Effect of Pd coverage

Similar to the results of TBBPA debromination, the rate and the extent of TCBPA dechlorination were dependent upon the relative amount of Pd loaded on the iron particles. Figure 61 shows the

time-dependent concentration profiles for the four different Pd coverages at a particle loading 5 g L^{-1}. For the system having the bimetallic particles at 0.0055% Pd coverage (Figure 61a), 11% of the initial TCBPA was dechlorinated after 120 min of reaction. Tri-CBPA was the dominant product, accounting for 10% of the total molar-based mass balance. Only 2% of Di-CBPA, 0.7 % of mono-CBPA and 0.5% of BPA were produced. For the system having the bimetallic particles at 0.011% Pd coverage (Figure 61b), 21% of the initial TCBPA was transformed after 120 min of reaction, and tri-CBPA was the dominant product, accounting for 18% of the total molar-based mass balance. Only 4% of di-CBPA, 0.8% of mono-CBPA and 1.3% BPA were produced. For the system having the bimetallic particles at 0.022% Pd coverage (Figure 61c), 58% of initial TCBPA was transformed within 120 min; tri- and di-CBPA were the dominant products, accounting for 37% and 18% of the total molar-based mass balance. Only 6% of mono-CBPA and 5% BPA were produced. For the system having the bimetallic particles at 0.044% Pd coverage (Figure 61d), 99% TCBPA was transformed within 90 min of reaction, tri- and di-CBPAs increased initially and reached a maximum, then decreased as time proceeds. After 90 min of reaction, tri-CBPA, di-CBPA, mono-CBPA and BPA accounted for 1%, 1%, 1% and 98% of the mass balance, respectively.

The k_{obs} values for the disappearance of TCBPA were 0.0682 (±0.0168), 0.141 (±0.032), 0.622 (±0.211) and 5.55 (±0.49) $\times 10^{-2}$ min^{-1} for the bimetallic particles with 0.0055%, 0.011%, 0.022% and 0.044% Pd coverage, respectively. Figure 60c shows a linear correlation between k_{obs} (min^{-1}) values versus the percentage of Pd coverage with a slope of 1.52±0.20 (R^2 = 0.952). Apparently, the dechlorination rate increased linearly as a function of surface coverage of Pd on the iron particles.

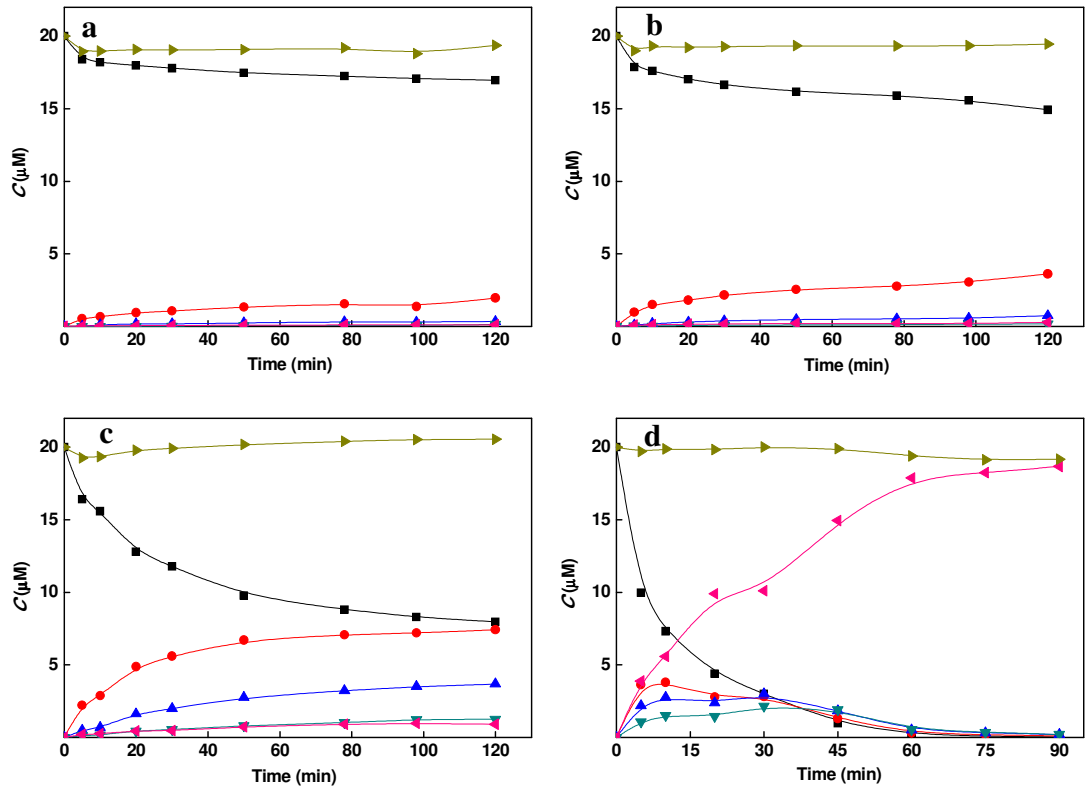

Figure 61 The effect of Pd coverage on the rate of TCBPA dechlorination

Experimental conditions: pH 4.0, Pd/Fe dosage of 5g L^{-1}, 20 μM initial concentration of TCBPA and Pd coverage of (a) 0.0055%, (b) 0.011%, (c) 0.022% and (d) 0.044% (captions**:** TBBPA - ■ and black line; Tri-BBPA - ● and red line; Di-BBPA - ▲ and blue line; mono-BBPA - ▼ and dark cyan line; BPA - ◀ and magenta line; mass balance - ▶ and dark yellow line).

4.8.5 Mechanism

Due to the high similarity observed for the TCBPA dechlorination to the TBBPA debromination, the same reaction mechanism is proposed. A similar correlation between the k_{obs} values and Pd dosage was also observed for TCBPA dechlorination (Figure 62). During the dechlorination reaction of TCBPA, the total amount of Pd added to the reactor appeared to be the dominating factor. As summarized in prior sections, the higher Pd dosage led to more complete transformation of TCBPA to BPA. Moreover, linear correlations were observed between the k_{obs} values and Pd surface coverage (Figure 60c) and the Pd/Fe dosage (Figure 60a), indicating high dependence of the observed rates of TCBPA dechlorination on the amount of Pd in the reactors.

Therefore, the results of TCBPA dechlorination re-emphasize the important role of Pd in the dehalogenation by Pd/Fe bimetallic particles.

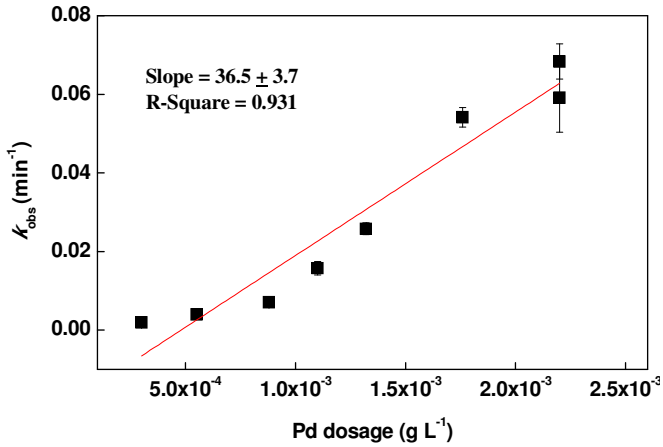

Figure 62 Correlation between the rate constant (k_{obs}) of TCBPA dechlorination and the Pd dosage

4.9 Summary

Bimetallic particles were synthesized at bench scale by chemically depositing a second transitional metal on the surface of zero valent iron. Surface characterization of the synthesized bimetallic particles revealed that the particles were not uniform in size and they appeared to be in small clusters. Elemental analysis of the second metal by XPS confirmed that the second metal was successfully deposited on the surface of iron as zero valent metal.

It was demonstrated that the synthesized bimetallic particles enhanced the observed dehalogenation rates of chlorinated/brominated benzenes compared to zero valent iron. In general, brominated benzenes reacted faster than chlorinated benzenes under the same conditions. The reactivity trend for 124-TCB/124-TBB was Pd/Fe >> Ni/Fe > Cu/Fe > Ag/Fe ≈ Fe. Under the same batch experimental conditions, 124-TFB remained virtually unchanged throughout the reaction period (4 days) and no daughter products were identified by GC-MS.

Reaction rate constants for 124-TCB/124-TBB with 4 different bimetallic particles were used to test two popular hypotheses for the rate enhancement by the second transitional metal. The results showed contrary observations against the galvanic couple hypothesis. However, a near linear correlation (R^2=0.937) was established between the $1/k_{obs}$ and the heat of hydrogen solution. The correlation between $\ln k_{obs}$ and the heat of hydrogen chemisorption was substantially less strong. This indicated that the hydrogen absorbed inside the metal played a more important role than the hydrogen adsorbed on the surface in the catalytic activity of the second noble metal. The results demonstrated the importance of hydrogen in the dehalogenation reaction by bimetallic particles and strongly supported that hydrogen atoms resulting from iron corrosion are the primary reactive species for reduction.

It was demonstrated that the debromination of TBBPA by Pd/Fe bimetallic particles of micron sizes was rapid at ambient temperature whereas ZVI alone showed little reaction under the same conditions. The debromination rate of TBBPA followed a pseudo-first-order rate model and the rate constant k_{obs} was proportional to the Pd/Fe particle dosage and surface loading of Pd. Lower solution pH also favored the debromination of TBBPA. More importantly, the k_{obs} values measured at constant solution pH correlated linearly with the Pd mass introduced to the reactors, regardless of Pd/Fe particle dosage or Pd surface coverage. The greater amount of Pd also resulted in more complete of transformation of TBBPA to BPA within very short time periods.

It was shown that the dechlorination of TCBPA by Pd/Fe bimetallic particles of micron sizes was rapid at ambient temperature whereas ZVI alone showed little reaction under the same conditions. The dechlorination rate of TCBPA followed a pseudo-first-order rate model and the rate constant k_{obs} was proportional to the Pd/Fe particle dosage and surface loading of Pd. Higher initial TCBPA concentrations had a negative impact on the k_{obs}. Similar to the debromination of TBBPA, the k_{obs} values measured for TCBPA dechlorination at constant solution pH correlated linearly with the Pd mass introduced to the reactors, regardless of Pd/Fe particle dosage or Pd

surface coverage. The greater amount of Pd also resulted in more complete of transformation of TCBPA to BPA within a short time period.

5 Chapter 5 Quantitative Structure–Activity Relationship Modeling

5.1 Introduction

Reductive transformation is the dominant reaction pathway for many organic pollutants in anoxic environments. Most interest in reductive transformations of environmental chemicals involves dehalogenation of chlorinated aliphatic or aromatic contaminants and the reduction of nitroaromatic compounds (Tratnyek et al., 2003). Recent trends in environmental regulatory strategies dictate that the U.S. Environmental Protection Agency and other regulatory organizations will have to rely more heavily on predictive modeling technologies for carrying out an increasingly complex array of exposure and risk assessments (Tratnyek et al., 2003). Quantitative structure–activity relationships (QSARs) and predictive modeling systems employing QSARs are being used increasingly to predict reductive dehalogenation of chlorinated aliphatics (Butler and Hayes, 2000), toxicity (Moore et al., 2003), potential ecological hazard of organic chemicals (Comber et al., 2003), et al.. However, established QSAR to predict dehalogenation rates of polychlorinated/polybrominated aromatics by ZVI based bimetallic particles is very limited in the literature. It is necessary to develop a theoretical technique to propose the dechlorination/debromination pathways and products, which use certain molecular descriptors calculated directly from chemical structures of the pollutants to indicate the eliminating activity of chlorines/bromines in different substituted positions (Lynam et al., 1998).

Quantum chemical descriptors can be easily obtained by computation to clearly describe specific molecular properties for structurally related compounds, and can also provide insight into the environmental behavior of chemicals not yet synthesized or those that cannot be examined experimentally due to their extremely hazardous nature (Lu et al., 2010). In the following

discussion, we will try to construct a QSAR model to predict reductive dehalogenation rates for polychlorinated benzenes and polybrominated benzenes. The QSAR model will shed light on the understanding of the dehalogenation mechanisms of our synthesized bimetallic particles.

5.2 **Background**

Structure-activity relationships (SARs) are based on the theory that a correlation exists between a chemical's structure and its physical or chemical properties. Three elements comprise the relationship (Walker et al., 2003): (1) a descriptor—this could be a physical property or a chemical property; (2) an end-point being predicted—perhaps another physical or chemical property or a biological activity; and (3) a derived relationship between the descriptors and the endpoint.

The starting point for a QSAR model is a series of compounds (usually congeners) that are related by a common reaction center that is responsible for the reaction of primary interest. The property to be described (predicted) is the dependent variable, referred to here as the response variable. Each member of the set of compounds on which the correlation is based (the training set) is distinguished by secondary differences in chemical structure, usually as differences in substituents. These differences are characterized by one or more independent variables that can be conveniently measured or otherwise determined. The independent variables are called the descriptor variables. When correlation of the response and descriptor variables yields a consistent functional relationship, the resulting fitted equation (the QSAR) can be used as a quantitative model for comparing and predicting properties of related compounds (Tratnyek et al., 2003).

The response variables that are most commonly used in QSARs for reduction reactions are summarized in Table 20. The descriptor variables that are most commonly used in QSARs for reduction reactions are summarized in Table 21.

Table 20 Response variables*

Variable	Description
k_{obs}, k_{FeOOH}, k_{FeS}, $k_{sulfidic}$	Pseudo-first-order reaction rate constants
k_{rel}	Rate constant relative to rate constant of a reference reaction
Q	Quotient of the rate constant for a substrate in the presence of a competing substrate normalized by the rate constant for a reference compound in the presence of the competing substrate
k_{SA}	First-order rate constant for a heterogenous reduction reaction normalized to reactive surface area of the reductant (usually Fe0)
$k^{s}S_{t}$	Product of the rate constant for surface-limited reaction and the total concentration of reactive surface sites
k, k_{FeP}, k_{Jug}	Second-order rate constant for reaction with specific model reductants in homogenous solution

* adapted from Table 1 (Tratnyek et al., 2003)

Table 21 Descriptor variables*

Variable	Description
Fragment properties	
σ, σ^*	Substituent constants for aromatics (various scales)
σ_1	Substitute constants for aliphatics (various scales)
D_{R-X}, *BS, BE, BDE*	Bond energies
Molecular properties	
$E_{1/2}$	Half-wave potentials from voltammetry
E_{LUMO}	Energy of lowest unoccupied molecular orbital
(V)EA, (V)AE	(Vertical) electron affinity or attachment energy
Reaction properties	

Variable	Description
E^2	Reduction potential for 2-electron (half) reaction
E^1	Reduction potential for 1-electron (half) reaction
$\Delta G^{0'}$	Free energy of reaction
k_{other}	Reaction rate constant

* adapted from Table 2 (Tratnyek et al., 2003)

5.3 **Computational method**

All calculations were carried out with the Gaussian 03 program (M.J. Frisch, 2003) running on an Intel Core 2 Duo 3.00 GHz CPU computer equipped with 5.00 GB of internal memory and the Microsoft Windows XP Professional operating system. HyperChem (Release 7.0, Hypercube Inc. 2002) was used as the molecular modeling system for constructing and viewing the molecular structures of all chemicals. Molecular geometry was optimized and quantum chemical descriptors were computed using the B3LYP hybrid functional of DFT (Density Functional Theory) in conjunction with 6-31G(d), a split-valence basis set with polarization function. B3LYP/6-31G(d) were selected because it was reliable in computing structure descriptors of organic compounds containing aromatic rings (Lu et al., 2007; Yang et al., 2006). The B3LYP calculations were performed using the quantum chemical computation software Gaussian 03.

5.4 QSAR modeling for halogenated benzenes

5.4.1 Response variables

Pseudo-first-order reaction rate constants (k_{obs}) were selected as the response variable for this study. Table 22 lists the k_{obs} of 124-TCB, DCBs, MCB, 124-TBB, DBBs and MBB. These k_{obs} were obtained at pH 7.2, with 0.011% Pd/Fe loading and a Pd/Fe dosage of 5g/L.

Table 22 Pseudo-first-order reaction rate constants (k_{obs}) for chemicals of interests

Chemical	k_{obs} (min^{-1})	Chemical	k_{obs} (min^{-1})
1,2,4-TCB	0.0042 ±0.00034	1,2,4-TBB	0.0098±0.00076
1,4-DCB	0.0058 ±0.00032	1,4-DBB	0.0102±0.00066
1,3-DCB	0.0052 ±0.00029	1,3-DBB	0.0110±0.00064
1,2-DCB	0.0049 ±0.00029	1,2-DBB	0.0122±0.00119
MCB	0.0083 ±0.00078	MBB	0.0129±0.00110

5.4.2 Descriptors

Density Functional Theory (DFT) contained in Gaussian 03 was used to compute all quantum chemical descriptors. DFT was selected because it has been widely used in recent applications of quantum chemistry (Lu et al., 2010; Zhou et al., 2005). In addition, the computational time of DFT calculations is now much shorter than before since the computing speed of the personal computer has increased rapidly.

According to chemometrics theory, a QSAR model should include as many relevant descriptors as possible to increase the likelihood of a good characterization for a class of compounds (Wold et al., 2001). The descriptors selected include: the eigenvalue of the highest occupied molecular orbital (E_{HOMO}), the eigenvalue of the lowest unoccupied molecular orbital (E_{LUMO}), molecular total energy (E_T), the electronic spatial extent (R_e), dipole moment (μ), the most positive Mulliken atomic charges on a carbon atom (Q_C^+), the most negative Mulliken atomic charges on a carbon

atom (Q_C^-), and the most positive Mulliken atomic charges on a chlorine/bromine atom (Q_x^+). All the above descriptors were obtained directly in the output files of each Gaussian 03 calculation after full optimization of the molecular structure using B3LYP/6-31G(d) FOPT. The values of these quantum chemical descriptors are listed in Table 23.

The units of energy, dipole moment, atomic charge and extent are hartree, debye, atomic charge unit and atom unit, respectively.

In addition, 3 combinations of frontier molecular orbital eigenvalues, E_{LUMO}–E_{HOMO}, $(E_{LUMO}–E_{HOMO})^2$ and E_{LUMO}+E_{HOMO} were also selected as independent variables.

Table 23 Descriptors for 124-TCB, DCBs, MCB, 124-TBB, DBBs and MBB

Comp.	E_{HOMO}	E_{LUMO}	E_T	R_e	μ	Q_C^+	Q_C^-	Q_x^+
1,2,4-TCB	–0.25445	–0.03758	–1611.0291898	2172.0486	1.4067	–0.062510	–0.125538	0.028829
1,4-DCB	–0.24789	–0.02734	–1151.4396805	1668.9728	0.0000	–0.065084	–0.125425	–0.014284
1,3-DCB	–0.25435	–0.02663	–1151.4395417	1539.6572	1.8073	–0.064481	–0.127202	–0.010686
1,2-DCB	–0.25151	–0.02412	–1151.4357336	1298.0858	2.7792	–0.073860	–0.125725	0.013386
MCB	–0.24641	–0.01255	–691.8449745	902.6424	1.9302	–0.064668	–0.128050	–0.028461
1,2,4-TBB	–0.24727	–0.03672	–7945.5573965	4271.9538	1.1722	0.086094	–0.166994	–0.078575
1,4-DBB	–0.24191	–0.02683	–5374.4572174	3206.0639	0.0000	0.084478	–0.146330	–0.120005
1,3-DBB	–0.24863	–0.02647	–5374.4571668	2785.4179	1.6565	0.080408	–0.164721	–0.115197
1,2-DBB	–0.24564	–0.02422	–5374.454901	1991.9006	2.4541	0.057540	–0.147024	–0.094751
MBB	–0.24192	–0.01259	–2803.3536793	1232.2921	1.8187	0.082135	–0.146362	–0.134064

5.4.3 Quantitative modeling

Since a large number of descriptors were selected in this study, intercorrelation of independent variables (multicollinearity) might become a technical problem. To overcome this problem, the

partial least squares (PLS) regression, a methodology that makes use of all available descriptors as opposed to subset regression, and is useful when the descriptors are strongly collinear, was used (Wold et al., 2001). PLS can find the relationship between a matrix Y and a matrix X by reducing the dimension of the matrices while concurrently maximizing the relationship between them (Chen et al., 2001). PLS modeling consists of simultaneous projections of both the X and Y spaces on low dimensional hyper planes. The coordinates of the points on these hyper planes constitute the elements of the matrices T and U. The analysis has the following objectives:

- To well approximated the X and Y spaces
- To maximized the correlation between X and Y

The PLS model accomplishing these objectives can be expressed as:

$$X = 1 \times \overline{X} + TP' + E \qquad \textbf{Equation 24}$$

$$Y = 1 \times \overline{Y} + UC' + F \qquad \textbf{Equation 25}$$

$$U = T + H \text{ (the inner relation)} \qquad \textbf{Equation 26}$$

Table 24 lists the symbols and their representation in Equations 24-26. Note that the coefficients of the inner relation are 1. In the PLS algorithm there are additional loadings, W, called weights. This modeling geometrically corresponds to fitting a line, plane or hyper plane to both the X and Y data represented as points in a multidimensional space, with the objective of well approximating the original data tables X and Y, and maximizing the covariance between the observation positions on the hyper planes (Umetrics, 2002).

SIMCA-P (Version 10.5, Umetrics AB, 2004) software was employed to perform the PLS analysis. The default values given by the software were used as the initial conditions for computation.

Table 24 Symbols in PLS model

T	Matrix of scores that summarizes the X variables
P	Matrix of weights expressing the correlation between X and U (Y)
U	Matrix of scores that summarizes the Y variables
C	Matrix of weights expressing the correlation between Y and T (X)
E, F, H	Matrices of residuals

According to the user's guide to SIMCA-P (Umetrics, 2002), the criterion used to determine the model dimensionality, *ie,* the number of significant PLS components (*h*), is cross validation (CV). With CV, observations are kept out of the model development, then the response values (Y) for the kept out observations are predicted by the model, and compared with the actual values. This procedure is repeated several times until every observation has been kept out once and only once. The prediction error sum of squares (PRESS) is the squared difference between observed Y and predicted values when the observations were kept out.

$$PRESS = \sum_i \sum_m (Y_{im} - \hat{Y}_{im})^2 \qquad \textbf{Equation 27}$$

For every component, the overall PRESS/SS is computed, where SS is the residual sum of the previous component, and also $(PRESS/SS)_m$ for each variable (m). These values are good measures of the predictive power of the model. A component is considered significant if PRESS/SS is statistically smaller than 1.0.

For every component, the fraction of the total variation of the dependent variables (Q^2) and the cumulative Q^2 for the extracted components (Q^2_{cum}) are computed. Q^2_{cum} was computed as:

$$Q^2_{cum} = (1.0 - \Pi(PRESS / SS)_a) \quad \textbf{[a=1, …A]} \qquad \textbf{Equation 28}$$

$\Pi(PRESS / SS)_a$ = the product of PRESS/SS for each individual component a.

The tested PLS component is thought significant if Q^2 is larger than a significance limit (0.0975) for the whole data set. The model is thought to have a good predicting ability when Q^2_{cum} is larger than 0.5. Model adequacy was assessed based primarily on the number of PLS principal components (h), Q^2_{cum}, the correlation coefficient between observed values and fitted values (R^2), the standard error of the estimate (SE), the variance ratio (F) in an analysis if variance, and the significance level (p).

Variable Importance in the Projection (VIP) is a parameter that shows the importance of a variable in the model. According to the manual for SIMCA-P, terms with large VIP (>1.0) are the most relevant for predicting dependent variables. Previous studies have found that not all independent variables were necessary for PLS modeling (Basak et al., 2002; Chen et al., 2003; Niu et al., 2005). To obtain an optimal model, the following PLS analysis procedure was adopted. A PLS model with all the predictor variables was first calculated and then the variable with the lowest VIP was eliminated and a new PLS regression was performed, yielding a new PLS model. This procedure was repeated until an optimal model was obtained. The optimal model was selected with respect to Q^2_{cum}, R^2, SE, F, and p. In accordance with statistical theory, a QSAR model with larger values of Q^2_{cum}, R^2, and F and smaller values of SE and p tends to be more stable and reliable than in the opposite case.

5.4.4 Modeling results

For the compounds comprising the data set, a PLS analysis was performed with all 11 variables as the initial predictor variables and k_{obs}, $\log k_{obs}$ and $1/k_{obs}$ as the dependent variables yielding QSAR (Quantitative Structure-Activity Relationship) models **I**, **II** and **III**. The parameters for these models are listed in Table 25. As we can see from Table 25, Model **II** is the best fitted model among the three models, with a R^2 value of 0.989 and the Q^2_{cum} (the cumulative fraction of

the total variation of the dependent variables) of 0.964. All three models are statistically significant.

Table 25 Fitting results for PLS models I, II and III

Model	Variables/ Descriptors	Dependent variables / Response variables	*h*	Q^2_{cum}	R^2
I	11	k_{obs}	2	0.951	0.983
II	11	$\log k_{obs}$	2	**0.964**	**0.989**
III	11	$1/k_{obs}$	2	0.892	0.969

The unscaled coefficients of the independent variables and constant transformed from the PLS results are listed in Table 26. Depending on the sign of the coefficient, one can evaluate the direction of a change in each independent variable on the observed dehalogenation rate of halogenated benzenes by Pd/Fe bimetallic particles.

Table 26 The variable coefficients of the Model II

Variables	**VIP***	**Coefficient**
E_{HOMO}	1.389	8.705
E_{LUMO}	0.6738	2.802
E_T	1.070	-9.519×10^{-6}
R_e	0.5985	8.628×10^{-6}
μ	0.2369	-3.430×10^{-3}
Q_C^+	1.408	0.4670
Q_C^-	1.211	-1.821
Q_X^+	1.529	-0.6910
$E_{LUMO}-E_{HOMO}$	0.3227	0.4023
$E_{LUMO}+E_{HOMO}$	1.030	2.903
$(E_{LUMO}-E_{HOMO})^2$	0.3210	0.9581
Constant		0.4417

* Variable Importance in the Projection (VIP) is a parameter that shows the importance of a variable in the model. According to the manual for SIMCA-P, terms with large VIP (>1.0) are the most relevant for predicting dependent variables.

Table 26 also listed the calculated VIP values for Model II. We see that the VIP values of Q_X^+、Q_C^+、E_{HOMO}、Q_C^-、E_T and $E_{LUMO}+E_{HOMO}$ are all greater than 1.0 (Figure 63), indicating they are

important in governing the observed dehalogenation rate of halogenated benzenes by Pd/Fe bimetallic particles. A new PLS regression was performed, eliminating the variables with the VIP values <1.0. Single variable correlation with logk_{obs} was also performed for all the 11 variables. Five variables (Q_X^+、Q_C^+、E_{HOMO}、Q_C^-、and E_{LUMO}+E_{HOMO}) were found to have significant ($p<0.05$) correlation with logk_{obs}. A new PLS model with the five variables that have VIP values larger than 1.0 and significant correlation with logk_{obs} was developed. Table 27 lists the coefficients of the five variables and constant of the optimized PLS model (Equation 29).

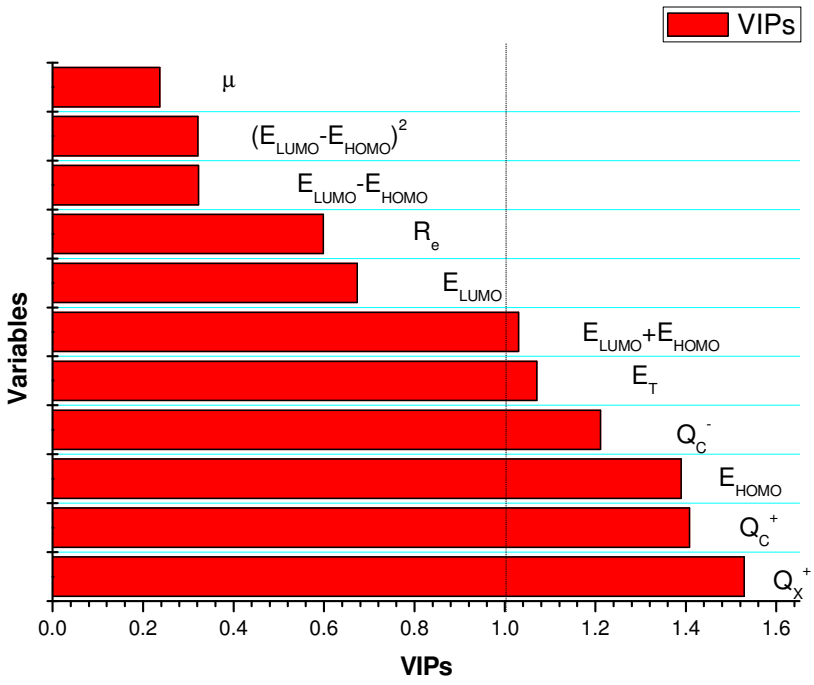

Figure 63 Importance of each variable in prediction model

$$\log k_{obs} = 10.01E_{HOMO} + 0.5890Q_C^+ - 2.363Q_C^- - 0.8187Q_X^+ + 2.875(E_{LUMO}+E_{HOMO}) + 0.7824$$

(h=1, R^2=0.980, Q^2_{cum}=0.977) **Equation 29**

Table 27 The variable coefficients of the optimized model

Variables	VIP*	Coefficient
E_{HOMO}	1.051	10.01
Q_C^+	1.066	0.5890
Q_C^-	0.913	-2.363
Q_X^+	1.160	-0.8187
E_{LUMO}+E_{HOMO}	0.761	2.875
Constant		0.7824

* Variable Importance in the Projection (VIP) is a parameter that shows the importance of a variable in the model. According to the manual for SIMCA-P, terms with large VIP (>1.0) are the most relevant for predicting dependent variables.

5.4.5 Analysis and discussion

The fact that Q_X^+ has the largest VIP value of all tested variables indicate that the most positive Mulliken atomic charges on a chlorine/bromine atom (Q_X^+) is the dominant factor in determining the observed dehalogenation rate of halogenated benzenes by Pd/Fe bimetallic particles. A significant correlation (R^2=0.924, $p<0.05$) between Q_X^+ and the observed $\log k_{obs}$ can be established and it is shown in Figure 64. Generally speaking, the more negative the Q_X^+ is, the faster the observed dehalogenation reaction is. It should be pointed out that Mulliken atomic charges are artificial and they do not represent an observable property of atoms or molecules. Therefore it is very important not to over interpret data provided by population analysis methods.

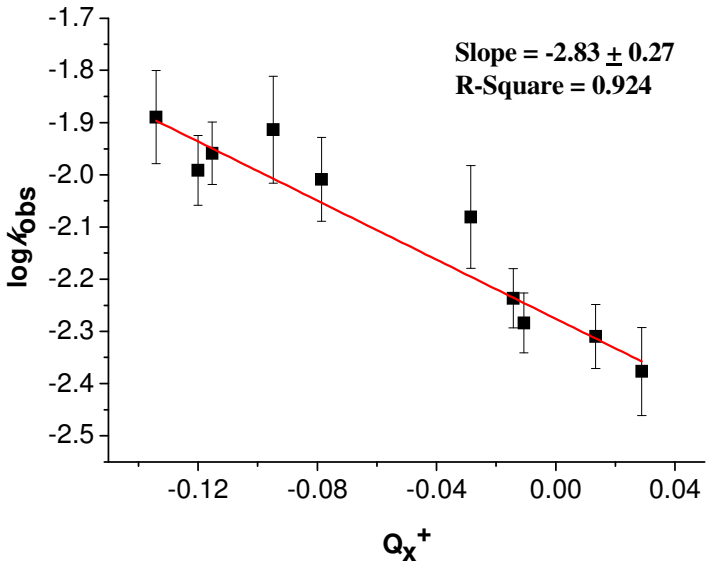

Figure 64 Correlation between Q_X^+ and the observed logk_{obs}

The predicted values of logk_{obs} for the 10 compounds computed using the optimized model are listed in Table 28. As can be seen from Table 28, the observed values are close to those predicted by the optimized model. A paired sample t test was conducted for the observed and predicted values. It was found that at the 0.05 level, the difference of the observed values means is NOT significantly different with the predicted values means. This indicates that the predicted values are acceptable. Note that the cross-validated the Q^2_{cum} value (0.977) of the optimized model is much larger than 0.5 and close to 1.0, so the model is apparently useful for prediction, and could be effectively used to predict the logk_{obs} of other chlorinated or brominated benzenes' reaction with Pd/Fe.

Table 28 Experimental and predicted logk_{obs} values for 10 compounds

Chemical	logk_{obs}- Experimental	logk_{obs} – Predicted
1,2,4-TCB	-2.38	-2.37
1,4-DCB	-2.24	-2.22
1,3-DCB	-2.28	-2.30
1,2-DCB	-2.31	-2.29
MCB	-2.08	-2.14
1,2,4-TBB	-2.01	-2.00
1,2-DBB	-1.99	-1.99
1,3-DBB	-1.96	-1.97
1,4-DBB	-1.91	-1.92
MBB	-1.89	-1.87

5.5 Dehalogenation pathway prediction for TBBPA/ TCBPA

Since there are no commercially available neat chemicals for intermediate products of TBBPA dehalogenation (tri-BBPA, di-BBPAs and mono-BBPA) or TCBPA dehalogenation (tri-CBPA, di-CBPAs and mono-CBPA), pathway elucidation was difficult. The combination of HPLC and GC-MS allowed us to differentiate tri-BBPA from Di-BBPAs and mon-BBPA, or tri-CBPA from di-CBPAs and mono-CBPA, but it could not tell which di-BBPA or di-CBPA was produced. To overcome this problem, a pathway prediction model was constructed based on the QSAR modeling results for the halogenated benzenes.

It was observed that among the intermediates produced during the dechlorination of 1, 2, 4-TCB, 1,2-DCB>1,4-DCB>1,3-DCB. Comparing the individual dechlorination rates among the DCBs, the order of dechlorination rates was 14-DCB ≥13-DCB≥12-DCB. Based on the calculation

results of B3LYP/6-31G(d) FOPT，the charge of each chlorine atom of the 1,2,4-TCB molecule is listed in Table 29.

Table 29 Charge on each chlorine atom of the 1,2,4-TCB molecule (Unit: atomic charge unit)

Position on 1,2,4-TCB	*ortho*-Cl (#1)	*meta*-Cl (#2)	*para*-Cl (#4)
Charge	0.024778	0.028829	-0.000430

Two hypotheses were proposed based on the dechlorination results of 1, 2, 4-TCB.

i. 1,2-DCB was the most produced intermediate during the dechlorination of 1, 2, 4-TCB. The favored chlorine to be removed is the *para*-Cl (#4), which has by far the lowest charge (Table 29).

ii. 1,4-DCB was the most produced intermediate during the dechlorination of 1, 2, 4-TCB. The favored chlorine to be removed is the *meta*-Cl (#2), which has the most positive charge by a small margin (Table 29).

Based on the QSAR modeling results of the 10 halogenated benzenes, it was found that Q_X^+ is the dominant factor in determining the observed dehalogenation rate of halogenated benzenes by Pd/Fe bimetallic particles. Therefore, the modeling results support hypothesis ii.

5.5.1 Pathway prediction for TBBPA debromination

Since the four bromine atoms on TBBPA are equal in terms of charges, no calculation was performed. Calculation was performed for tri-BBPA and the charges of each bromine atoms are marked in Figure 65. Since the most positive Mulliken atomic charges on a bromine atom (Q_X^+) is found on the aromatic ring where two bromine atoms are located, it is predicted that the bromine atom with the largest Q_X^+ will be removed first, and the primary di-BBPA product has one bromine atom on each aromatic ring. The same conclusion was reached for TCBPA (Figure 67 and Figure 68).

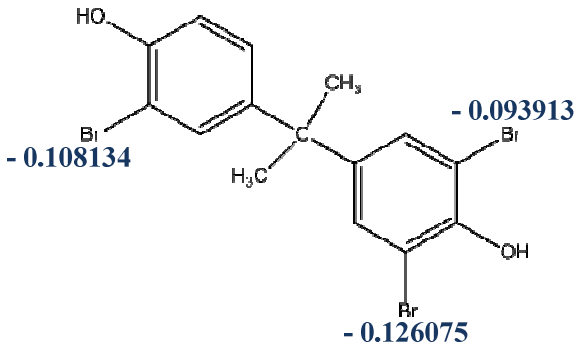

Figure 65 Calculated charges of each bromine atoms for tri-BBPA

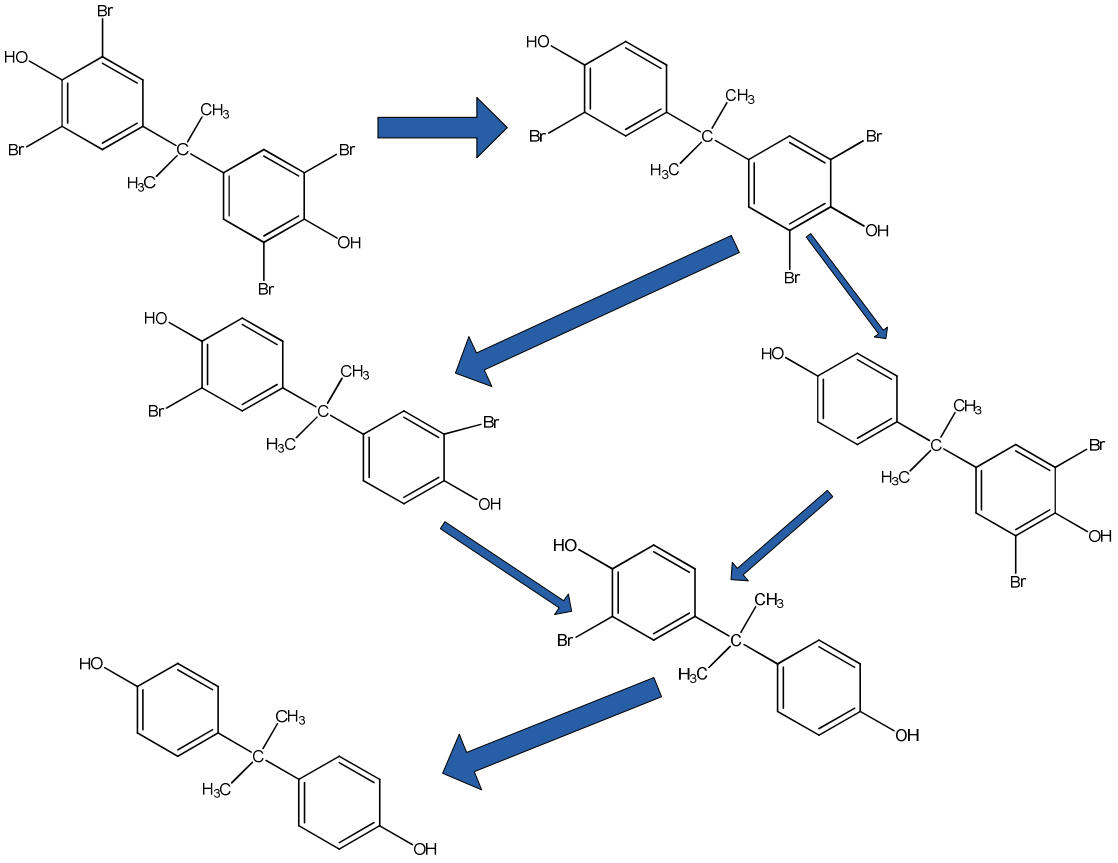

Figure 66 Predicted debromination pathway for TBBPA

5.5.2 Pathway prediction for TCBPA dechlorination

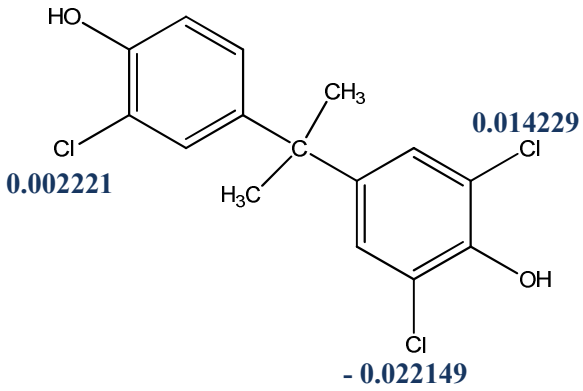

Figure 67 Calculated charges of each chlorine atoms for tri-CBPA

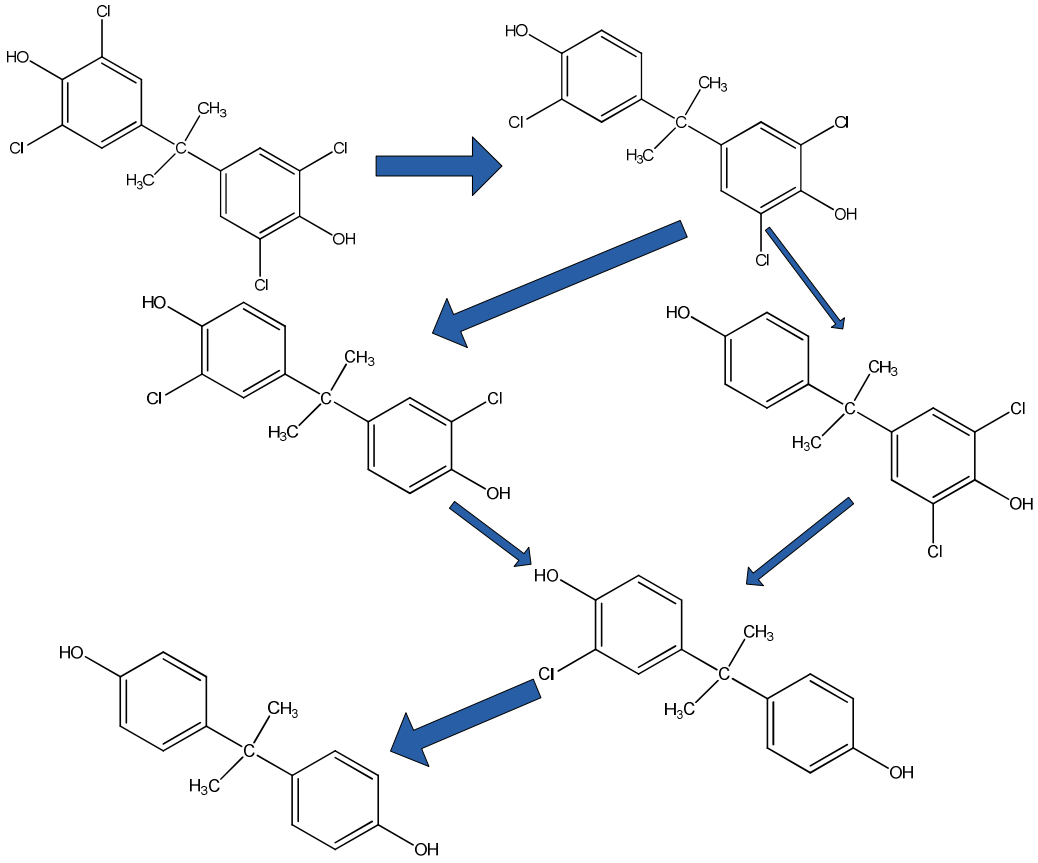

Figure 68 Predicted dechlorination pathway for TCBPA

6 Chapter 6 Conclusions

6.1 Summary of results

This research work has been based on the hypothesis that the unique electrochemical and physicochemical properties of zero valent iron based bimetallic particles can be used to enhance the degradation kinetic of polyhalogenated compounds. Iron-based microscale particles with a second dopant metal were shown to be able to catalyze the reaction kinetics substantially. The benefits of using microscale zero valent iron based bimetallic particles were retained by keeping the reductive power of economically advantaged zero valent iron yet overcoming a key technical barrier that the nanosized particles tend to agglomerate in minutes and thereby lose their mobility and chemical reactivity rapidly.

Fundamental Science and Engineering Advancements:

- A second catalytic dopant can be incorporated to enhance the physical and chemical properties of the base metallic element.
- Microscale zero valent iron based Pd/Fe and Ni/Fe particles can be used to enhance the reactions kinetically.
- The catalytic effect of the second metal is sensitive to the chemical identity of the transition metal additive and correlates with thermodynamic descriptors for the solubility of hydrogen in the transition metal additive.
- A quantitative structure-activity relationship (QSAR) model was constructed and it indicates that the most positive Mulliken atomic charges on a chlorine/bromine atom (Q_X^+) is the dominant factor in determining the observed dehalogenation rate of halogenated benzenes by Pd/Fe bimetallic particles.

Specific conclusions drawn from this work include:

- Surface characterization of synthesized bimetallic particles revealed that the particles were not uniform in size and they appeared to be in small clusters. Elemental analysis of the second metal by XPS confirmed that the second metal was successfully deposited on the surface of iron as zero valent metal.
- The 0.011% Pd/Fe bimetallic particles were found to be effective in dechlorination of 124-TCB, DCBs and chlorobenzene (MCB) under neutral conditions (pH=7.2). Benzene was the major final product. The half-lives for MCB, DCBs and 124-TCB ranged from 84 minutes (MCB) to 165 minutes (124-TCB). The order of dechlorination rates among DCBs was 14-DCB ≥ 13-DCB ≥ 12-DCB.
- The following reactivity trend towards 124-TCB was identified: Pd/Fe >> Ni/Fe > Cu/Fe > Ag/Fe ≈ Fe. The results showed contrary observations against the galvanic couple hypothesis. However, a near linear correlation (R^2=0.937) was established between the $1/k_{obs}$ and the heat of hydrogen solution. The correlation between $\ln k_{obs}$ and the heat of hydrogen chemisorption was substantially less strong. This indicated that the hydrogen absorbed inside the metal played a more important role than the hydrogen adsorbed on the surface in the catalytic activity of the second noble metal. The results demonstrated the importance of hydrogen in the dehalogenation reaction by bimetallic particles and strongly supported that hydrogen atoms resulting from iron corrosion are the primary reactive species for reduction.
- The 0.011% Pd/Fe bimetallic particles were demonstrated to be effective in debromination of 124-TBB, DBBs and bromobenzene (MBB) under neutral conditions (pH=7.2). Benzene was the major final product. The half-lives for MBB, DBBs and 124-TBB ranged from 54 minutes (MBB) to 71 minutes (124-TBB). The order of debromination rates among DBBs was 14-DBB ≥ 13-DBB ≥ 12-DBB.

- The following reactivity trend was found for 124-TBB: Pd/Fe >> Ni/Fe > Cu/Fe > Ag/Fe ≈ Fe. This is consistent with the reactivity trend found for 124-TCB.
- 124-trifluorobenzene (TFB) was subjected to the same batch experimental procedure with 0.011% Pd/Fe. However, the initial concentration of 124-TFB remained virtually unchanged throughout the reaction period (4 days). No daughter products were identified by GC-MS.
- It was demonstrated that the debromination of TBBPA by Pd/Fe bimetallic particles of micron sizes was rapid at ambient temperature whereas ZVI alone showed little reaction under the same conditions. The debromination rate of TBBPA followed a pseudo-first-order rate model and the rate constant k_{obs} was proportional to the Pd/Fe particle dosage and surface loading of Pd. Lower solution pH also favored the debromination of TBBPA. More importantly, the k_{obs} values measured at constant solution pH correlated linearly with the Pd mass introduced to the reactors, regardless of Pd/Fe particle dosage or Pd surface coverage. The greater amount of Pd also resulted in more complete transformation of TBBPA to BPA within very short time period.
- It was shown that the dechlorination of TCBPA by Pd/Fe bimetallic particles of micron sizes was rapid at ambient temperature. The dechlorination rate of TCBPA followed a pseudo-first-order rate model and the rate constant k_{obs} was proportional to the Pd/Fe particle dosage and surface loading of Pd. Higher initial TCBPA concentrations had a negative impact on the k_{obs}. Similar to the debromination of TBBPA, the k_{obs} values measured for TCBPA dechlorination at constant solution pH correlated linearly with the Pd mass introduced to the reactors, regardless of Pd/Fe particle dosage or Pd surface coverage. The greater amount of Pd also resulted in more complete of transformation of TCBPA to BPA within a short time period.

- An optimized quantitative structure–activity relationships (QSAR) model was constructed using 5 descriptors. The VIP values of Q_X^+、Q_C^+、E_{HOMO}、Q_C^- and E_{LUMO}+E_{HOMO} are all greater than 1.0, indicating they are important in governing the observed dehalogenation rate of halogenated benzenes by Pd/Fe bimetallic particles. The fact that Q_X^+ has the largest VIP value of all tested variables indicate that the most positive Mulliken atomic charges on a chlorine/bromine atom (Q_X^+) is the dominant factor in determining the observed dehalogenation rate of halogenated benzenes by Pd/Fe bimetallic particles. A significant correlation (R^2=0.924, $p<0.05$) between Q_X^+ and the observed logk_{obs} was established. Generally speaking, the more negative the Q_X^+ is, the faster the observed dehalogenation reaction is. The cross-validated Q^2_{cum} value (0.977) of the optimized model is much larger than 0.5 and close to 1.0, hence the model is useful for prediction, and could be effectively used to predict the logk_{obs} of other chlorinated or brominated benzenes' reaction with Pd/Fe.
- A pathway prediction model for TBBPA/TCBPA was constructed based on the QSAR modeling results for the halogenated benzenes. It is predicted that the bromine atom with the largest Q_X^+ will be removed first, and the primary di-BBPA product has one bromine atom on each aromatic ring. For TCBPA, it is predicted that the chlorine atom with the largest Q_X^+ will be removed first, and the primary di-CBPA product has one chlorine atom on each aromatic ring.

6.2 **Further research needs**

In this study a QSAR model was developed. Further testing and verification of the model could provide more information on the predictability of the model. If further validation is achieved, the model could bridge numerous data gaps.

The chlorinated/brominated benzenes and tetrabromobisphenol A (TBBPA)/ tetrachlorobisphenol A (TCBPA) degradation by Pd/Fe bimetallic particles has been demonstrated successfully at bench scale in this research. However, in reality, the chlorinated solvents in a source zone are usually adsorbed in the soil or present as a separate DNAPL phase. The degradation behavior of soil-related chlorinated solvents or DNAPL using bimetallic particles may substantially differ from their degradation behavior in water. Field testing must be carried out to assess the effectiveness of bimetallic particle reactivity under environmental conditions.

Since the recovery of bimetallic particles in an underground remediation setting is usually not feasible, the fate and transport of these bimetallic particles should be well understood. More investigations on toxicology and fate of the bimetallic particles are needed in order to gain regulatory and public acceptance. Table 30 lists the secondary maximum contaminant levels for the metals and major final products in this study. As can be seen from the table, benzene is a regulated drinking water contaminant, so are copper, iron, nickel and silver. Although no legal limit has been set for bisphenol A in drinking water, bisphenol A has been considered a toxic substance due to the possible hazards to fetuses, infants and young children (FDA, 2010). Dehalogenation may stop at benzene or bisphenol A, but remediation does not. The fate of the metals and dehalogenation byproducts needs to be thoroughly studied.

Table 30 Secondary maximum contaminant levels for public water systems

Contaminant	Secondary maximum contaminant levels (MCL) (mg/L)[a]
Copper	1.0
Iron	0.3
Nickel	0.1[b]
Silver	0.1
Palladium	N/A[c]
Benzene	0.005
Bisphenol A	N/A[d]

[a] 40 CFR 143.3;[b] The MCL for Nickel were remanded on February 9, 1995. This means that while many water suppliers continue to monitor nickel levels in their water, there is currently no EPA legal limit on the amount of nickel in drinking water. [c] There is currently no EPA legal limit on the amount of palladium in drinking water. [d] There is currently no EPA legal limit on the amount of bisphenol A in drinking water.

It has been observed that microbial activity does occur in iron based permeable reactive barriers. It is worthwhile studying the co-effects of microbial activity in the reactive barriers or down gradient of the reactive barriers. Chen et al. (2011) simulated benzene and toluene biodegradation down gradient of a zero-valent iron permeable reactive barrier (ZVI PRB) that reduces trichloroethylene (TCE). Their data suggested that alkaline pH (pH 10.5), often observed down gradient of ZVI PRBs, inhibited Fe(III)-mediated biotransformation of both benzene and toluene. For microbial benzene and toluene removal down gradient of a ZVI PRB, it may be necessary to provide pH control.

7 References

Agrawal A, Tratnyek PG. Reduction of Nitro Aromatic Compounds by Zero-Valent Iron Metal. Environmental Science & Technology (1995) 30:153-160.

Alvarez-Cohen L, Speitel GE. Kinetics of aerobic cometabolism of chlorinated solvents. Biodegradation (2001) 12:105-126.

Arnold WA, Roberts AL. Pathways and Kinetics of Chlorinated Ethylene and Chlorinated Acetylene Reaction with Fe(0) Particles. Environmental Science & Technology (2000) 34:1794-1805.

Atkins P. Physical Chemistry, 6th edition (1997): W.H. Freeman and Company, New York.

Aulenta F, Majone M, Tandoi V. Enhanced anaerobic bioremediation of chlorinated solvents: environmental factors influencing microbial activity and their relevance under field conditions. Journal of Chemical Technology & Biotechnology (2006) 81:1463-1474.

Bard AJ, Parsons, R., and Jordan, J. . Standard Potentials in Aqueous Solutions (1985): Marcel Dekker, New York.

Basak SC, Mills D, Hawkins DM, El-Masri HA. Prediction of tissue-air partition coefficients: A comparison of structure-based and property-based methods. SAR and QSAR in Environmental Research (2002) 13:649-665.

Behm RJ PV, Cattina MG, Christmann K, Ertl G. Evidence for subsurface hydrogen in Pd(110): an intermediate between chemisorbed and dissolved species. J. Chem. Phys. (1983) 78:7486-7490.

Bennett P, He F, Zhao D, Aiken B, Feldman L. In situ testing of metallic iron nanoparticle mobility and reactivity in a shallow granular aquifer. Journal of Contaminant Hydrology (2010) 116:35-46.

Blowes DW, Ptacek CJ, Benner SG, McRae CWT, Bennett TA, Puls RW. Treatment of inorganic contaminants using permeable reactive barriers. Journal of Contaminant Hydrology (2000) 45:123-137.

Bokare AD, Chikate RC, Rode CV, Paknikar KM. Iron-nickel bimetallic nanoparticles for reductive degradation of azo dye Orange G in aqueous solution. Applied Catalysis B: Environmental (2008) 79:270-278.

Borgschulte A, Westerwaal RJ, Rector JH, Schreuders H, Dam B, Griessen R. Catalytic activity of noble metals promoting hydrogen uptake. Journal of Catalysis (2006) 239:263-271.

Boudouch O, Ying Y, Benadda B. The Influence of Surface Covers on the Performance of a Soil Vapor Extraction System. CLEAN – Soil, Air, Water (2009) 37:621-628.

Bransfield SJ, Cwiertny DM, Roberts AL, Fairbrother DH. Influence of copper loading and surface coverage on the reactivity of granular iron toward 1,1,1-trichloroethane. Environmental Science & Technology (2006) 40:1485-1490.

Butler EC, Hayes KF. Kinetics of the Transformation of Halogenated Aliphatic Compounds by Iron Sulfide. Environmental Science & Technology (2000) 34:422-429.

Casey FXM, Ong SK, Horton R. Degradation and transformation of trichloroethylene in miscible displacement experiments through zerovalent metals. Environmental Science & Technology (2000) 34:5023-5029.

Chen J, et al. Is it possible to develop a QSPR model for direct photolysis half-lives of PAHs under irradiation of sunlight? Environmental Pollution (2001) 114:137-143.

Chen JW, et al. Quantitative structure-property relationships for vapor pressures of polybrominated diphenyl ethers. SAR and QSAR in Environmental Research (2003) 14:97-111.

Chen L, Liu F, Liu Y, Dong H, Colberg PJS. Benzene and toluene biodegradation down gradient of a zero-valent iron permeable reactive barrier. Journal of Hazardous Materials (2011) 188:110-115.

Cheng R WJ, Zhang WX. Reductive dechlorination of p-chlorophenol by nanoscale iron. Biomed Environ Sci. (2007) 20:410-413.

Choi JH, Choi SJ, Kim YH. Hydrodechlorination of 2,4,6-trichlorophenol for a permeable reactive barrier using zero-valent iron and catalyzed iron. Korean Journal of Chemical Engineering (2008) 25:493-500.

Clement TP, Johnson CD, Sun Y, Klecka GM, Bartlett C. Natural attenuation of chlorinated ethene compounds: model development and field-scale application at the Dover site. Journal of Contaminant Hydrology (2000) 42:113-140.

Comber MHI, Walker JD, Watts C, Hermens J. Quantitative structure-activity relationships for predicting potential ecological hazard of organic chemicals for use in regulatory risk assessments. Environmental Toxicology and Chemistry (2003) 22:1822-1828.

Council ITR. Regulatory Guidance for Permeable Reactive Barriers Designed to Remediate Chlorinated Solvents, www.itrcweb.org/Documents/pbw-1.pdf. (1999a).

Council ITR. Overview of In Situ Bioremediation of Chlorinated Ethene DNAPL Source Zones, www.itrcweb.org/Documents/bioDNPL.../BioDNAPL-2.pdf (2005).

Council ITR. Permeable Reactive Barrier:Technology Update, www.itrcweb.org/Documents/PRB-5.pdf. (2011).

Council NR. Alternatives for Ground Water Cleanup. (1994): The National Academies Press.

Council NR. Innovations in Ground Water and Soil Cleanup:From Concept to Commercialization. (1997): The National Academies Press.

Council NR. Groundwater and Soil Cleanup:Improving Management of Persistent Contaminants. (1999b): The National Academies Press.

Cousins IT, Staples CA, Klečka GM, Mackay D. A Multimedia Assessment of the Environmental Fate of Bisphenol A. Human and Ecological Risk Assessment: An International Journal (2002) 8:1107-1135.

Cwiertny DM, Bransfield SJ, Livi KJT, Fairbrother DH, Roberts AL. Exploring the influence of granular iron additives on 1,1,1-trichloroethane reduction. Environmental Science & Technology (2006) 40:6837-6843.

De Jong V, Louw R. Performance of supported nickel and other metal catalysts in the hydrodechlorination of chlorobenzene and 1-chlorohexane. Applied Catalysis A: General (2004) 271:153-163.

Ding M, Schroeder NC, Reimus PW. Zero-valent iron as a reducing "getter" for immobilization of technetium. Abstr.Pap.Am.Chem.Soc. (2001) 222:U443-U443.

Elliott DW, Zhang WX. Field assessment of nanoscale bimetallic particles for groundwater treatment. Environmental Science & Technology (2001) 35:4922.

Ellis DE, et al. Bioaugmentation for Accelerated In Situ Anaerobic Bioremediation. Environmental Science & Technology (2000) 34:2254-2260.

Elsner M, Cwiertny DM, Roberts AL, Lollar BS. 1,1,2,2-tetrachloroethane reactions with OH-, Cr(II), granular iron, and a copper-iron bimetal: Insights from product formation and associated carbon isotope fractionation. Environmental Science & Technology (2007) 41:4111-4117.

Fang Y, Al-Abed SR. Correlation of 2-Chlorobiphenyl Dechlorination by Fe/Pd with Iron Corrosion at Different pH. Environmental Science & Technology (2008) 42:6942-6948.

FDA. Update on Bisphenol A for Use in Food Contact Applications, http://www.fda.gov/downloads/NewsEvents/PublicHealthFocus/UCM197778.pdf (2010).

Feng J, Lim TT. Pathways and kinetics of carbon tetrachloride and chloroform reductions by nano-scale Fe and Fe/Ni particles: comparison with commercial micro-scale Fe and Zn. Chemosphere (2005) 59:1267.

Fennelly JP, Roberts AL. Reaction of 1,1,1-trichloroethane with zero-valent metals and bimetallic reductants. Environmental Science & Technology (1998) 32:1980.

Ferguson JF, Pietari JMH. Anaerobic transformations and bioremediation of chlorinated solvents. Environmental Pollution (2000) 107:209-215.

Fukai Y. he Metal-hydrogen System, Basic Bulk Properties. (1992): Springer-Verlag, Berlin, Heidelberg.

Ghauch A, Tuqan A. Reductive destruction and decontamination of aqueous solutions of chlorinated antimicrobial agent using bimetallic systems. Journal of Hazardous Materials (2009) 164:665-674.

Gillham RW. Cleaning halogenated contaminants from groundwater (1993).

Gillham RW, O'Hannesin SF. Enhanced Degradation of Halogenated Aliphatics by Zero-Valent Iron. Ground Water (1994) 32:958-967.

Gillham RW OHS. Metal-catalyzed abiotic degradation of halogenated organic compounds. In: International Association of Hydrologists Conference, Modern Trends in Hydrology, (1992) Hamilton, ON, Canada.

Graham LJ, Jovanovic G. Dechlorination of p-chlorophenol on a Pd/Fe catalyst in a magnetically stabilized fluidized bed; Implications for sludge and liquid remediation. Chemical Engineering Science (1999) 54:3085.

Grieger KD, Fjordbøge A, Hartmann NB, Eriksson E, Bjerg PL, Baun A. Environmental benefits and risks of zero-valent iron nanoparticles (nZVI) for in situ remediation: Risk mitigation or trade-off? Journal of Contaminant Hydrology (2010) 118:165-183.

Grittini C, Malcomson M, Fernando Q, Korte N. Rapid Dechlorination of Polychlorinated Biphenyls on the Surface of a Pd/Fe Bimetallic System. Environmental Science & Technology (1995) 29:2898-2900.

Guasp E, Wei R. Dehalogenation of trihalomethanes in drinking water on Pd–Fe° bimetallic surface. Journal of Chemical Technology & Biotechnology (2003) 78:654-658.

Hans Stroo CHW, Bruce C. Alleman. In Situ Remediation Of Chlorinated Solvent Plumes. (2010): Springer.

He F, Zhao D. Hydrodechlorination of trichloroethene using stabilized Fe-Pd nanoparticles: Reaction mechanism and effects of stabilizers, catalysts and reaction conditions. Applied Catalysis B: Environmental (2008) 84:533-540.

He F, Zhao DY. Preparation and characterization of a new class of starch-stabilized bimetallic nanoparticles for degradation of chlorinated hydrocarbons in water. Environmental Science & Technology (2005) 39:3314.

He F, Zhao DY, Paul C. Field assessment of carboxymethyl cellulose stabilized iron nanoparticles for in situ destruction of chlorinated solvents in source zones. Water Research (2010) 44:2360-2370.

Hoffman F. Ground-Water Remediation Using “Smart Pump and Treat”. Ground Water (1993) 31:98-106.

Hu C-Y, Lo S-L, Liou Y-H, Hsu Y-W, Shih K, Lin C-J. Hexavalent chromium removal from near natural water by copper–iron bimetallic particles. Water Research (2010) 44:3101-3108.

ITRC tITRC. Permeable Reactive Barrier:Technology Update. (2011a).

ITRC tITRC. Permeable Reactive Barrier:Technology Update. (2011b).

Jovanovic GN, Znidarsic Plazl P, Sakrittichai P, Al-Khaldi K. Dechlorination of 0RW1S34RfeSDcfkexd09rT2p1RW1S34RfeSDcfkexd09rT2-Chlorophenol in a Microreactor with Bimetallic Pd/Fe Catalyst. Ind Eng Chem Res (2005) 44:5099.

Keane MA, Pina G, Tavoularis G. The catalytic hydrodechlorination of mono-, di- and trichlorobenzenes over supported nickel. Applied Catalysis B: Environmental (2004) 48:275-286.

Kim Y-H, Carraway ER. Dechlorination of Pentachlorophenol by Zero Valent Iron and Modified Zero Valent Irons. Environmental Science & Technology (2000) 34:2014-2017.

Kim YH, Carraway ER. Reductive dechlorination of TCE by zero valent bimetals. Environmental Technology (2003) 24:69-75.

Klaassen C.D. WIJB. The Basic Science of Poisons, Companion Handbook (1999): The McGraw-Hill Companies, Inc.

Klausen J, Vikesland PJ, Kohn T, Burris DR, Ball WP, Roberts AL. Longevity of granular iron in groundwater treatment processes: solution composition effects on reduction of organohalides and nitroaromatic compounds. Environmental Science & Technology (2003) 37:1208-1218.

Kohn T, Livi KJT, Roberts AL, Vikesland PJ. Longevity of Granular Iron in Groundwater Treatment Processes: Corrosion Product Development. Environmental Science & Technology (2005) 39:2867-2879.

Lawson DR, Tierney MJ, Cheng IF, Van Dyke LS, Espenscheid MW, Martin CR. Use of a coulometric assay technique to study the variables affecting deuterium loading levels within palladium electrodes. Electrochimica Acta (1991) 36:1515-1522.

Li L, et al. Synthesis, properties, and environmental applications of nanoscale iron-based materials: A review. Crit.Rev.Environ.Sci.Technol. (2006a) 36:405.

Li X-q, Elliott DW, Zhang W-x. Zero-Valent Iron Nanoparticles for Abatement of Environmental Pollutants: Materials and Engineering Aspects. Critical Reviews in Solid State and Materials Sciences (2006b) 31:111-122.

Li X-q, Zhang W-x. Sequestration of Metal Cations with Zerovalent Iron NanoparticlesA Study with High Resolution X-ray Photoelectron Spectroscopy (HR-XPS). The Journal of Physical Chemistry C (2007) 111:6939-6946.

Li XD, Schwartz FW. DNAPL remediation with in situ chemical oxidation using potassium permanganate: II. Increasing removal efficiency by dissolving Mn oxide precipitates. Journal of Contaminant Hydrology (2004) 68:269-287.

Liang C, Bruell CJ, Marley MC, Sperry KL. Persulfate oxidation for in situ remediation of TCE. I. Activated by ferrous ion with and without a persulfate–thiosulfate redox couple. Chemosphere (2004) 55:1213-1223.

Liao C-H, Kang S-F, Hsu Y-W. Zero-valent iron reduction of nitrate in the presence of ultraviolet light, organic matter and hydrogen peroxide. Water Research (2003) 37:4109-4118.

Lien HL, Zhang WX. Enhanced dehalogenation of halogenated methanes by bimetallic Cu/Al. Chemosphere (2002) 49:371.

Lin C-F, Lu W-D, Wang IW, Wu M-J. Synthesis of 2-(Diarylmethylene)-3-benzofuranones Promoted via Palladium-Catalyzed Reactions of Aryl Iodides with 3-Aryl-1-(2-tert-butyldimethylsilyloxy)phenyl-2-propyn-1-ones. ChemInform (2004a) 35:no-no.

Lin CJ, Lo SL, Liou YH. Dechlorination of trichloroethylene in aqueous solution by noble metal-modified iron. Journal of Hazardous Materials (2004b) 116:219.

Liou YH, Lo SL, Lin CJ, Kuan WH, Weng SC. Chemical reduction of an unbuffered nitrate solution using catalyzed and uncatalyzed nanoscale iron particles. Journal of Hazardous Materials (2005) 127:102-110.

Liu Y, Majetich SA, Tilton RD, Sholl DS, Lowry GV. TCE Dechlorination Rates, Pathways, and Efficiency of Nanoscale Iron Particles with Different Properties. Environmental Science & Technology (2005) 39:1338-1345.

Liu Y, Phenrat T, Lowry GV. Effect of TCE Concentration and Dissolved Groundwater Solutes on NZVI-Promoted TCE Dechlorination and H2 Evolution. Environmental Science & Technology (2007) 41:7881-7887.

Liu Y, Yang F, Yue PL, Chen G. Catalytic dechlorination of chlorophenols in water by palladium/iron. Water Research (2001) 35:1887-1890.

Lu G-N, Dang Z, Fennell DE, Huang W, Li Z, Liu C-Q. Rules of thumb for assessing reductive dechlorination pathways of PCDDs in specific systems. Journal of Hazardous Materials (2010) 177:1145-1149.

Lu G-N, Dang Z, Tao X-Q, Yang C, Yi X-Y. Modeling and prediction of photolysis half-lives of polycyclic aromatic hydrocarbons in aerosols by quantum chemical descriptors. Science of the Total Environment (2007) 373:289-296.

Luo S, Yang S, Wang X, Sun C. Reductive degradation of tetrabromobisphenol A over iron–silver bimetallic nanoparticles under ultrasound radiation. Chemosphere (2010) 79:672-678.

Lynam MM, Kuty M, Damborsky J, Koca J, Adriaens P. Molecular orbital calculations to describe microbial reductive dechlorination of polychlorinated dioxins. Environmental Toxicology and Chemistry (1998) 17:988-997.

M.J. Frisch GWT, H.B. Schlegel, G.E. Scuseria, M.A. Robb, J.R. Cheeseman et al. Gaussian 03, Revision B.01 (2003) Pittsburgh, PA Gaussian Inc.

Mackenzie K, Frenzel H, Kopinke F-D. Hydrodehalogenation of halogenated hydrocarbons in water with Pd catalysts: Reaction rates and surface competition. Applied Catalysis B: Environmental (2006) 63:161-167.

Matheson LJ, Tratnyek PG. Reductive Dehalogenation of Chlorinated Methanes by Iron Metal. Environmental Science & Technology (1994) 28:2045-2053.

McMahon PB, Dennehy KF, Sandstrom MW. Hydraulic and Geochemical Performance of a Permeable Reactive Barrier Containing Zero-Valent Iron, Denver Federal Center. Ground Water (1999) 37:396-404.

Moore DRJ, Breton RL, MacDonald DB. A comparison of model performance for six quantitative structure-activity relationship packages that predict acute toxicity to fish. Environmental Toxicology and Chemistry (2003) 22:1799-1809.

Morales J, Hutcheson R, Cheng IF. Dechlorination of chlorinated phenols by catalyzed and uncatalyzed Fe(0) and Mg(0) particles. Journal of Hazardous Materials (2002a) 90:97.

Morales J, Hutcheson R, Noradoun C, Cheng IF. Hydrogenation of Phenol by the Pd/Mg and Pd/Fe Bimetallic Systems under Mild Reaction Conditions. Ind Eng Chem Res (2002b) 41:3071.

Muegge JP, Hadley PW. An evaluation of permeable reactive barrier projects in California. Remediation Journal (2009) 20:41-57.

Mueller N, et al. Application of nanoscale zero valent iron (NZVI) for groundwater remediation in Europe. Environmental Science and Pollution Research (2012) 19:550-558.

Muftikian R, Fernando Q, Korte N. A method for the rapid dechlorination of low molecular weight chlorinated hydrocarbons in water. Water Research (1995) 29:2434.

Nagpal V, Bokare AD, Chikate RC, Rode CV, Paknikar KM. Reductive dechlorination of [gamma]-hexachlorocyclohexane using Fe-Pd bimetallic nanoparticles. Journal of Hazardous Materials (2010) 175:680-687.

Nicole C. Müller BN. Nano zero valent iron – THE solution for water and soil remediation? (2010).

Niu J, Huang L, Chen J, Yu G, Schramm K-W. Quantitative structure–property relationships on photolysis of PCDD/Fs adsorbed to spruce (Picea abies (L.) Karst.) needle surfaces under sunlight irradiation. Chemosphere (2005) 58:917-924.

Nobre MMM, Nobre RCM. Soil vapor extraction of chlorinated solvents at an industrial site in Brazil. Journal of Hazardous Materials (2004) 110:119-127.

Noubactep C, Meinrath G, Merkel BJ. Investigating the mechanism of uranium removal by zerovalent iron. Environmental Chemistry (2005) 2:235-242.

Nyer EK, Vance DB. Nano-Scale Iron for Dehalogenation. Ground Water Monitoring & Remediation (2001) 21:41-46.

P. C. Hayes SHA. Process principles in minerals and materials production, 2nd edition. (1993): Hayes Publishing, 1993.

Panel TACCsBFRI. Data summary and test plan for phenol, 4,4'-isopropylidenbis[2,6-dibromo-(Tetrabromobisphenol A, TBBPA) (2004).

Pankow JF, Cherry.J.A. . Dense chlorinated solvents and other DNAPLs in groundwater: History, Behavior and Remediation. (1996).

Phenrat T, Fagerlund F, Illangasekare T, Lowry GV, Tilton RD. Polymer-modified Fe0 nanoparticles target entrapped NAPL in two dimensional porous media: effect of particle concentration, NAPL saturation, and injection strategy. Environmental Science & Technology (2011) 45:6102-6109.

Phenrat T, Saleh N, Sirk K, Tilton RD, Lowry GV. Aggregation and Sedimentation of Aqueous Nanoscale Zerovalent Iron Dispersions. Environmental Science & Technology (2007) 41:284-290.

Powell RM, Puls RW, Hightower SK, Sabatini DA. Coupled Iron Corrosion and Chromate Reduction: Mechanisms for Subsurface Remediation. Environmental Science & Technology (1995) 29:1913-1922.

Pundt A, Kirchheim R. HYDROGEN IN METALS: Microstructural Aspects. Annual Review of Materials Research (2006) 36:555-608.

Quinn J, Geiger, Cherie, Clausen, Chris, Brooks, Kathleen, Coon, Christina, O'Hara, Suzanne, Krug, Thomas, Major, David, Yoon, Woong-Sang, Gavaskar, Arun, Holdsworth, Thomas. Field Demonstration of DNAPL Dehalogenation Using Emulsified Zero-Valent Iron. Environmental Science & Technology (2005) 39:1309-1318.

Rangsivek R, Jekel MR. Removal of dissolved metals by zero-valent iron (ZVI): Kinetics, equilibria, processes and implications for stormwater runoff treatment. Water Research (2005) 39:4153-4163.

Reynolds GW, Hoff JT, Gillham RW. Sampling bias caused by materials used to monitor halocarbons in groundwater. Environmental Science & Technology (1990) 24:135-142.

Rivero-Huguet M, Marshall WD. Reduction of hexavalent chromium mediated by micro- and nano-sized mixed metallic particles. Journal of Hazardous Materials (2009) 169:1081-1087.

Roh Y, Lee SY, Elless MP, Cho KS. Electro-enhanced remediation of radionuclide-contaminated groundwater using zero-valent iron. Journal of Environmental Science and Health Part a-Toxic/Hazardous Substances & Environmental Engineering (2000) 35:1043-1059.

Sayles GD, You G, Wang M, Kupferle MJ. DDT, DDD, and DDE Dechlorination by Zero-Valent Iron. Environmental Science & Technology (1997) 31:3448-3454.

Schrick B, Blough JL, Jones AD, Mallouk TE. Hydrodechlorination of trichloroethylene to hydrocarbons using bimetallic nickel-iron nanoparticles. Chemistry of Materials (2002) 14:5140.

Semprini L. Strategies for the aerobic co-metabolism of chlorinated solvents. Current Opinion in Biotechnology (1997) 8:296-308.

Senzaki T. Removal of Chlorinated Organic Compounds by Iron and Manganese Powders in Buffered Water and Landfill Leachate. Chemosphere (1988) 29:1743-1753.

Shih Y-h, Chen Y-C, Chen M-y, Tai Y-t, Tso C-P. Dechlorination of hexachlorobenzene by using nanoscale Fe and nanoscale Pd/Fe bimetallic particles. Colloids and Surfaces A: Physicochemical and Engineering Aspects (2009) 332:84-89.

Shih YH, Chen MY, Su YF. Pentachlorophenol reduction by Pd/Fe bimetallic nanoparticles: Effects of copper, nickel, and ferric cations. Appl.Catal.B-Environ. (2011) 105:24-29.

Smuleac V, Varma R, Sikdar S, Bhattacharyya D. Green synthesis of Fe and Fe/Pd bimetallic nanoparticles in membranes for reductive degradation of chlorinated organics. Journal of Membrane Science (2011) 379:131-137.

SRC. PhysProp database, http://www.srcinc.com/what-we-do/databaseforms.aspx?id=386 (2012).

Su C, Puls RW. Kinetics of Trichloroethene Reduction by Zerovalent Iron and Tin: Pretreatment Effect, Apparent Activation Energy, and Intermediate Products. Environmental Science & Technology (1998) 33:163-168.

Susarla S, Medina VF, McCutcheon SC. Phytoremediation: An ecological solution to organic chemical contamination. Ecological Engineering (2002) 18:647-658.

Sweeny KH. The Reductive Treatment of Industrial Wastewater: I. Process Description. In: American Institute of Chemical Engineers, Symposium Series --G.F.Bennett, ed. (1981a). 67-71.

Sweeny KH. The Reductive Treatment of Industrial Wastewater: II. Process Description In: American Institute of Chemical Engineers Symposium Series--G.F.Bennett, ed. (1981b). 72-88.

Sweeny KH, Fischer, J.R. Reductive degradation of halogenated pesticides (1972).

Taghavy A, Costanza J, Pennell KD, Abriola LM. Effectiveness of nanoscale zero-valent iron for treatment of a PCE-DNAPL source zone. Journal of Contaminant Hydrology (2010) 118:128-142.

Takigami H, Suzuki G, Hirai Y, Sakai S-i. Brominated flame retardants and other polyhalogenated compounds in indoor air and dust from two houses in Japan. Chemosphere (2009) 76:270-277.

Totten LA, Gigliotti, Cari L., VanRy,Daryl A., Offenberg,John H., Nelson,Eric D., Dachs,Jordi, Reinfelder,John R., Eisenreich,Steven J. Atmospheric Concentrations and Deposition of Polychorinated Biphenyls to the Hudson River Estuary. Environmental Science & Technology (2004) 38:2568-2573.

Tratnyek PG, Johnson RL. Nanotechnologies for environmental cleanup. Nano Today (2006) 1:44-48.

Tratnyek PG, Johnson TL, Scherer MM, Eykholt GR. Remediating Ground Water with Zero-Valent Metals: Chemical Considerations in Barrier Design. Ground Water Monitoring & Remediation (1997) 17:108-114.

Tratnyek PG, Weber EJ, Schwarzenbach RP. Quantitative structure-activity relationships for chemical reductions of organic contaminants. Environmental Toxicology and Chemistry (2003) 22:1733-1742.

Umetrics. User's Guide to SIMCA-P, SIMCA-P+, Version 10.0. (2002) Umetrics AB, Umeå, Sweden.

USEPA. A Citizen's Guide to Permeable Reactive Barriers (2001).

USEPA. Nanotechnology white paper. (2007).

USEPA. Nanotechnology for Site Remediation Fact Sheet. (2008).

Vanýsek P. Handbook of Chemistry and Physics: 88thEdition (2007): Chemical Rubber Company.

Vogan JL, Focht RM, Clark DK, Graham SL. Performance evaluation of a permeable reactive barrier for remediation of dissolved chlorinated solvents in groundwater. Journal of Hazardous Materials (1999) 68:97-108.

Wagner CD, Gale LH, Raymond RH. Two-dimensional chemical state plots: a standardized data set for use in identifying chemical states by x-ray photoelectron spectroscopy. Anal.Chem. (1979) 51:466-482.

Walker JD, Jaworska J, Comber MHI, Schultz TW, Dearden JC. Guidelines for developing and using quantitative structure-activity relationships. Environmental Toxicology and Chemistry (2003) 22:1653-1665.

Wang CB, Zhang WX. Synthesizing Nanoscale Iron Particles for Rapid and Complete Dechlorination of TCE and PCBs. Environmental Science & Technology (1997) 31:2154.

Wang X, Chen C, Chang Y, Liu H. Dechlorination of chlorinated methanes by Pd/Fe bimetallic nanoparticles. Journal of Hazardous Materials (2009) 161:815-823.

Wang Y, Salvage K. Immobilization of uranium in the presence of Fe-0(s): Model development and simulation of contrasting experimental conditions. Appl.Geochem. (2005) 20:1268-1283.

Wang Z, Huang W, Peng Pa, Fennell DE. Rapid transformation of 1,2,3,4-TCDD by Pd/Fe catalysts. Chemosphere (2010) 78:147-151.

Warren KD, Arnold RG, Bishop TL, Lindholm LC, Betterton EA. Kinetics and mechanism of reductive dehalogenation of carbon tetrachloride using zero-valence metals. Journal of Hazardous Materials (1995) 41:217-227.

Wei J, Xu X, Liu Y, Wang D. Catalytic hydrodechlorination of 2,4-dichlorophenol over nanoscale Pd/Fe: Reaction pathway and some experimental parameters. Water Research (2006) 40:348.

Witt ME, Klecka GM, Lutz EJ, Ei TA, Grosso NR, Chapelle FH. Natural attenuation of chlorinated solvents at Area 6, Dover Air Force Base: groundwater biogeochemistry. Journal of Contaminant Hydrology (2002) 57:61-80.

Wold S, Sjöström M, Eriksson L. PLS-regression: a basic tool of chemometrics. Chemometrics and Intelligent Laboratory Systems (2001) 58:109-130.

Wu D-l, Wang H-w, Fan J-h, Ma L-m. Catalytic reduction of CCl4 in water by Fe0 and amended Fe0. Huan jing ke xue= Huanjing kexue / [bian ji, Zhongguo ke xue yuan huan jing ke xue wei yuan hui "Huan jing ke xue" bian ji wei yuan hui.] (2008) 29:3433-3438.

Wu D-l, Wang H-w, Ma L-m. Reductive dechlorination of chlorinated hydrocarbons in water by Ag/Fe catalytic reduction system. Huan jing ke xue= Huanjing kexue / [bian ji, Zhongguo ke xue yuan huan jing ke xue wei yuan hui "Huan jing ke xue" bian ji wei yuan hui.] (2006) 27:1802-1807.

Xu F, et al. Highly Active and Stable Ni–Fe Bimetal Prepared by Ball Milling for Catalytic Hydrodechlorination of 4-Chlorophenol. Environmental Science & Technology (2012) 46:4576-4582.

Xu X, Wo J, Zhang J, Wu Y, Liu Y. Catalytic dechlorination of p-NCB in water by nanoscale Ni/Fe. Desalination (2009) 242:346-354.

Xu X, Zhou H, He P, Wang D. Catalytic dechlorination kinetics of p-dichlorobenzene over Pd/Fe catalysts. Chemosphere (2005a) 58:1135-1140.

Xu X, Zhou H, Wang D. Structure relationship for catalytic dechlorination rate of dichlorobenzenes in water. Chemosphere (2005b) 58:1497-1502.

Xu X, Zhou H, Zhou M. Catalytic amination and dechlorination of para-nitrochlorobenzene (p-NCB) in water over palladium-iron bimetallic catalyst. Chemosphere (2006) 62:847-852.

Xu X, Zhou M, He P, Hao Z. Catalytic reduction of chlorinated and recalcitrant compounds in contaminated water. Journal of Hazardous Materials (2005c) 123:89-93.

Xu Y, Zhang W-x. Subcolloidal Fe/Ag Particles for Reductive Dehalogenation of Chlorinated Benzenes. Ind Eng Chem Res (2000) 39:2238-2244.

Yang G, Zhang X, Wang Z, Liu H, Ju X. Estimation of the aqueous solubility (−lgSw) of all polychlorinated dibenzo-furans (PCDF) and polychlorinated dibenzo-p-dioxins (PCDD) congeners by density functional theory. Journal of Molecular Structure: THEOCHEM (2006) 766:25-33.

Yang GCC, Hung C-H, Tu H-C. Electrokinetically enhanced removal and degradation of nitrate in the subsurface using nanosized Pd/Fe slurry. Journal of environmental science and health. Part A, Toxic/hazardous substances & environmental engineering (2008) 43:945-951.

Yi Z-j, Lian B, Yang Y-q, Zou J-l. Treatment of simulated wastewater from in situ leaching uranium mining by zerovalent iron and sulfate reducing bacteria. Transactions of Nonferrous Metals Society of China (2009) 19:S840-S844.

Yuan S, Zheng Z, Meng X-Z, Chen J, Wang L. Surfactant mediated HCB dechlorination in contaminated soils and sediments by micro and nanoscale Cu/Fe Particles. Geoderma (2010a) 159:165-173.

Yuan SH, Wen H, Wu XH, Chen J, Wang LL. Effect of nonionic and cationic surfactants on the dechlorination kinetics and products distribution of various polychlorinated benzenes by Cu/Fe particles. Separation and Purification Technology (2010b) 74:130-137.

Zhang W-x. Nanoscale Iron Particles for Environmental Remediation: An Overview. Journal of Nanoparticle Research (2003) 5:323-332.

Zhang W-x, Wang C-B, Lien H-L. Treatment of chlorinated organic contaminants with nanoscale bimetallic particles. Catalysis Today (1998) 40:387-395.

Zhang Y, Amrhein C, Chang A, Frankenberger WT, Jr. Effect of zero-valent iron and a redox mediator on removal of selenium in agricultural drainage water. Science of the Total Environment (2008) 407:89-96.

Zhang YQ, Wang JF, Amrhein C, Frankenberger WT. Removal of selenate from water by zerovalent iron. J Environ Qual (2005) 34:487-495.

Zhou W, Zhai Z, Wang Z, Wang L. Estimation of n-octanol/water partition coefficients (Kow) of all PCB congeners by density functional theory. Journal of Molecular Structure: THEOCHEM (2005) 755:137-145.

Zhu B-W, Lim T-T. Catalytic Reduction of Chlorobenzenes with Pd/Fe Nanoparticles: Reactive Sites, Catalyst Stability, Particle Aging, and Regeneration. Environmental Science & Technology (2007) 41:7523-7529.

Zhu NM, Yi L, Zhang FS. Catalytic dechlorination of polychlorinated biphenyls in subcritical water by Ni/Fe nanoparticles. Chemical Engineering Journal (2011) 171:919-925.

Zhu NR, Luan HW, Yuan SH, Chen J, Wu XH, Wang LL. Effective dechlorination of HCB by nanoscale Cu/Fe particles. Journal of Hazardous Materials (2010) 176:1101-1105.